PEOPLE'S DEMOCRATIC REPUBLIC OF ALGERIA

MINISTRY OF HIGHER EDUCATION AND SCIENTIFIC RESEARCH

UNIVERSITY OF ECHAHID HAMMA LAKHDAR EL-OUED

Faculty of Sciences and Technology

Department of Electrical Engineering

Thesis

Submitted in partial fulfillment of the requirements for Doctorate degree

Option: Telecommunications Systems

Presented by **MENAA SABER**

Thesis Title:

Novel NOMA MIMO designs for 5G and beyond

Jury:

President	Hettiri Messaoud	Professor	El-Oued University
Examiner	Djellab Hanane	MCA	Tebessa University
Examiner	Saidi Riad	MCA	Batna 2 University
Examiner	Hima Abdelkader	MCA	El-Oued University
Supervisor	Khelil Abdellatif	Professor	El-Oued University

March 2024


بسم الله الرحمن الرحيم

Acknowledgements

Initially, Gratitude to the Almighty God, who has blessed me with faith, courage, and patience to undertake and complete this endeavor.

I would like to express my deep appreciation and gratitude to my thesis supervisor, Khelil Abdellatif. His consistent support, invaluable guidance, and dedicated commitment have been instrumental in shaping my research journey. Khelil Abdellatif has served as an exemplary mentor, providing expertise, insights, and unwavering dedication to this research project. His constructive feedback, scholarly wisdom, and constant encouragement have greatly enhanced the quality of my work.

I am equally thankful to Professor Khaled Rabie for his invaluable contributions and guidance during this research endeavor. His expertise and insights have brought a multifaceted dimension to my work, and his support has been instrumental in its success.

I would like to express my deep appreciation to the jury members who so kindly agreed to be part of this humble endeavour. My sincere thanks to all of you.

I extend my heartfelt thanks to my mother, wife, brother, and sisters for their unwavering support and invaluable guidance, which have been the pillars of my journey. In this humble work, I aim to convey the profound depth of my feelings and eternal gratitude for all that you have done.

To my beloved children, Mirna and Mostafa Amir, who bring boundless joy and inspiration into my life.

Finally, I would like to express my gratitude to my friends and colleagues at Echahid Hamma Lakhdar University El-Oued. Your friendship and support mean a great deal to me.

Dedication

I dedicate this work to my beloved mother:

whose prayers and unwavering love have been my constant source of inspiration.

To my esteemed wife, I deeply appreciate your endless patience throughout this journey.

This thesis stands as a tribute to your continuous encouragement and steadfast belief in my potential.

In honor of my cherished brothers and sisters, whose unwavering love and support have illuminated my path, I deeply appreciate your continued encouragement.

To all my friends and supporters, I extend my sincere gratitude for your unwavering encouragement and wish you continued success.

Thanks

Menaa Saber

Abstract

The evolution of future generations of mobile wireless communication systems has intensified the demand for higher data rates, reduced latency, and improved spectral efficiency. Non-orthogonal multiple access (NOMA) has emerged as a groundbreaking solution to meet these demands. Which enables the sharing of time-frequency resources and utilizes successive interference cancellation (SIC) to mitigate interference among multiple users. As well, cooperative communications based on relays offer dependable connectivity and extend system coverage. While multiple inputs multiple outputs (MIMO) technology significantly contributes to the evolution of NOMA systems. The integration of MIMO using antenna selection (AS) schemes in NOMA enhances overall performance, decreases complexity and power consumption, which is a novel and appealing approach in this context. Within this thesis, we evaluate the effectiveness of implementing multi-antenna techniques within NOMA networks under realistic conditions, considering practical challenges such as SIC error, channel estimation error (CEE), and feedback delay error. The analysis begins with an examination of the single-input single-output (SISO) system in Downlink and Uplink NOMA networks, deriving mathematical expressions for ergodic capacity (EC), outage probability (OP), and bit error rate (BER). Subsequently, we investigate the MIMO-NOMA network, utilizing the joint transmit and receive antenna selection (JTRAS) protocol, and derive the expression for EC under realistic conditions. Later, we assess the performance of the Downlink cooperative NOMA network employing a relay selection strategy, incorporating both best relay selection (BRS) and partial relay selection (PRS) through the implementation of a transmit antenna selection (TAS) protocol. Finally, the thesis concludes with a comprehensive analysis of the results, highlighting challenges while offering valuable insights that can significantly influence future research in the field.

Keywords: antenna selection (AS), best relay selection (BRS), bit error rate (BER), channel estimation error (CEE), ergodic capacity (EC), joint transmit and receive antenna selection (JTRAS), multiple inputs multiple outputs (MIMO), non-orthogonal multiple access (NOMA), outage probability (OP), partial relay selection (PRS), single input single output (SISO), successive interference cancellation (SIC), transmit antenna selection (TAS).

Résumé

L'évolution des générations futures des systèmes de communication sans fil mobile a intensifié la demande de débits plus élevés, de latence réduite et d'une meilleure efficacité spectrale. L'accès multiple non orthogonal (NOMA) a émergé comme une solution révolutionnaire pour répondre à ces exigences. Il permet le partage des ressources temps-fréquence et utilise l'annulation successive des interférences (SIC) pour atténuer les interférences entre plusieurs utilisateurs. De plus, les communications coopératives basées sur des relais offrent une connectivité fiable et étendent la couverture du système, tandis que la technologie d'entrées multiples et de sorties multiples (MIMO) contribue de manière significative à l'évolution des systèmes NOMA. L'intégration du MIMO à l'aide de schémas de sélection d'antennes (AS) dans le NOMA améliore les performances globales, réduit la complexité et la consommation d'énergie, ce qui constitue une approche nouvelle et attrayante dans ce contexte. Dans cette thèse, nous évaluons l'efficacité de la mise en œuvre de techniques multi-antennes au sein des réseaux NOMA dans des conditions réalistes, en tenant compte de défis pratiques tels que l'erreur SIC, l'erreur d'estimation de canal (CEE) et l'erreur de retard de rétroaction. L'analyse commence par un examen du système d'entrée unique et de sortie unique (SISO) dans les réseaux NOMA en liaison descendante et montante, avec des expressions mathématiques dérivées pour la capacité ergodique (EC), la probabilité de panne (OP) et le taux d'erreur binaire (BER). Ensuite, nous étudions le réseau MIMO-NOMA, en utilisant le protocole de sélection d'antennes conjointes d'émission et de réception (JTRAS), et dérivons l'expression de la capacité ergodique (EC) dans des conditions réalistes. Enfin, nous évaluons la performance d'un réseau coopératif NOMA en liaison descendante en utilisant une stratégie de sélection de relais, en incorporant à la fois la meilleure sélection de relais (BRS) et la sélection partielle de relais (PRS) grâce à la mise en œuvre d'un protocole de sélection d'antennes d'émission (TAS). En conclusion, la thèse propose une analyse approfondie des résultats, mettant en évidence les défis tout en offrant des perspectives précieuses qui peuvent influencer de manière significative les futures recherches dans le domaine.

Mots clés : sélection d'antenne (AS), meilleure sélection de relais (BRS), taux d'erreur binaire (BER), erreur d'estimation de canal (CEE), capacité ergodique (EC), sélection conjointe d'antenne d'émission et de réception (JTRAS), entrées multiples sorties multiples (MIMO), accès multiple non orthogonal (NOMA), probabilité de panne (OP), sélection partielle de relais (PRS), entrée unique à sortie unique (SISO), annulation d'interférence successive (SIC), sélection d'antenne d'émission (TAS).

ملخص

أدى تطور الأجيال القادمة من أنظمة الإتصالات اللاسلكية المتنقلة إلى تكثيف الطلب على معدل بيانات أعلى، تقليل زمن الوصول وتحسين الكفاءة الطيفية. وقد برز الوصول المتعدد غير المتعامد (NOMA) كحل رائد لتلبية هذه المطالب. والذي يتيح مشاركة موارد التردد الزمني ويستخدم إلغاء التداخل المتتالي (SIC) لتخفيف التداخل بين العديد من المستخدمين. بالإضافة إلى أن الإتصالات التعاونية القائمة على المرحلات توفر إتصالاً يمكن الإعتماد عليه وتوسع نطاق تغطية النظام، فإن تقنية المدخلات المتعددة والمخرجات المتعددة (MIMO) تساهم بشكل كبير في تطور أنظمة NOMA، فيؤدي دمج MIMO بإستخدام مخططات إختيار الهوائي (AS) في NOMA إلى تحسين الأداء العام وتقليل التعقيد وإستهلاك الطاقة، وهو نهج جديد وجذاب في هذا السياق. ضمن هذه الأطروحة، نقوم بتقييم فعالية تنفيذ تقنيات الهوائيات المتعددة داخل شبكات NOMA في ظل ظروف واقعية، مع الأخذ في الاعتبار التحديات العملية مثل خطأ SIC، خطأ تقدير القناة (CEE)، وخطأ تأخير التغذية الراجعة. يبدأ التحليل بفحص نظام المدخلات الفردية والمخرجات الفردية (SISO) في شبكات NOMA للوصلة الهابطة والصاعدة باشتقاق التعبيرات الرياضية للسعة المريحة (EC)، إحتمال الإنقطاع (OP) ومعدل خطأ البت (BER). بعد ذلك، قمنا بدراسة شبكة MIMO-NOMA، بإستخدام بروتوكول إختيار هوائي الإرسال والإستقبال المشترك (JTRAS)، وإشتقاق التعبير عن EC في ظل ظروف واقعية. لاحقاً، نقوم بتقييم أداء شبكة NOMA التعاونية للوصلة الهابطة التي تستخدم إستراتيجية إختيار الترحيل، والتي تتضمن كلاً من إختيار أفضل الترحيل (BRS) وإختيار الترحيل الجزئي (PRS) من خلال تنفيذ بروتوكول اختيار هوائي الإرسال (TAS). أخيراً، تُختتم الأطروحة بتحليل شامل للنتائج، مع تسليط الضوء على التحديات و تقديم رؤى قيمة يمكن أن تؤثر بشكل كبير على الأبحاث المستقبلية في هذا المجال.

كلمات مفتاحية: اختيار الهوائي (AS)، اختيار أفضل الترحيل (BRS)، معدل خطأ البت (BER)، خطأ تقدير القناة (CEE)، السعة المريحة (EC)، اختيار هوائي الإرسال والاستقبال المشترك (JTRAS)، المدخلات المتعددة والمخرجات المتعددة (MIMO) والوصول المتعدد غير المتعامد (NOMA)، واحتمال الانقطاع (OP)، واختيار الترحيل الجزئي (PRS)، الإدخال الفردي والإخراج الفردي (SISO)، وإلغاء التداخل المتتالي (SIC)، واختيار هوائي الإرسال (TAS).

Contents

List of Figures

List of Tables

List of Abbreviations

1G	1^{st} Generation
2G	2^{nd} Generation
3G	3^{rd} Generation
3GPP	3^{rd} Generation Partnership Project
4G	4^{th} Generation
5G	5^{th} Generation
6G	6^{th} Generation
AF	Amplify-and-Forward
AR	Augmented Reality
AWGN	Additive White Gaussian Noise
BF	Beamforming
BER	Bit Error Rate
BRS	Best Relay Selection
BS	Base Station
CDF	Cumulative Distribution Function
CDMA	Code Division Multiple Access
CEE	Channel Estimation Error
CoMP	Coordinated Multi-Point
CNOMA	Cooperative Non-Orthogonal Multiple Access
CSI	Channel State Information
DF	Decode-and-Forward
E2E	End-2-End
EC	Ergodic Capacity
EE	Energy Efficiency
eMBB	enhanced Mobile BroadBand
FD	Full Duplex
FDMA	Frequency Division Multiple Access

GPRS	General Packet Radio Service
GSM	Global System for Mobile
H2H	Human-to-Human
HAP	High Altitude Platform
HD	Half Duplex
IMT	International Mobile Telecommunications
IRS	Intelligent Reflecting Surfaces
ISTN	Integrated Space and Terrestrial Network
JTRAS	Joint Transmit and Receive Antenna Selection
KPI	Key Performance Indicator
LED	Light-emitting diode
LOS	Line-of-Sight
LTE	Long-Term Evolution
MIMO	Multiple Input Multiple Output
MISO	Multiple Input Single Output
ML	Maximum Likelihood
mMIMO	massive Multiple Input Multiple Output
mMTC	massive Machine Type Communications
MR	Mixed Reality
MRC	Maximum Ratio Combining
MUST)	Multi-User Superimposed Transmission
NFV	Network Functions Virtualization
NOMA	Non-Orthogonal Multiple Access
OFDMA	Orthogonal Frequency Division Multiple Access
OMA	Orthogonal Multiple Access
OP	Outage Probability
PA	Power Allocation
PDF	Probability Density Function
PRS	Partial Relay Selection
QoS	Quality of Service
RAS	Receive Antenna Selection
RB	Resource Bloc
RS	Relay Selection
SDN	Software Defined Networking

SC	Superposition Coding
SE	Spectral Efficiency
SIC	Successive Interference Cancellation
SINR	Signal-to-Interference-plus-Noise Ratio
SISO	Single Input Single Output
SWIPT	Simultaneous Wireless Information and power Transfer
TAS	Transmit Antenna Selection
THz	TeraHertz
TDMA	Time Division Multiple Access
UAV	Unmanned Aerial Vehicle
UE	User Equipment
UMTS	Universal Mobile Telecommunications System
URLLC	Ultra-Reliable and Low Latency Communications
VLC	Visible-Light Communications
VR	Virtual Reality
WCDMA	Wideband Code Division Multiple Access
Wi-Fi	wireless fidelity

List of Symbols

n	Additive white Gaussian noise
h_j	Channel coefficient between the BS and UE$_j$
κ_j	Channel estimation error CEE
$F_X(.)$	Cumulative distribution function of X
$\hat{h}_j$	Estimated channel coefficients of h_j
$\widehat{h}_j^{(\tau)}$	Feedback delayed of the estimated channel $\hat{h}_j$
e_{fd}	Feedback error
ξ	Imperfect SIC effect coefficient
f_d	Maximum Doppler frequency characterizing the time-varying channel
$f_d\tau$	Normalized Doppler frequency
$P_{j.out}$	Outage Probability of UE$_j$
α_j	Power allocation coefficient
$f_{\gamma_j}(\gamma_j)$	Probability density function of γ_j
y_j	Received signal at UE$_j$
γ_j	SINRs at UE$_j$
ρ	Time correlation coefficient
τ	Time delay associated with the feedback information
P_t	Transmit power through BS
P_r	Transmit power through relay
γ_0	Transmit SNR
σ_j^2	Variance of h_j
$\widehat{\sigma}_j^2$	Variance of $\widehat{h}_j$
σ_κ^2	Variance the CEE

General introduction

Today's interconnected world heavily relies on wireless communication networks, which enable seamless connectivity and data exchange among various devices and locations. These networks use electromagnetic waves to transmit data wirelessly, offering flexibility and mobility. As the use of mobile devices continues to grow, the demand for efficient and dependable wireless communication networks has increased, driving ongoing advancements in technology and infrastructure. From cellular networks and wireless fidelity (Wi-Fi) to emerging technologies such as 5^{th} generation (5G) and the Internet of Things (IoT) [1, 2, 3].

Mobile wireless communication through global systems for mobile (GSM) played a pivotal role in transforming the landscape of communication networks, paving the way for the ongoing development of global mobile networks. Introduced in the 1990s, GSM brought about a revolutionary change in communication by establishing a universal standard, allowing users to connect seamlessly worldwide. The emergence of GSM marked the beginning of the global mobile communication era, laying the foundation for subsequent standards such as 3^{rd} generation (3G), 4^{th} generation (4G), and the current 5G. This continuous evolution has elevated mobile communication to a fundamental aspect of modern connectivity, significantly influencing our lifestyles, work environments, and interactions with the world [4].

Each generation represented a technological leap, bringing improvements in terms of capacity, data transmission speed, and features. The transition from analog to digital and the evolution of access techniques laid the groundwork for more advanced and efficient wireless communication networks, as we know them today. These multiple access (MA) techniques define the methods and protocols through which devices access the network, share resources, and exchange information. So, these techniques can be classified into orthogonal multiple access (OMA) and non-orthogonal multiple access (NOMA) approaches [5, 6, 7].

While OMA, characterized by its allocation of orthogonal resources to different users, aims to prevent interference by ensuring that each user operates independently including frequency-

division multiple access (FDMA), time-division multiple access (TDMA), code-division multiple access (CDMA), and orthogonal frequency-division multiple access (OFDMA) [8]. In contrast, NOMA is a groundbreaking wireless communication paradigm that outperforms OMA. NOMA's key advantage lies in its improved spectral efficiency, enabling multiple users to share time and frequency resources non-orthogonally. This leads to higher capacity and better user diversity compared to OMA. Furthermore, NOMA offers advantages in terms of low transmission latency and signaling costs compared to conventional OMA, where each user needs to send a channel scheduling request to its serving base station (BS). With these compelling features, NOMA emerges as a promising access technology for 5G networks and beyond (B5G), addressing the demand for extensive connectivity and coverage within limited radio resources [9]. NOMA's potential to reduce latency and support various services, including enhanced mobile broadband (eMBB) and IoT applications, makes it a compelling choice for evolving wireless communication systems, especially for future generations of mobile. However, its suitability depends on specific communication scenario requirements, and both NOMA and OMA offer viable options for different use cases [10].

In the power domain, NOMA's adaptive power allocation based on individual channel conditions enhances system flexibility and fairness [11]. So, the simultaneous transmission to users with diverse channel conditions further enhances its superiority. NOMA accomplishes this by utilizing advanced signal processing techniques, including superposition coding (SC) at BS to enable simultaneous transmission to users with differing channel conditions. Moreover, successive interference cancellation (SIC) at receivers is utilized to efficiently separate and decode signals from different users [12].

On the other hand, multiple input multiple output (MIMO) technology plays a pivotal role in enhancing the performance and capabilities of mobile wireless communication systems. In MIMO systems, multiple antennas are used at both the transmitter and receiver, enabling the simultaneous transmission and reception of multiple data streams [13]. This technique leverages spatial diversity and multiplexing gains to improve link reliability, increase data rates, and enhance overall system efficiency [14].

While MIMO systems offer substantial advantages, challenges such as increased power consumption and heightened hardware complexity due to multiple radio frequency (RF) chains arise. In response, antenna selection (AS) schemes serve as a practical solution, addressing these challenges through simplicity and reduced complexity. Three antenna selection protocols; transmit antenna selection (TAS), receive antenna selection (RAS), and joint transmit and receive antenna selection (JTRAS) have been implemented as effective strategies to minimize costs while maximizing the throughput benefits of multiple antennas. The straightforward implementation of antenna selection proves particularly beneficial in scenarios where hardware constraints and deployment simplicity

are paramount. Additionally, it provides a cost-effective alternative by selecting a subset of antennas, potentially reducing expenses compared to more intricate MIMO systems while retaining their advantages [15, 16]. Consequently, MIMO remains a cornerstone technology, integral to modern wireless standards like 4G long-term evolution (LTE) and 5G, enhancing spectral efficiency and overall network performance.

Recent attention has focused on exploring the interactions between NOMA and various other physical layer techniques, including cooperative communication [17, 18], MIMO systems [19], millimeter-wave (mm-W) communication [20], cognitive radio (CR) [21], and visible light communication (VLC) [22]. NOMA is considered a strong candidate for massive machine type communications (mMTC) due to its high spectral efficiency and ability to support massive communications, already implemented in 3^{rd} Generation Partnership Project (3GPP) standards [23]. Given these considerations, this thesis aims to deepen the study and the amelioration of the interaction between NOMA and MIMO systems. It proposes two models that support this interaction, showcasing our main contributions. From this perspective, the contributions of the thesis can be summarized as follows:

- In the first considered system, we analyze SISO-NOMA downlink and uplink networks with successive interference cancellation (SIC) error, channel estimation error (CEE), and feedback delay. Closed-form expressions are derived for the ergodic capacity (EC), outage probability (OP), and bit error rate (BER) of the considered Network. In addition, comprehensive simulations for downlink and uplink NOMA are presented, comparing them to related OMA networks. Based on simulation results, it is evident that SISO-NOMA networks have been adversely affected by the practical impairments.

- Secondly, we explore the incorporation of MIMO technology using the JTRAS protocol in the NOMA paradigm, establishing a direct link between the BS and users. Simulation results unequivocally demonstrate that the antenna selection strategy, implemented at both the transmitter and receiver, significantly enhances the performance in terms of EC for the considered system.

- Finally, we delve into the implementation of MIMO technology through the TAS protocol at both the BS and relay. This enriches the NOMA model and establishes an interaction between NOMA and cooperative communications. We investigate this interaction in three scenarios: conventional CNOMA as a benchmark, partial relay selection (PRS-TAS CNOMA), and best relay selection (BRS-TAS CNOMA) in terms of OP and throughput metrics under imperfections like SIC error, CEE, and feedback delay error. Simulation results indicate that the selection strategies in the antenna and relay significantly enhance the performance of the considered model.

The remainder of the thesis is organized as follows:

In chapter 1, we provide a general overview of future generations of mobile wireless communication and the fundamentals of NOMA and MIMO paradigms. The first part of this chapter includes a detailed literature review related to the requirements, features, and use cases of beyond 5G (B5G) and 6^{th} generation (6G). The second part of this chapter covers the fundamental principles of NOMA in the power domain, including SC and SIC techniques, considering both downlink and uplink transmissions in a multi-user scenario. Additionally, the concepts of multiple antennas are presented.

Chapter 2 serves as an introduction to a SISO-NOMA system, establishing it as a benchmark. This chapter delves into a comprehensive examination of practical impairments such as SIC error, CEE, and feedback delay, impacting both downlink and uplink NOMA systems over the Rayleigh fading channel. The analysis in this context focuses on key metrics such as EC, OP, and BER.

In Chapter 3, we delve into the application of the JTRAS protocol to the NOMA system, leading to the creation of a MIMO-NOMA-based JTRAS protocol system. With a focus on addressing imperfections such as SIC and CEE, we derive closed-form expressions for the EC in a multi-user system. The chapter provides a detailed analysis and comparison of the performance of the investigated system, shedding light on its capabilities and limitations.

Chapter 4 explores the application of TAS protocol and relay selection (RS) to the NOMA system, resulting in the formation of a CNOMA-based TAS protocol system. The chapter involves a detailed analysis and comparison of two RS strategies, namely BRS and PRS, evaluating the system's performance in terms of OP and throughput over the Rayleigh fading channel. The analysis takes practical impairments into account, including SIC error, CEE, and feedback delay.

In the concluding part of our thesis, we summarize the essential findings and insights obtained during the research. Additionally, we offer a glimpse into potential directions for future research in NOMA networks, including the expansion of multiple antenna techniques to introduce alternative designs in upcoming studies.

Chapter 1

Future Generations of Mobile Wireless Communications: NOMA and MIMO Paradigms

1.1 Introduction

The evolution of mobile phone technology has progressed from 1^{st} generation (1G), utilizing frequency division multiple access (FDMA) for voice communication, to 2^{nd} generation (2G), implementing time division multiple access (TDMA) for digital voice transmission. The introduction of general packet radio service (GPRS) marked 2.5G, providing data rates of approximately 144 kbps per channel and ensuring constant connectivity. GPRS facilitated various services, including web browsing and media sharing. The subsequent stage, known as enhanced data for GSM evolution (EDGE), represented 2.75G, offering theoretical data rates of up to 384 kbps and efficiently utilizing the existing global system for mobile (GSM) spectrum [24, 25]. These advancements laid the foundation for future generations of mobile communication.

The transition to 3^{rd} generation (3G) technologies, specifically universal mobile telecommunications system (UMTS) using wideband code division multiple access (WCDMA) as its primary air interface, responded to increasing data rate needs and technological progress. UMTS facilitated data transfer rates of up to 2 Mbps [26]. Initially focused on applications like video telephony, 3G systems experienced a surge in demands in the post-3G era, requiring greater bandwidth, consistent performance, and high-quality service (QoS).

The introduction of 4^{th} generation (4G) in 2010 marked a significant leap in service quality, data rates, and internet speed. Its primary objective was to provide wireless services with reliabil-

ity, accessibility, and the capacity to handle substantial data loads. It leveraged technologies such as orthogonal frequency division multiple access (OFDMA) and carrier aggregation, enabling speeds ranging from 100 Mbit/s to 1 Gbit/s, whether indoors or outdoors, all while maintaining stringent standards of quality and security [27].

Today, 5^{th} generation (5G) networks are globally available in non-standalone (NSA) configurations [28]. Operating across diverse frequency bands, including sub-6 GHz and millimeter-wave (mmWave), early 5G deployments initially focused on non-standalone mode, leveraging existing long-term evolution (LTE) infrastructure and frequencies. The primary goal was to provide enhanced mobile broadband (eMBB) services, emphasizing high-speed data for applications like HD video streaming, online gaming, IoT, and mission-critical communications with reduced latency [29]. The 5G landscape remains dynamic, characterized by ongoing spectrum auctions, network enhancements, and the continual emergence of new applications, shaping an evolving ecosystem.

Beyond 5G (B5G) and 6^{th} generation (6G) represent the next stages in the evolution of wireless communication, pushing boundaries to meet diverse digital demands. These generations promise faster speeds and innovative capabilities, further building upon the foundation laid by 5G. They introduce intelligent reflecting surfaces, integrated space, terrestrial networks, and new frequency bands to enhance performance and reliability. These advancements unlock applications like augmented reality, high-speed, low-latency communication for critical services, and more. B5G and 6G aren't just evolutionary steps; they signify a significant technological leap, driving our society's digital transformation.

Previous generations of mobile cellular networks used multiple access schemes such as FDMA, TDMA, CDMA, and OFDMA. These conventional schemes divide resources orthogonally, assigning each user a distinct portion of the spectrum. However, NOMA enables multiple users to share the same frequency, time, and code resources non-orthogonally. NOMA was developed to meet the increasing demands for wireless communication services, particularly in the context of 5G and beyond. As the number of devices and applications requiring connectivity continues to rise, there is a pressing need for more efficient resource allocation and support for massive connectivity.

In this chapter, we will delve deeper into this topic, with a particular emphasis on the essential prerequisites and emerging technologies. We will explore how networks are expanded and the ultimate applications that B5G and 6G aspire to realize. Additionally, we delve into discussions about NOMA and multiple input multiple output (MIMO) models, anticipated to play a substantial role in realizing the envisioned applications of B5G and 6G.

1.2 Towards future generations of mobile wireless communications

1.2.1 Requirements for future generations

Referring to the international mobile telecommunications (IMT) framework for 2020 and beyond [30, 31], Figure 1.1 presents a comparative analysis of the fundamental features of 5G and 6G. Both networks are assessed based on eight crucial performance metrics: peak data rate, user-experienced data rate, spectral efficiency (SE), energy efficiency (EE), mobility, latency, connectivity density, and area traffic capacity. The diagram depicts an inner red polygon symbolizing the criteria for 5G requirements, surrounded by an outer blue octagon representing the specifications for 6G. [32].

The following sections will offer a comprehensive examination of these eight key performance metrics.

- **Peak data rate:** The peak data rate is the maximum achievable data transmission speed under ideal conditions, where all available radio resources are allocated to a single mobile station. This metric has historically been crucial in differentiating between generations of mobile communication systems. With evolving user demands and technological advancements, including the emergence of Terahertz (THz) communications, the peak data rate is expected to surpass 1 Tbps. This projection exceeds the peak data rates offered by 5G, which provides 20 Gbps for downlink and 10 Gbps for uplink communications [31].

- **The user-experienced data rate:** The user-experienced data rate is defined as 5 % on the cumulative distribution function, representing user throughput. Simply put, this rate ensures that a user can expect to receive at least this data rate with a 95 % probability at any time or location. This metric is crucial for evaluating perceived performance, especially at the cell edge, and serves as an indicator of network design quality, considering factors like site density, architectural considerations, and inter-cell optimization [31].

  In a dense urban 5G deployment, the target user-perceived data rate is set at 100 Mbps for downlink and 50 Mbps for uplink. With the advent of 6G, these rates are expected to rise to 1 Gbps or higher, marking a significant tenfold increase compared to 5G technology. .

- **Latency:** Latency can be categorized into two distinct types: user plane latency and control plane latency. User plane latency represents the time delay within a radio network from the moment a packet is sent from the source until it is received by the destination, assuming a mobile station is in an active state. In the context of 5G, the minimum requirement for user plane latency stands at 4 ms for enhanced mobile broadband (eMBB) and 1 ms for ultra-reliable low latency communications (URLLC). It is envisioned that this value will see further reductions, possibly down to 100 μs or even as low as 10 μs.

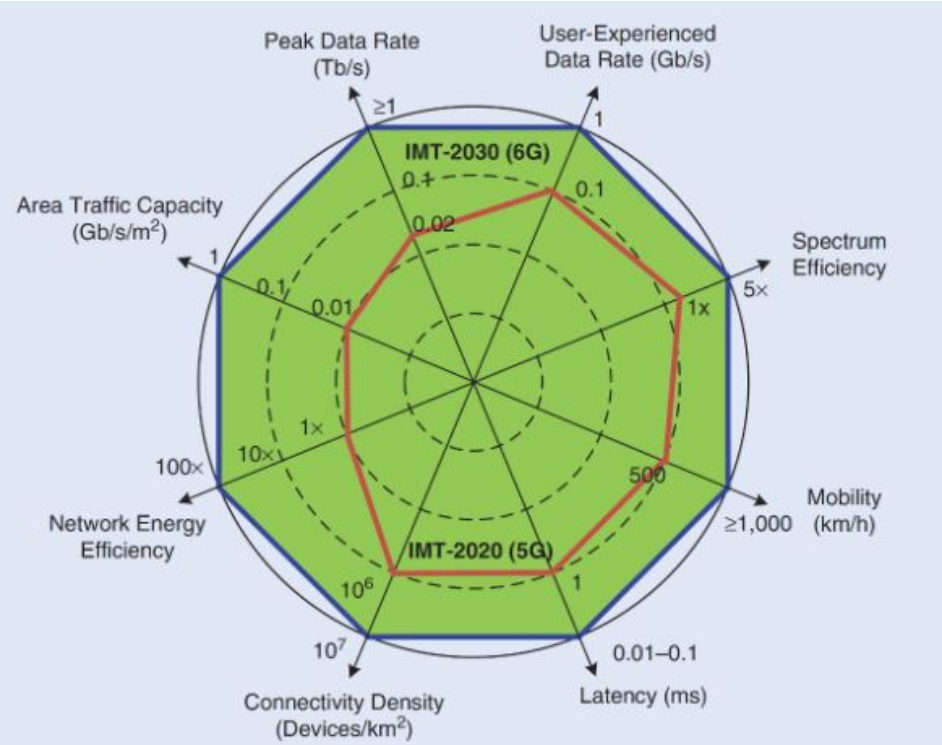

Figure 1.1: Key requirements of 5G and 6G networks [33].

Control plane latency, on the other hand, pertains to the transition time from the most "battery-efficient" state (e.g., idle state) to the initiation of continuous data transfer (e.g., active state). In 5G, the minimum requirement for control plane latency is set at 10 ms, and this is also expected to see significant improvements in 6G [34].

- **Mobility:** Mobility represents the highest achievable speed of a mobile station while maintaining acceptable QoS. In the context of 5G, mobility requirements are defined based on various use cases as follows:

  For scenarios involving higher-speed user mobility, the network should support speeds of up to 500 km/h.
  In dense urban areas, the requirement is a maximum speed of 30 km/h.
  In indoor hotspot situations, the network should support speeds of up to 10 km/h.

  However, in anticipation of 6G, the aim is to support speeds of up to 1000 km/h for high-speed applications like airline systems and hyperloop transportation.

- **Connectivity density:** Connectivity density, often assessed as a key performance indicator (KPI), is especially relevant in the context of massive machine-type communications (mMTC) use cases. In 5G, with a finite number of available radio resources, the minimum requirement for devices with a relaxed QoS per km^2 is set at 10^6 (1,000,000) devices per km^2. It is

Table 1.1: The KPI Requirements of 4G, 5G and 6G

	4G	B5G	6G
Peak data rate	• 100 Mb/s	• 20 Gb/s	• more than 1 Tb/s
Experienced data rate	• 10Mb/s	• 0.1 Gb/s	• 1 Gb/s
Spectral efficiency	• 1×	• 3× that of 4G	• 5–10× that of 5G
Energy efficiency	• 1×	• 10–100× that of 4G	• 10–100× that of 5G
Area traffic capacity	• 0.1 Mb/s/m^2	• 10 Mb/s/m^2	• 1 Gb/s/m^2
Connectivity density	• 10^5 Devices/km^2	• 10^6 Devices/km^2	• 10^7 Devices/km^2
Latency	• 10 ms	• 1 ms	• 10–100 μs
Mobility	• 350 km/h	• 500 km/h	• 1000 km/h
Reliability	• 99.99 %	• 99.999 %	• 99.99999 %

expected that this density will see a tenfold increase, reaching 10^7 (10,000,000) devices per km^2 in future 6G networks.

- **Energy efficiency:** is measured as the amount of information that can be consistently transmitted per Joule of energy consumed. It stands as a critical performance indicator for 5G networks. However, in the context of 6G networks, there's an expectation that this performance metric will exhibit a remarkable improvement, reaching levels that are 10 to 100 times more efficient than those of 5G.

- **Area traffic capacity:** is a metric that quantifies the total mobile traffic a network can handle per unit area, taking into account factors like available bandwidth, spectral efficiency, and network densification. In the context of 5G, the minimum requirement for area traffic capacity is set at 10 Mbps per m^2. However, it is anticipated that in specific deployment scenarios, such as indoor hotspots and the emergence of 6G, this capacity could significantly increase to 1 Gbps per m^2 [35].

  The notable surge in area traffic capacity highlights the evolving capabilities and escalating demands of future wireless communication systems, emphasizing the imperative to accommodate diverse connectivity needs across various scenarios, including 6G and beyond.

- **Spectral efficiency:** SE pertains to the performance metric that evaluates the maximum data throughput achievable per unit of spectrum resource under error-free conditions. For 5G, the target for user peak SE is set at 30 bps/Hz for the downlink (DL) and 15 bps/Hz for the uplink (UL). In contrast, 6G aims for a five-fold increase in SE compared to 5G, promising significantly higher data rates through more efficient spectrum resource utilization.

A comparative analysis of the requirements of 5G and 6G is presented in Table 1.1

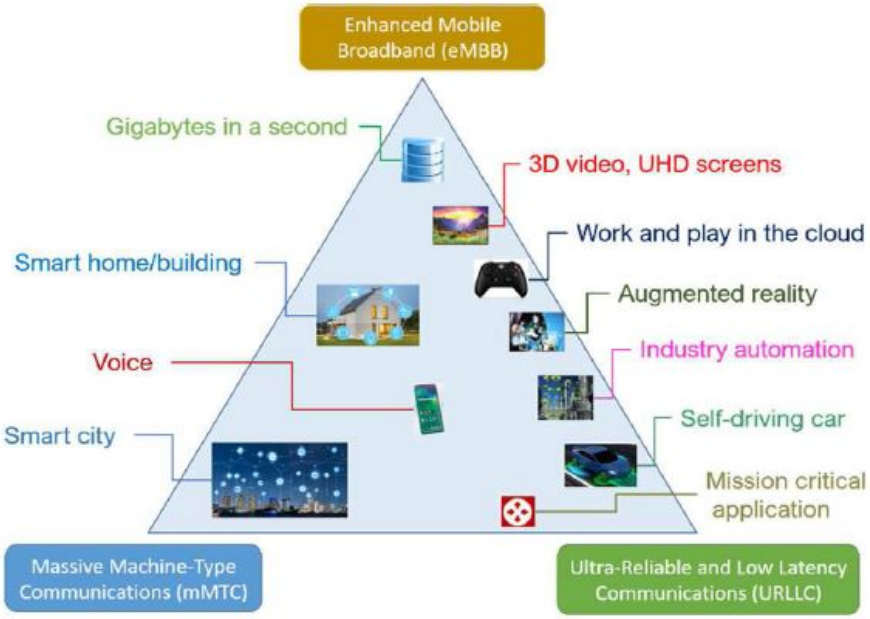

Figure 1.2: Use-cases and applications for 5G and beyond [36].

1.2.2 Usage scenarios for future generations

The evolution from 5G and beyond represents a paradigm shift beyond traditional human-to-human (H2H) communication. It introduces a diverse range of applications, including automotive communication, remote control, augmented reality (AR), virtual reality (VR), mixed reality (MR), high-definition videos, and low-data-rate applications like remote sensors. Three recommended groups of use cases by the IMT for B5G and 6G are illustrated in Figures 1.2 and 1.3.

- **Enhanced mobile broadband (eMBB):** Among the three primary 5G New Radio (NR) use cases outlined by 3GPP, eMBB stands out as a natural progression from existing 4G networks. Its primary objective is to deliver faster data rates, ultimately providing an enhanced user experience compared to current mobile broadband services. Within the realm of eMBB use cases, 5G is tasked with delivering three distinct attributes: increased capacity, improved connectivity, and enhanced user mobility. These advancements pave the way for innovative mobile applications, including high-definition video streaming, as well as immersive experiences in AR, VR, and 4K media [37, 35].

- **Massive machine-type communications (mMTC):** The primary goal of the mMTC system is to establish extensive connectivity for a multitude of devices that typically exchange small amounts of data. This use case boasts the capacity to support connectivity densities of up to one million devices per square kilometer, surpassing the capabilities of 4G networks by more than tenfold. With this remarkable capability, 5G lays the foundation for the essential

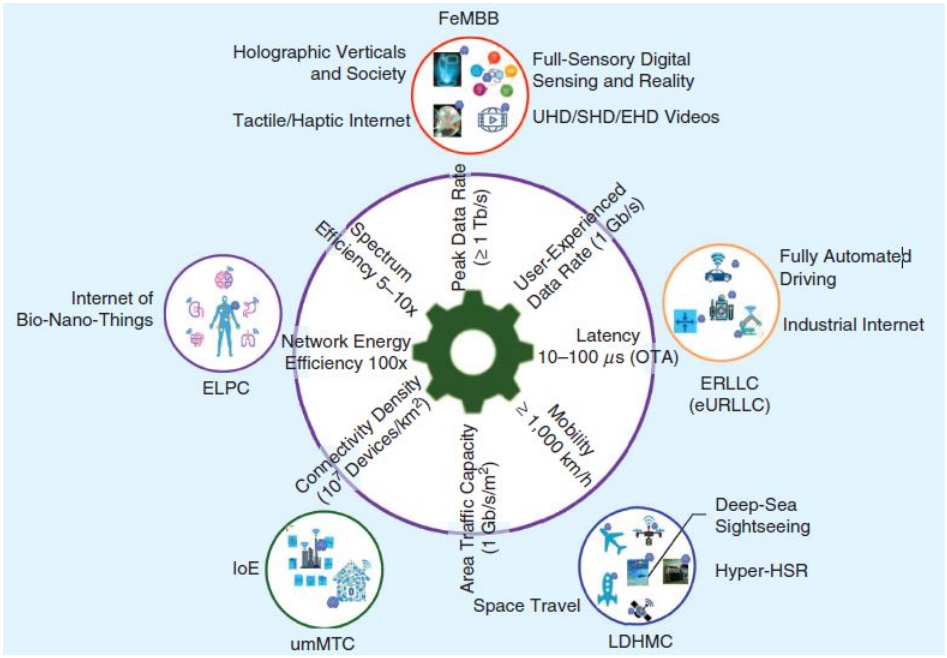

Figure 1.3: Use-cases and applications for 6G [33].

infrastructure required to underpin expansive networks of cellular-connected sensors. mMTC plays a pivotal role in enabling smart cities, industrial automation, environmental monitoring, and various IoT applications that demand scalable, widespread coverage and efficient connectivity across a diverse device ecosystem [38].

- **Ultra-reliable and low latency communications (URLLC):** In the context of 5G technology, URLLC places a strong emphasis on ensuring an exceptionally high level of reliability and minimizing communication delays. Its primary goal is to serve applications that demand real-time responsiveness, where even the slightest delay can have significant consequences. URLLC plays a critical role in mission-critical scenarios, including industrial automation, autonomous vehicles, virtual/augmented reality, and safety-critical applications that depend on instantaneous communication. The 3GPP aims to achieve URLLC applications with extremely low latencies, targeting 1ms for the user plane and 10ms for the control plane. Additionally, it strives to provide an exceptionally high level of reliability, with a success rate of up to 99.999 % in terms of packet delivery [35].

Beyond the usage scenarios covered in B5G, 6G technology introduces advanced capabilities rooted in precision and the evolution of KPIs. This paves the way for a diverse range of applications, including further enhanced mobile broadband (FeMBB), enhanced ultra-reliable low latency communications (eURLLC), ultra-massive machine-type communications (umMTC), long-range and high-mobility communications (LDHMC), and extremely low-power communications (ELPC).

These advancements represent a significant leap from 5G to 6G, raising the bar for service quality [39].

1.2.3 Key enabling techniques for future generations

To effectively enable groundbreaking use cases and applications, the B5G and 6G systems will experience the development and subsequent application of advanced technologies in transmission, networking, and computing. This section provides a comprehensive overview of the most important potential B5G and 6G technological catalysts, organized into distinct categories: New spectrum frequency bands comprising of millimeter wave (mm-Wave) technology, terahertz (THz) communications, and visible-light communications (VLC); new air interface including massive multiple-input multiple-output (mMIMO), supermassive MIMO (smMIMO), intelligent reflecting surfaces (IRS), coordinated multi-point (CoMP), non-orthogonal multiple access (NOMA), beamforming (BF), and holographic beamforming (HBF). An innovative network infrastructure encompassing cloudization, softwarization, virtualization, slicing, and intelligentization [34, 40].

We present the fundamental principles, advantages, challenges, and open research topics for each technology:

1.2.3.1 New spectrum

In the next generation of cellular networks, there is a strong capacity to support various radio access technologies (RATs), encompassing both traditional RATs with lower radio frequencies and line-of-sight (LOS) dependent RATs like THz, VLC, and optical wireless communication (OWC) as shown in Figure 1.4. These emerging RATs could potentially constitute a new layer in the hierarchical radio access network (RAN) architecture, possibly as pico cells, where diverse cells with varying RATs overlap, similar to the introduction of mmWave technology in 5G networks.

- **Millimeter wave:** The introduction of mmWave technology by 5G New Radio represents a significant leap in wireless communication and is expected to continue playing a vital role in future 6G networks. Unlike traditional RF technologies, mmWave technology provides access to a much broader spectrum of carrier frequencies, reaching up to 300 GHz. One of the remarkable advantages of mmWave technology is its shorter wavelength, which results in smaller antenna sizes. [41]. In the mmWave band, atmospheric and molecular absorption characteristics vary across frequencies. Bands like 35 GHz, 94 GHz, 140 GHz, and 220 GHz exhibit low attenuation, whereas others like 60 GHz, 120 GHz, and 180 GHz show severe propagation loss. Current standardization efforts in the mmWave domain predominantly focus on the 60 GHz band for indoor applications [34]. As a result, mmWave channels are primarily characterized by LOS paths [42].

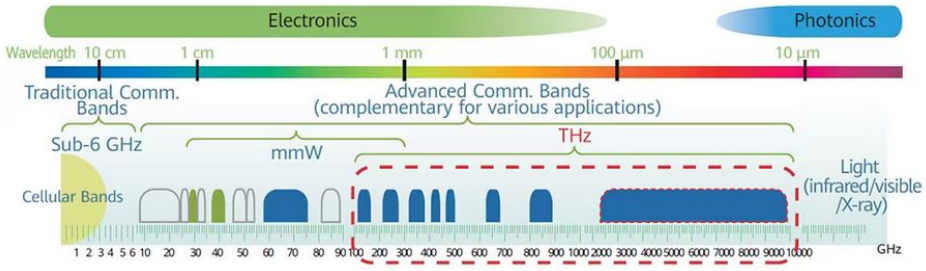

Figure 1.4: Position of mmWaves and THz waves in the radio spectrum [43].

- **Terahertz communications:** The THz band, ranging from 0.1 to 10 THz, is considered one of the promising foundational technologies that can meet the demands of 6G networks for the year 2030 and beyond. THz communications can support a vast number of connected devices while providing ultra-high user data rates, on the order of terabits per second (Tbit/s). This is primarily due to the THz band's access to extremely wide available bandwidth resources, enabling ultra-high communication rates [40, 44]. Furthermore, the THz frequency band offers the advantage of integrating more antennas to provide hundreds of beams due to its significantly shorter wavelength compared to the mm-wave band. It is expected that more than 10,000 antenna elements can be integrated into THz base stations (BS), enabling the formation of super-narrow beams [33].

- **Visible light communications:** Also known as light fidelity (Li-Fi), is a promising technology that utilizes visible light for data transmission. While it has primarily been associated with indoor communication due to its reliance on line-of-sight, VLC is evolving and gaining attention for its potential role in Beyond 5G (B5G) and 6G networks. VLC operates within the frequency spectrum ranging from 400 terahertz (THz) to 800 THz [45, 46]. In contrast to radiofrequency (RF) technologies that utilize antennas in the lower THz range, VLC uses light sources, primarily light-emitting diodes (LEDs). VLC is expected to find applications in Beyond 5G and 6G networks, particularly in indoor and dense urban environments and applications that require high data rates, low latency, and security.

1.2.3.2 New air interface

The integration of orthogonal frequency division multiplexing (OFDM) and small-scale active multiple input multiple output (MIMO) antenna arrays has been dominant in 4G and continues to be crucial in recent 5G developments. MIMO technologies are expected to play pivotal roles in the transition to 6G, leveraging new spectrum and meeting the demands of future use cases. This evolution anticipates substantial transformations, shifting from small-scale to massive MIMO and transitioning from active antennas to passive reflective surfaces.

- **Massive-MIMO:** In traditional cellular networks, MIMO technology is typically divided into two primary categories: single-user MIMO and multi-user MIMO, each serving specific roles within the network structure. Recognizing the need to enhance user experiences, boost data throughput, and leverage the benefits of statistical multiplexing gain, the concept of massive MIMO was introduced to overcome the limitations of conventional MIMO. Additionally, the use of supermassive MIMO can achieve super-high spectrum efficiency through spatial multiplexing, transmitting hundreds of parallel data streams on the same frequency channel and providing hundreds of beams, simultaneously serving more users in the form of massive-user MIMO rather than multi-user MIMO [33].

- **Beamforming and holographic beamforming:** Beamforming (BF) and holographic BF (HBF) are advanced techniques in the context of wireless communication, particularly in B5G and 6G networks. These methods are employed to optimize signal transmission and reception.

  Beamforming is a well-established technology that involves directing electromagnetic signals in a specific direction, typically toward a user or device, using an array of antennas. In analog beamforming, the phase and amplitude of the signals are controlled at the antenna level. On the other hand, Digital beamforming involves processing the signals digitally at the baseband level [47].

  Holographic beamforming is an emerging technology that combines principles of holography with beamforming to enable advanced control over signal propagation. In this approach, the amplitude and phase of signals are intelligently adjusted using holographic principles to shape and steer beams [48, 49].

- **Intelligent reflecting surfaces:** The concept of IRS has recently emerged as a highly promising and innovative approach for creating intelligent and adaptable wireless channels and radio propagation conditions in the context of advanced wireless communication systems beyond 5G and into 6G [50]. IRS is a two-dimensional surface comprised of numerous passive reflecting elements. Each of these elements can autonomously adjust the amplitude and/or phase of incoming signals [51, 52]. By strategically placing IRSs in a dense configuration within wireless networks and intelligently orchestrating their reflective properties, it becomes possible to dynamically reconfigure the propagation of signals and wireless channels between transmitters and receivers. This reconfiguration enables the achievement of specific desired outcomes and signal distributions.

- **Coordinated multi-point and cell-free:** are pivotal technologies anticipated to play essential roles in the evolution of B5G and 6G wireless networks.

  CoMP: is a technology that enables multiple base stations to coordinate their transmissions to improve network performance. It allows for more efficient utilization of radio resources and

mitigates interference, resulting in enhanced spectral efficiency and better user experiences. CoMP was initially introduced by 3GPP in its Release 11 for LTE Advanced systems [53] and is expected to continue playing an important role in 5G [54].

Cell-free communication: is an innovative network architecture that departs from the traditional cell-based approach. Cell-free networks employ distributed antenna elements throughout the coverage area. These distributed elements collaboratively serve users, offering improved coverage, capacity, and flexibility [55].

- **Non-orthogonal multiple access:** NOMA has garnered significant attention in the development of radio access methods for fifth-generation (5G) wireless networks and beyond. NOMA's fundamental idea is to serve multiple users within the same resource block, whether a time slot, subcarrier, spreading code, or spatial allocation. This approach offers several advantages, including enabling extensive connectivity, reducing latency, enhancing user fairness and spectral efficiency, and improving reliability when compared to conventional orthogonal multiple access (OMA) techniques [56, 57, 58].

1.2.3.3 New Networking

To deploy the aforementioned use cases utilizing the discussed key technologies, the network must be flexible, intelligent, and support multi-vendor equipment and multi-tenancy. Achieving this involves softwarization and virtualization in B5G and 6G networks. This shift emphasizes network slicing and reducing complexity. Software-defined networking (SDN) and network functions virtualization (NFV) enable RAN slicing, providing flexibility. This discussion covers these aspects, addressing privacy and security concerns in the context of future mobile network generations.

- **Software-defined networking:** Is a networking approach that separates the control plane from the data plane in a network. Traditionally, network devices such as switches and routers integrated both the control and data planes. With SDN, the control plane is centralized and managed by a software controller, while the data plane remains distributed across the network devices. This separation allows for greater flexibility, programmability, and automation in network management and configuration [59].

- **Network functions virtualization:** NFV focuses on virtualizing network functions that were traditionally performed by dedicated hardware appliances. NFV aims to replace these specialized hardware devices with software-based virtual network functions (VNFs) that can run on standard servers or even in the cloud [60]. By virtualizing network functions, NFV enables greater scalability, agility, and cost-efficiency in deploying and managing network services.

- **Radio access network slicing :** Is a concept that allows for the partitioning of the radio access network within 5G networks into multiple virtual slices. Slicing the RAN architecture, using SDN and NFV technologies, is an emerging research direction aimed at the cloudification, virtualization, and centralization of RAN resources in mobile networks beyond 5G and into the 6G era [61].

  The sliced next-generation radio access network (NG-RAN) architecture allows mobile operators to efficiently partition the infrastructure based on end-user and industry-specific requirements, including slicing into eMBB, URLLC, and mMTC subnets. Each slice is dedicated to a specific use case, allowing customization for different applications and ensuring optimal performance and resource allocation [62].

  The resources for the three RAN slices are divided into physical and virtual components. The 3GPP network slicing management system oversees physical resources [63], while the European Telecommunication Standards Institute (ETSI) manages virtual resources [64].

- **Cloudization:** In B5G and 6G, cloudization integrates cloud computing technologies to enhance network capabilities, flexibility, and scalability. It relies on key techniques such as Cloud Infrastructure, SDN, NFV, slicing, and service orchestration. cloudization is expected to advance network performance, service delivery, and user experience, enabling efficient resource utilization, diverse applications, and flexible infrastructure for evolving wireless communication systems.

- **Intelligentization:** softwarization, virtualization, cloudization, and slicing remain crucial for autonomous networks, with SDN, NFV, and network slicing continuing from 5G to 6G [65]. However, intelligence emerges as the primary focus for 6G, with AI techniques, particularly machine learning and deep learning, playing a pivotal role. AI optimizes network performance, aids in creating intelligent services, and facilitates predictive maintenance by preemptively detecting potential faults or degradation. The integration of AI makes it the most innovative technique for designing autonomous 6G networks [66].

1.2.3.4 New architecture

Until now, traditional mobile networks have heavily relied on land-based cellular infrastructure, limiting coverage in remote areas. To address this, the integrated space and terrestrial network (ISTN) is emerging in 6G, comprising ground-based, airborne (HAP and UAV) [34]. ISTN aims to comprehensively enhance coverage, improve global connectivity, and support diverse applications in challenging areas like open seas and wilderness regions.

- **Terrestrial-network tier:** In B5G and 6G, the terrestrial network remains the primary solution for wireless coverage, utilizing a spectrum range from sub-6 GHz to mmWave and

Table 1.2: The Network Features of 4G, 5G and 6G

	4G	B5G	6G
Service objects	People	People and things	People and world
Usage scenarios	• MBB	• eMBB • uRLLC • mMTC	• FeMBB • ERLLC • umMTC • LDHMC • ELPCs
Networking	• Flat and All-IP	• Softwarization • Virtualization • Cloudization • Slicing	• Intelligentization • Softwarization • Virtualization • Cloudization • Slicing
Main key techniques	• MIMO • OFDM • Carrier Aggregation • D2D communications	• mMIMO • mm-waves • NOMA • Beamforming	• smMIMO • THz communications • NOMA • OWC and VLC • RIS and HBF • AI /ML /DL
Applications	• HD Videos • VoLTE • Mobile TV • Mobile Internet	• UHD Videos • V2X • IoT • Smart City • Telemedicine • Wearable Devices	• Holographic Verticals and Society, • Tactile/Haptic Internet • Full-sensory digital Sensing and Reality, • Automated Driving • Industrial Internet, Space Travel

beyond. While B5G enhances capacity, 6G leverages a broader spectrum, including sub-THz and THz frequencies. To overcome path loss challenges, 6G adopts numerous small BSs, creating a highly heterogeneous network for exceptional data rates and coverage.

- **Space-network tier:** Integrating large-scale satellite constellations into the network is crucial for global coverage, especially in remote and underserved areas.

  This tier supports orbit or space Internet services, catering to space travel and meeting IoT connectivity needs, such as remote environmental monitoring and smart grids. Densely deploying low-Earth-orbit (LEO), medium-Earth-orbit (MEO), and Geostationary-Earth-orbit (GEO) satellites in areas not covered by terrestrial networks ensure wide-area ubiquitous coverage [67].

- **Air-network tier:** HAPs and UAVs play vital roles in enhancing wireless communication infrastructure alongside space satellite and terrestrial networks. They extend network coverage to challenging areas and provide connectivity in remote, rural, or disaster-stricken locations [68, 69]. Their features facilitate the connection between space and terrestrial networks, aligning with the requirements and techniques of future mobile communication generations.

- **Underwater-network tier:** This tier is designed to cover and offer internet services for diverse maritime and deep-sea activities, spanning military and commercial applications. Utilizing the distinctive propagation properties of underwater environments, the network employs acoustic and laser communication techniques for high-speed data transmission, facilitating the deployment of multiple underwater hubs [33].

The vision, architecture, and key technologies of the future generations are summarized in Table 1.2.

1.3 Towards non-orthogonal multiple access in wireless networks

Non-orthogonal multiple access (NOMA) is a multiple access scheme used in wireless communications systems, allowing multiple users to share the same time-frequency resource non-orthogonally. The basic concept of NOMA is to serve multiple users simultaneously in the same frequency band and time period, using different power levels and/or coding schemes. This approach optimizes spectrum utilization and improves overall system capacity [70].
The fundamental concepts of NOMA include:

- **Superposition coding:** SC is a fundamental technique used in NOMA to multiplex multiple users in the power domain. Distinct power levels are assigned to different users for their data transmissions, enabling simultaneous communication over the same resources. Superposition coding is applied at the transmitter to combine the data intended for different users in a way that permits their separation at the receiver [71].

- **Successive interference cancellation:** SIC is designed to detect and eliminate interference from each user. The mechanism behind SIC in Figure 1.5 is as follows: The far user with a weaker channel condition treats the signal from a user with a stronger channel as noise and decodes its data from the received signal. Conversely, the near user with a stronger channel performs SIC by first decoding the weaker user's data, subtracting it from the received signal, and then decoding its data [71].

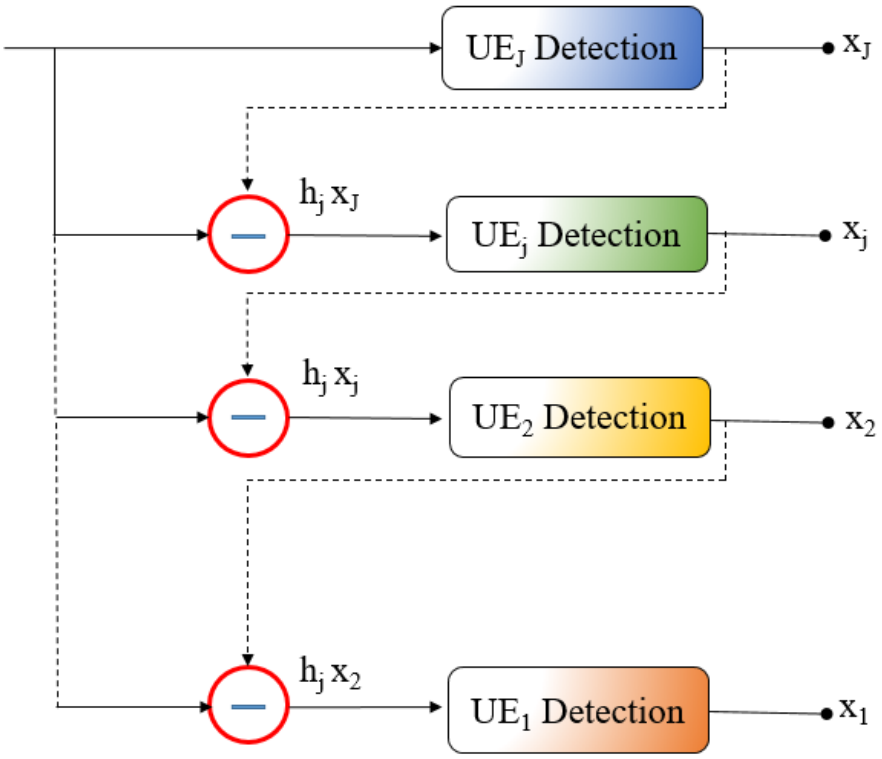

Figure 1.5: Successive interference cancellation process.

1.3.1 Downlink NOMA

In the Downlink NOMA system, where the BS communicates with multiple users as illustrated in Figure 1.6, the BS transmits an SC signal for each user as follows:

$$x = \sum_{j=1}^{J} \sqrt{P_t \alpha_j} x_j, \tag{1.1}$$

where, P_t is the transmit power from the BS, α_j are power allocation coefficients for users and x_j are the messages for users.

At the receiving end, users experiencing weaker channel conditions are provided with higher power levels, whereas those with stronger channel conditions receive lower power levels. This disparity in power allocation allows users facing challenging channel conditions to accurately decode their intended signals, even amidst interference from other users. In contrast, users with robust channel conditions employ SIC to decode their signals, effectively eliminating interference introduced by signals from stronger users in a step-by-step manner.
The signal received by the users can be expressed as:

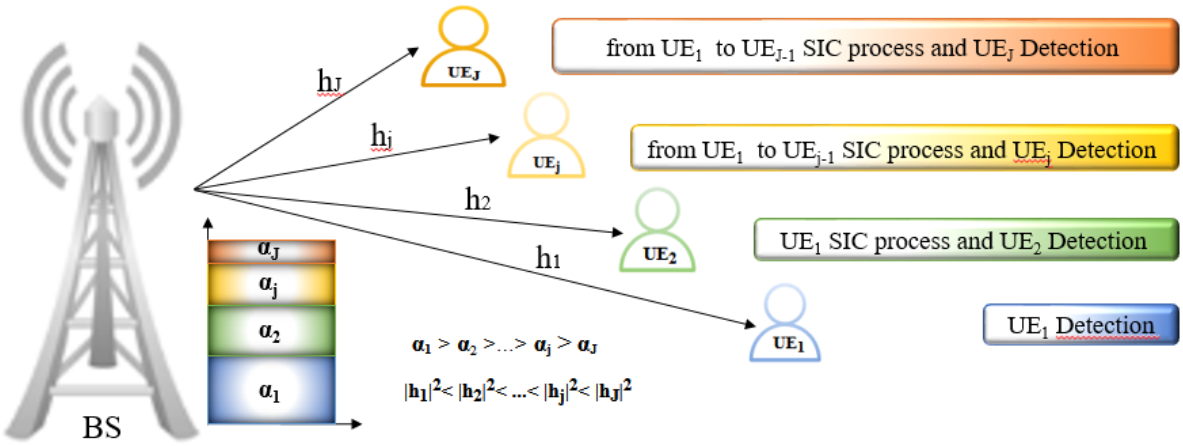

Figure 1.6: Downlink NOMA system.

$$y_j = h_j \sum_{j=1}^{J} \sqrt{P_t \alpha_j} x_j + n_j, \tag{1.2}$$

where h_j are the channel coefficients between the BS and users and n_j are the additive white Gaussian noises (AWGN) with zero mean and variance N_0.

1.3.2 Uplink NOMA

In the uplink NOMA scenario illustrated in Figure 1.7, each user's equipment transmits signals to the BS. Users are allocated different transmit power levels based on their channel conditions. This means that users with stronger channel conditions are assigned higher power levels for transmission, while those with weaker channel conditions operate at lower power levels. Subsequently, the BS employs SIC to segregate the signals of users with different power allocation coefficients. Unlike the downlink scenario, in the uplink, SIC is performed at the BS to identify signals from multiple users. The process begins by detecting the signal from the strongest user while treating the signal from the other user as interference. Then, the BS identifies and cancels signals from stronger users iteratively to enhance the detection performance of the weaker user [72].
The received signal at the BS can be depicted as follows:

$$y = \sum_{j=1}^{J} h_j \sqrt{P_t \alpha_j} x_j + n. \tag{1.3}$$

1.4 Towards multiple input multiple output in wireless networks

Traditional communication systems typically feature a single transmitting antenna paired with a single receiving antenna. Nevertheless, the increasing demands of contemporary wireless mobile

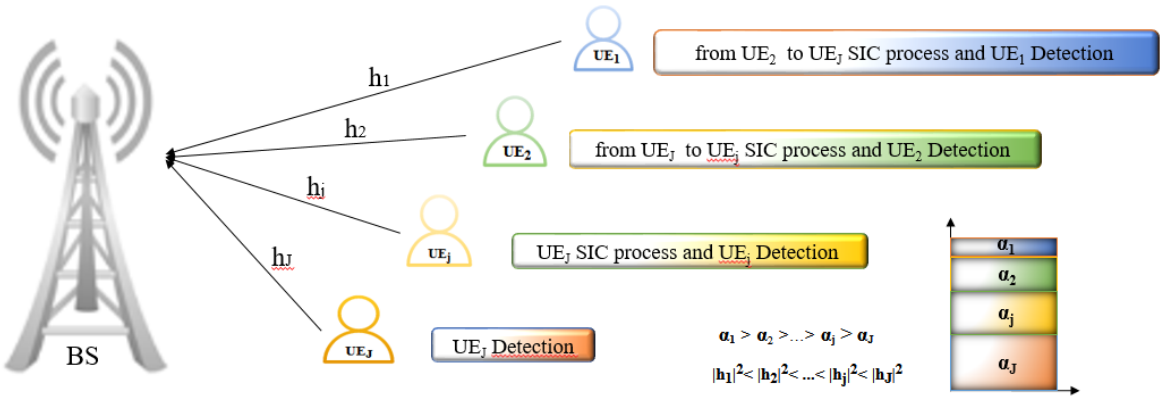

Figure 1.7: Uplink NOMA system.

communication services require enhanced data transmission capabilities. In response, the conventional approach involves substantial increases in both system bandwidths and the power levels of transmitted signals within single input single output (SISO) systems. However, recent advancements reveal that employing multiple antennas for both transmission and reception provides a pathway to enhance data transmission rates without the need to expand the bandwidth or amplify the power of the transmitting signal. This innovative transmission technique is commonly referred to as multiple input multiple output (MIMO) [73]. Thus, MIMO techniques serve as the primary means to significantly boost wireless communication performances.

As MIMO continues to be a valuable tool for optimizing and enhancing capabilities, its technology finds innovative applications in the context of NOMA. Integrating MIMO with NOMA allows the system to exploit the spatial diversity provided by multiple antennas, and enable simultaneous data transmission to multiple users [74]. This integration highlights the adaptability of MIMO techniques, expanding their impact to diverse communication paradigms like NOMA and paving the way for new possibilities in efficient and robust future wireless communication. Figure 1.8. illustrates the structure of MIMO system.

However, the deployment of multiple antennas in wireless communication systems, particularly in MIMO systems, may incur elevated power consumption, increased complexity, and higher hardware costs. In response, antenna selection (AS) emerges as a novel technique to mitigate these challenges. AS involves the strategic choice of antennas, considering criteria such as signal quality, SNR, and other performance metrics, from an available pool for transmission or reception. This selection process enhances data rates, signal quality, and minimizes interference. Notably, useful cases include transmit antenna selection (TAS), receive antenna selection (RAS), and joint transmit and receive antenna selection (JTRAS) protocols, which serve as practical solutions to keep the benefits of

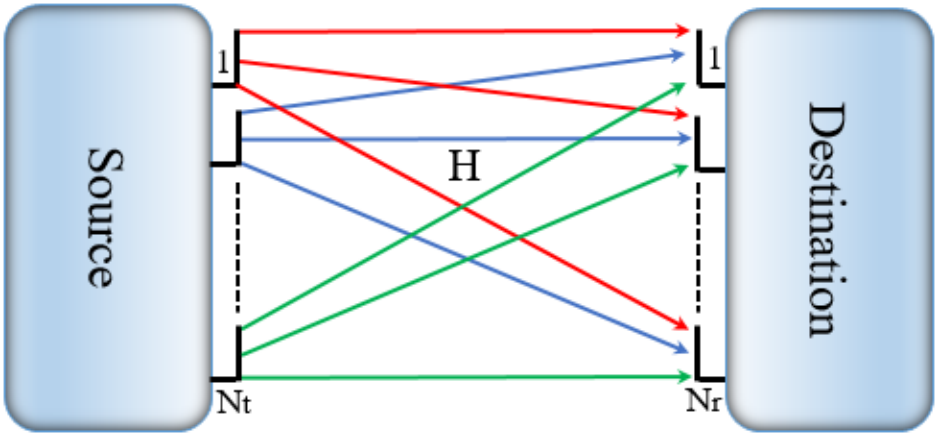

Figure 1.8: Multiple input multiple output structure.

MIMO systems [75].

1.4.1 Transmit antenna selection:

The primary objective of a TAS scheme is to maximize signal quality at the receiver while minimizing interference and power consumption. TAS can help achieve higher data rates, improved coverage, and a more robust wireless connection by carefully selecting antennas that offer the best transmission performance for a specific communication link. In the TAS scheme, the source employs multiple transmit antennas N_t, while the destination utilizes a single receive antenna, as illustrated in Figure 1.9. The selected transmit antenna index (t^*) is transmitted to the source through a feedback channel [75]. Based on this selection criterion, t^* can be determined as

$$t^* = \underset{1<t<N_t}{\arg\max} |h_t|^2, \tag{1.4}$$

where, h_t represents the fading channel coefficient connecting the t^{th} transmit antenna at the source to the destination.

1.4.2 Receive antenna selection:

In RAS scheme, the goal is to enhance the performance of the receiving system by strategically selecting one or more antennas from a set of available antennas N_r as illustrated in Figure 1.10. This scheme is often employed in wireless communication systems to mitigate the impact of fading, interference, and noise. Hence, the selected index for the receive antenna [75], denoted as r^*, can be ascertained as

$$r^* = \underset{1<r<N_r}{\arg\max} |h_r|^2, \tag{1.5}$$

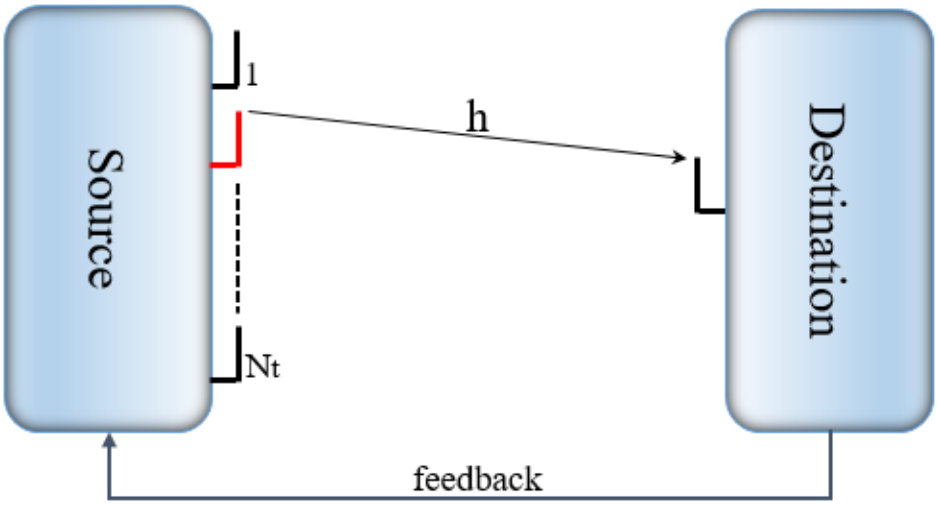

Figure 1.9: Transmit antenna selection structure.

where, h_r represents the fading channel coefficient connecting the r^{th} receive antenna at the destination from the source.

1.4.3 Joint transmit and receive antenna selection:

JTRAS scheme presented in Figure 1.11 involves simultaneously selecting optimal transmit and receive antennas to enhance communication performance. This scheme considers both ends of the communication link. Subsequently, the selected transmit antenna index is transmitted to the source through a feedback channel. Then, The selected pair of transmit and receive antennas, denoted as (t^*, r^*), is determined as [19].

$$(t^*, r^*) = \underset{1<t<N_t, 1<r<N_r}{\arg\max} |h_{t,r}|^2, \tag{1.6}$$

where, $h_{t,r}$ represents the fading channel coefficient connecting the t^{th} transmit antenna at the source to the r^{th} receive antenna at the destination.

1.5 Practical impairments

Practical impairments in wireless communication encompass real-world factors and limitations that significantly affect performance, reliability, and data quality. Our research thoroughly investigates some of these impairments, including:

- **Successive interference cancellation:** In the context of NOMA, the process of SIC is executed at the receivers to decode the signals of mobile users. It's important to consider

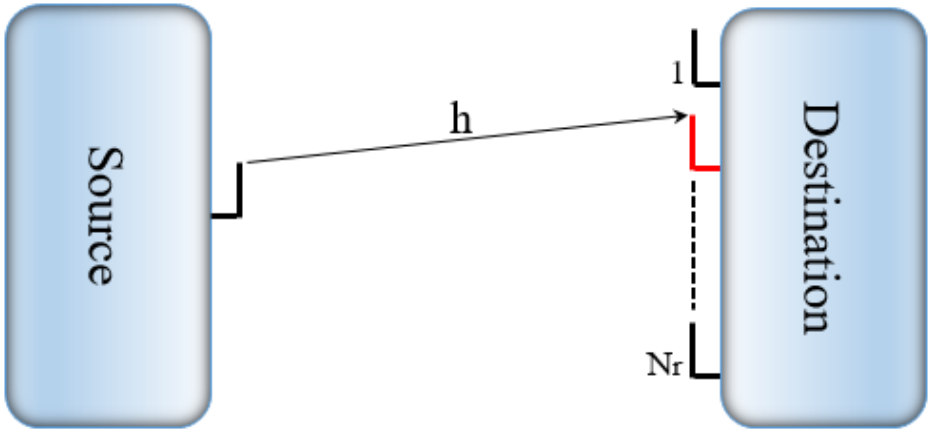

Figure 1.10: Receive Antenna Selection structure.

that errors may occur during the SIC process in real-world systems, resulting in what we can describe as propagation errors. These errors can be modeled as complex Gaussian random variables, denoted as $\sim CN\left(0,\sigma_{\zeta}^{2}\right)$. The term σ_{ζ}^{2} includes the error propagation factor, where $0<\zeta<1$. This factor quantifies the extent of the error introduced during the SIC process.

- **Channel estimation error:** CEE refers to inaccuracies in estimating the CSI at either the transmitter or receiver. In other words, in wireless communication, the existence of CEE implies that the precise determination of channel conditions between the transmitter and receiver is not perfect. let's define $h\sim CN\left(0,\sigma^{2}\right)$ as the fading channel coefficient between the transmit antenna at the BS and UE. Then, by including the CEE, the estimated channel coefficients of h can expressed by $\hat{h}=h-\kappa$, where κ is the CEE independent of $\hat{h}$ and modeled as $\kappa\sim CN\left(0,\sigma_{\kappa}^{2}\right)$. The variance $\sigma_{\kappa}^{2}=\sigma^{2}-\widehat{\sigma}^{2}$, where $\sigma^{2}=E\left\{\left|h\right|^{2}\right\}$ and $\widehat{\sigma}^{2}=E\left\{\left|\widehat{h}\right|^{2}\right\}$ are the variances of h and $\widehat{h}$, respectively [76].

- **Feedback delay:** Feedback delay denotes the duration takes to transmit channel state information from the receiver to the transmitter. During the evaluation of the destination, the channel coefficients are estimated and sent to the source through the feedback link. However, the existence of strong fading channels introduces a feedback delay. Therefore, considering this delay, the expression for the estimated channel coefficient is as follows: $\hat{h}=\rho\widehat{h}^{(\tau)}+e_{fd}$ where $\widehat{h}^{(\tau)}$ is the feedback delayed of the estimated channel $\hat{h}$ and e_{fd} the feedback error modeled as $e_{fd}\sim CN\left(0,\sigma_{fd}^{2}\right)$, which $\sigma_{fd}^{2}=\left(1-\rho\right)\widehat{\sigma}^{2}$ and $\rho=J_{0}(2\pi f_{d}\tau)$ $0<\rho<1$, ρ represents the time correlation coefficient, which serves as a measure of the quality of the feedback data, while $f_{d}\tau$ stands for the normalized Doppler frequency. In this context, f_{d} and τ refer to the maximum Doppler frequency characterizing the time-varying channel and the time delay associated with the feedback information, respectively. We assume e_{fd} and κ are independent random variables, we define a new error $e=\kappa+e_{fd}$, then $e\sim CN\left(0,\sigma_{e}^{2}\right)$ where $\sigma_{e}^{2}=\sigma_{\kappa}^{2}+\sigma_{fd}^{2}$

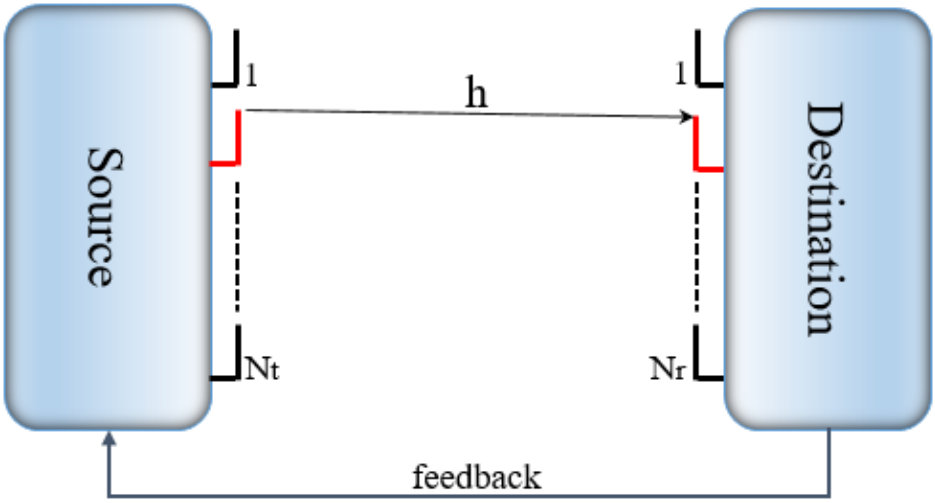

Figure 1.11: Joint Transmit and Receive Antenna Selection structure.

is the variance of each element in the error term e [76].

1.6 Wireless communications performance criteria

In this thesis, we employ the following performance metrics to evaluate the considered wireless communication systems:

- **Ergodic capacity**: The ergodic capacity (EC) of a user is computed by averaging the achievable rates R across various instantaneous channel coefficients. Mathematically, the EC can be expressed as [19]:

$$C = E\left[R\right] = E\left[\log_2(1+SINR)\right] = \int_0^{\infty} \log_2(1+SINR) f_X\left(x\right) dx, \tag{1.7}$$

  where, $f_X\left(x\right)$ is the probability density function (PDF) of X.

- **Outage probability**: The outage probability (OP) represents the likelihood of the signal-to-interference-and-noise ratio (SINR) dropping below a predefined threshold (γ_{th}). Mathematically, expressing the OP using this definition, it can be formulated as [77]:

$$P_{out} = pr\left(SINR < \gamma_{th}\right). \tag{1.8}$$

- **Bit error rate**: The bit error rate (BER) is the probability of decoding a received signal incorrectly, favoring a bit different from the one transmitted. Mathematically, the BER can be expressed as [77]:

$$P(e) = \int_0^\infty P_r(e/x) f_X(x) dx, \tag{1.9}$$

where $P_r(e/x)$ is the conditional error probability.

1.7 Conclusion

B5G and 6G mark the promising future of wireless communication, transcending the goal of speed enhancement to introduce revolutionary capabilities that cater to the diverse and expanding needs of our interconnected world. Featuring technologies such as intelligent reflecting surfaces, integrated space, and terrestrial networks, and the exploration of untapped frequency bands, these advancements promise unparalleled performance, reliability, and coverage.

These advancements unlock transformative applications, from augmented and virtual reality experiences to high-speed, low-latency communication for critical services like autonomous vehicles and remote medical procedures. The transition from 5G to B5G and 6G is not just an incremental progression; it signifies a technological leap that will profoundly influence and propel the digital transformation of our society. Looking forward, B5G and 6G are poised to redefine how we connect, communicate, and interact with the world, shaping the future of wireless technology.

On the other hand, the integration of NOMA and MIMO technologies in the realm of B5G and 6G holds the potential to propel the capabilities of future wireless communication systems. NOMA, with its ability to efficiently allocate resources to multiple users, while MIMO capitalizes on spatial diversity and multiplexing gains, collectively enhancing SE, enhanced data rates, and improved network performance. As we envision B5G and 6G, the seamless integration of NOMA and MIMO is poised to be a pivotal force in shaping the landscape of future generations of mobile wireless networks, offering transformative advantages for end-users and the broader digital ecosystem.

Chapter 2

A Comprehensive Analysis of SISO-NOMA Under Practical Impairments

2.1 Introduction

With the ever-increasing demand for wireless data, driven by the proliferation of mobile devices, the growth of the Internet of Things (IoT), and the vast volume of big data, future networks are poised to experience a significant surge in wireless traffic. Researchers have identified non-orthogonal multiple access (NOMA) as a promising candidate for the next wave of wireless communication technology, extending from the fifth generation (5G) to beyond fifth generation (B5G) networks [78].

At the essence of NOMA lies a fundamental concept that delves into the pivotal role of the power domain in facilitating multiple access (MA) within mobile networks. In more straightforward terms, NOMA enables the simultaneous multiplexing of multiple users within the power domain. This achievement is made possible by implementing superposition coding (SC) at the transmitter and successive interference cancellation (SIC) at the receiver. In the NOMA framework, the base station (BS) employs superposition coding to multiplex non-orthogonal users, apportioning higher power to those positioned at greater distances. Subsequently, each user can eliminate interference emanating from users subjected to less favorable channel conditions, courtesy of the successive interference cancellation (SIC) process [79, 80].

On the other hand, SIC plays a pivotal role in the success of NOMA by enabling multiple users to efficiently share resources. However, it introduces challenges related to computational complexity

and latency. Furthermore, imperfect channel state information (CSI) encompasses a wide range of factors that contribute to inaccuracies in the CSI; channel estimation error (CEE) may degrade performance, but accurate estimation techniques can mitigate its impact. Feedback delay (f_d) can impede real-time adaptability, yet strategies such as shorter intervals and predictive algorithms can help alleviate its effects. Striking a balance among these factors is crucial when implementing efficient NOMA systems in wireless communication networks.

In the early stages, it was a common practice for researchers to perform evaluations that compared NOMA and OMA systems. These comparisons aimed to understand their respective strengths in terms of the sum data rate and system capacity [81, 82]. Additionally, in [83, 84], a detailed exploration was carried out to investigate aspects related to NOMA's outage probability (OP) behavior and the ergodic data rate. average bit error rate (BER) formulas are derived for the downlink NOMA scheme with imperfect SIC under Rayleigh fading channels in [85, 86] and over Nakagami-m fading channels in [87]. Despite system complexity, DL-NOMA outperformed the conventional OMA scheme in terms of spectral efficiency.

Researchers have introduced numerous technological advancements to enhance the performance of NOMA systems, with cooperative communication standing out as a notable example [88]. In [89], the authors derive analytical expressions for end-to-end BER and OP while investigating a downlink CNOMA system with multiple relays to extend the coverage and connectivity, even in the presence of imperfect CSI and SIC.

Furthermore, utilizing multiple antennas enhances NOMA performance [90]. In [91], the authors derive precise OP expressions for both CSI-based and fixed gain AF relay scenarios in Nakagami-m fading channels with CSI to analyze system performance through OP and ergodic sum rate. The performance of a downlink MIMO-NOMA system over Nakagami-m fading channels is analyzed, accounting for imperfect SIC, CEE, and feedback delay [92].

Previous investigations highlight imperfect SIC, CEE, and feedback delay (f_d) as key factors in degrading NOMA network performance. Notably, closed-form expressions for EC and BER in the presence of these practical impairments are lacking in prior studies.

Hence, this chapter focuses on examining the performance of a single input single output NOMA (SISO-NOMA) system over the Rayleigh fading channel, taking into consideration imperfect SIC, CEE, and feedback delay in the downlink, as well as imperfect SIC and CEE in the uplink network. To achieve this, firstly, We formulate the signal-to-interference-plus-noise ratio (SINR) expression for both users. Subsequently, we derive closed-form expressions for EC, OP, and BER to evaluate

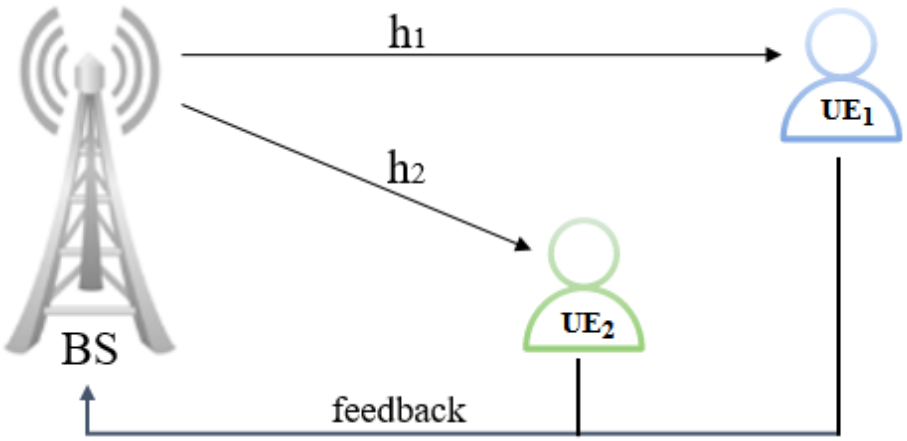

Figure 2.1: System model of downlink NOMA.

the impact of these impairments on the SISO-NOMA system. Finally, we show a close agreement between the analytical and simulation results in the numerical results section.

2.2 Modeling of SISO-NOMA downlink system

We are investigating the downlink NOMA system, which includes a base station (BS) and two users: a far user UE_1 and a near user UE_2. As depicted in Figure 2.1, all nodes are equipped with a single antenna. To model the system in practical scenarios in the presence of imperfect CSI, let's define $h_j \sim CN\left(0, \sigma_j^2\right)$ as the fading channel coefficient between the transmit antenna at the BS and UE_j. Then, by including the CEE, the estimated channel coefficients of h_j can expressed by $\hat{h}_j = h_j - \kappa_j$, where κ_j is the CEE independent of $\hat{h}_j$ and modeled as $\kappa \sim CN\left(0, \sigma_\kappa^2\right)$. The variance $\sigma_\kappa^2 = \sigma_j^2 - \widehat{\sigma}_j^2$, where $\sigma_j^2 = E\left\{|h_j|^2\right\}$ and $\widehat{\sigma}_j^2 = E\left\{\left|\widehat{h}_j\right|^2\right\}$ are the variance of h_j and $\widehat{h}_j$, respectively, with $j = 1, 2$.

Simultaneously, as the BS transmits the estimated channel gains to the users via the feedback channel, there can be a delay in the process. Thus, when accounting for this delay, the estimated channel can be formulated as follows $\hat{h}_j = \rho \widehat{h}_j^{(\tau)} + e_{j.fd}$ where $\widehat{h}_j^{(\tau)}$ is the feedback delayed of the estimated channel $\hat{h}_j$ and $e_{j.fd}$ the feedback error modelled as $e_{j.fd} \sim CN\left(0, \sigma_{j.fd}^2\right)$, which $\sigma_{j.fd}^2 = (1-\rho)\,\widehat{\sigma}_j^2$ and $\rho = J_0(2\pi f_d \tau)$ $0 < \rho < 1$, ρ represents the time correlation coefficient, which serves as a measure of the quality of the feedback data, while $f_d\tau$ stands for the normalized Doppler frequency. In this context, f_d and τ refer to the maximum Doppler frequency characterizing the time-varying channel and the time delay associated with the feedback information, respectively. We assume $e_{j.fd}$ and κ_j are independent random variables, we define a new error $e_j = \kappa_j + e_{j.fd}$, then $e \sim CN\left(0, \sigma_{e_j}^2\right)$ where $\sigma_{e_j}^2 = \sigma_{\kappa_j}^2 + \sigma_{j.fd}^2$ is the variance of each element in the error term e_j. To simplify the calculation, we make the assumption, $\sigma_\kappa^2 = \sigma_{\kappa_1}^2 = \sigma_{\kappa_2}^2$ and $\sigma_{fd}^2 = \sigma_{1,fd}^2 = \sigma_{2,fd}^2$.

In the downlink NOMA we consider that $d_2 < d_1$, resulting in $\sigma_2^2 > \sigma_1^2$.Therefore, the BS transmits a superimposed signal $x = \sum_{j=1}^{J} \sqrt{P_t \alpha_j} x_j$ to both users with distinct power levels. Following the NOMA protocol, the signal received by the UE_j users can be expressed as follows:

$$y_j = \left(\rho \widehat{h}_j^{(\tau)} + e\right) \sum_{j=1}^{J} \sqrt{P_t \alpha_j} x_j + n_j, \tag{2.1}$$

$$y_j = \underbrace{\rho \widehat{h}_j^{(\tau)} \sqrt{P_t \alpha_j} x_j}_{\text{desired signal}} + \underbrace{\rho \widehat{h}_j^{(\tau)} \sum_{j \neq i}^{J} \sqrt{P_t \alpha_i} x_i}_{\text{interference signal}} + \underbrace{e \sum_{i=1}^{J} \sqrt{P_t \alpha_i} x_i}_{\text{error signal}} + \underbrace{n_j}_{\text{noise}}, \tag{2.2}$$

where n_j is the additive white Gaussian noise (AWGN) $n_j \sim CN(0, N_o)$.

The instantaneous signal-to-interference-plus-noise ratio (SINR) for the far user UE_1 is derived as follows:

$$\gamma_1 = \frac{\alpha_1 \gamma_0 \left|\widehat{h}_1^{(\tau)}\right|^2}{\alpha_2 \gamma_0 \left|\widehat{h}_1^{(\tau)}\right|^2 + \frac{\gamma_0}{\rho^2}\left(\sigma_\kappa^2 + \sigma_{f_d \tau}^2\right) + \frac{1}{\rho^2}}. \tag{2.3}$$

The SINR received by the near user UE_2, for decoding UE_1's signal is expressed as follows:

$$\gamma_{2 \to 1} = \frac{\alpha_1 \gamma_0 \left|\widehat{h}_2^{(\tau)}\right|^2}{\alpha_2 \gamma_0 \left|\widehat{h}_2^{(\tau)}\right|^2 + \frac{\gamma_0}{\rho^2}\left(\sigma_\kappa^2 + \sigma_{f_d \tau}^2\right) + \frac{1}{\rho^2}}. \tag{2.4}$$

Considering imperfect SIC, the SINR for the near user UE_2 can be formulated as follows:

$$\gamma_2 = \frac{\alpha_2 \gamma_0 \left|\hat{h}_2^{(\tau)}\right|^2}{\alpha_1 \gamma_0 \xi \left|\hat{h}_2^{(\tau)}\right|^2 + \frac{\gamma_0}{\rho^2}\left(\sigma_\kappa^2 + \sigma_{f_d \tau}^2\right) + \frac{1}{\rho^2}}, \tag{2.5}$$

where $\gamma_0 = \frac{P_t}{N_0}$ is the transmit SNR and ξ defines the imperfect SIC effect coefficient.

2.3 Performance analysis of downlink SISO-NOMA

In this section, we investigate the ergodic capacity (EC), outage probability (OP), and bit error rate (BER) for the downlink NOMA network in the presence and absence of SIC, CEE, and feedback delay over a Rayleigh fading channel. Then, we derive the closed-form expressions for the following performance metrics.

2.3.1 Ergodic capacity analysis

In this part, we derive the closed-form of ergodic capacity for the SISO-NOMA system, considering imperfect SIC, CEE, and feedback delay. The ergodic capacity for UE_1 and UE_2 is determined by averaging achievable rates over instantaneous channel coefficients.
The achievable rates of UE_j for the SISO-NOMA system can be expressed as follows:

$$R_j = \log_2\left(1+\gamma_j\right). \tag{2.6}$$

The EC of UE_j for the SISO-NOMA system can be expressed as follows:

$$C_{j,erc} = \int_0^\infty \log_2\left(1+\gamma_j\right) f_{\gamma_j}\left(\gamma_j\right) d\gamma_j, \tag{2.7}$$

where $f_{\gamma_j}\left(\gamma_j\right)$ is the pdf of γ_j.

2.3.1.1 Ergodic capacity at far user

Based on the provided SINRs at the users, the achievable rates for UE_1, after substituting (2.3) into (2.6), can be expressed as follows:

$$R_1 = \log_2\left(1+\frac{\alpha_1\gamma_0\left|\widehat{h}_1^{(\tau)}\right|^2}{\alpha_2\gamma_0\left|\widehat{h}_1^{(\tau)}\right|^2+\frac{\gamma_0}{\rho^2}\left(\sigma_\kappa^2+\sigma_{f_d\tau}^2\right)+\frac{1}{\rho^2}}\right). \tag{2.8}$$

Substituting (2.8) into (2.7) the EC of UE_1 can be written as follows:

$$C_{1,erc} = \int_0^\infty \log_2\left(1+\frac{\alpha_1\gamma_0\left|\widehat{h}_1^{(\tau)}\right|^2}{\alpha_2\gamma_0\left|\widehat{h}_1^{(\tau)}\right|^2+\frac{\gamma_0}{\rho^2}\left(\sigma_\kappa^2+\sigma_{f_d\tau}^2\right)+\frac{1}{\rho^2}}\right) f_{\gamma_1}\left(\gamma_1\right) d\gamma_1. \tag{2.9}$$

To solve (2.9), we use some mathematical expressions:

- $\log_2\left(\frac{x}{y}\right) = \log_2\left(x\right) - \log_2\left(y\right)$.
- $\int_0^\infty \log_2\left(\beta+x\right) f_X\left(x\right) dx = \frac{1}{\ln(2)} \int_0^\infty \frac{1-F_X(x)}{\beta+x} dx$.
- $\int_0^\infty \frac{\exp(-\mu x)}{\beta+x} dx = -\exp\left(\mu\beta\right) Ei\left(-\mu\beta\right)$ [[93] eq(3.352.4)].

After some algebraic manipulations, the closed-form expression for UE_1's EC was derived as follows:

$$C_{1,erc}^{NOMA} = \frac{1}{\ln(2)} \times \left(\exp\left(\frac{\frac{\gamma_0}{\rho^2}\left(\sigma_\kappa^2 + \sigma_{f_d\tau}^2\right) + \frac{1}{\rho^2}}{\gamma_0 \alpha_2 \hat{\sigma}_1^2} \right) \mathrm{Ei}\left(-\frac{\frac{\gamma_0}{\rho^2}\left(\sigma_\kappa^2 + \sigma_{f_d\tau}^2\right) + \frac{1}{\rho^2}}{\gamma_0 \alpha_2 \hat{\sigma}_1^2} \right) \right)$$

$$- \frac{1}{\ln(2)} \times \left(\exp\left(\frac{\frac{\gamma_0}{\rho^2}\left(\sigma_\kappa^2 + \sigma_{f_d\tau}^2\right) + \frac{1}{\rho^2}}{\gamma_0 \hat{\sigma}_1^2} \right) \mathrm{Ei}\left(-\frac{\frac{\gamma_0}{\rho^2}\left(\sigma_\kappa^2 + \sigma_{f_d\tau}^2\right) + \frac{1}{\rho^2}}{\gamma_0 \hat{\sigma}_1^2} \right) \right), \quad (2.10)$$

where Ei(.) denotes the exponential integral function.
Please see Appendix A for the proof.

2.3.1.2 Ergodic capacity at near user

Based on the provided SINRs at the users, the achievable rates for UE_2, after substituting (2.5) into (2.6), can be expressed as follows:

$$R_2 = \log_2 \left(1 + \frac{\alpha_2 \gamma_0 \left| \hat{h}_2^{(\tau)} \right|^2}{\alpha_1 \gamma_0 \xi \left| \hat{h}_2^{(\tau)} \right|^2 + \frac{\gamma_0}{\rho^2}\left(\sigma_\kappa^2 + \sigma_{f_d\tau}^2\right) + \frac{1}{\rho^2}} \right). \quad (2.11)$$

Following the same steps as above, the EC of UE_2, after proofing, can be expressed as follows:

$$C_{2,erc}^{NOMA} = \frac{1}{\ln(2)} \times \left(\exp\left(\frac{\frac{\gamma_0}{\rho^2}\left(\sigma_\kappa^2 + \sigma_{f_d\tau}^2\right) + \frac{1}{\rho^2}}{\xi \gamma_0 \alpha_1 \hat{\sigma}_2^2} \right) \mathrm{Ei}\left(-\frac{\frac{\gamma_0}{\rho^2}\left(\sigma_\kappa^2 + \sigma_{f_d\tau}^2\right) + \frac{1}{\rho^2}}{\xi \gamma_0 \alpha_1 \hat{\sigma}_2^2} \right) \right)$$

$$- \frac{1}{\ln(2)} \times \left(\exp\left(\frac{\frac{\gamma_0}{\rho^2}\left(\sigma_\kappa^2 + \sigma_{f_d\tau}^2\right) + \frac{1}{\rho^2}}{\left(\alpha_2 + \alpha_1 \xi\right) \gamma_0 \hat{\sigma}_2^2} \right) \mathrm{Ei}\left(-\frac{\frac{\gamma_0}{\rho^2}\left(\sigma_\kappa^2 + \sigma_{f_d\tau}^2\right) + \frac{1}{\rho^2}}{\left(\alpha_2 + \alpha_1 \xi\right) \gamma_0 \hat{\sigma}_2^2} \right) \right). \quad (2.12)$$

2.3.2 Outage probability analysis

The OP is the probability of signal-to-interference-and-noise ratio (SINR) falling below γ_{th}. According to this definition, the OP can be given by:

$$P_{out} = Pr(\gamma < \gamma_{th}). \quad (2.13)$$

where γ_{th} is the SINR threshold. We also consider the definition of the Cumulative Distribution Function (CDF), which is given as in [94]:

$$F_{\gamma_j}(\lambda_j) = 1 - \exp\left(-\frac{\lambda_j}{{\sigma_j}^2} \right), \quad (2.14)$$

where $F_{\gamma_j}(.)$ is the CDF of γ_j.

2.3.2.1 Outage probability at far user

The OP of UE_1 can be determined by applying the CDF definition as

$$P_{out.1} = Pr(\gamma_1 < \gamma_{th,1}) = F_{\gamma_1}(\lambda_1), \tag{2.15}$$

$$\Pr(\gamma_1 < \gamma_{th.1}) = \Pr\left(\left|\widehat{h}_1^{(\tau)}\right|^2 < \frac{\frac{\gamma_{th.1}}{\rho^2}\left(1+\gamma_0\left(\sigma_\kappa^2+\sigma_{f_d\tau}^2\right)\right)}{\gamma_0\left(\alpha_1-\alpha_2\gamma_{th.1}\right)}\right). \tag{2.16}$$

We put $\lambda_1 = \frac{\frac{\gamma_{th.1}}{\rho^2}\left(1+\gamma_0\left(\sigma_\kappa^2+\sigma_{f_d\tau}^2\right)\right)}{\gamma_0(\alpha_1-\alpha_2\gamma_{th.1})}$. Thus, aligning it with the definition of the CDF in (2.14), the OP of UE_1 is derived as:

$$P_{out.1} = 1 - \exp\left(\frac{-\left(\frac{\gamma_{th.1}}{\rho^2}\left(1+\gamma_0\left(\sigma_{\kappa_j}^2+\sigma_{fd_j}^2\right)\right)\right)}{\gamma_0\hat{\sigma}_1^2\left(\alpha_1-\alpha_2\gamma_{th.1}\right)}\right). \tag{2.17}$$

Remark: It's important to emphasize that, to prevent UE_1 from being in a constant state of outage, the condition $\alpha_1 \geq \alpha_2\gamma_{th.1}$ must be met.

2.3.2.2 Outage probability at near user

The OP of UE_2 can be determined by applying the union probability of two events. The first event occurs when $\gamma_{2\to1} < \gamma_{th.1}$, while the second event occurs when $\gamma_2 < \gamma_{th.2}$. Therefore, the outage probability condition for UE_2 can be expressed as follows:

$$P_{out.2} = F_{\gamma_{2\to1}}(\lambda_1) + F_{\gamma_2}(\lambda_2) - F_{\gamma_{2\to1}}(\lambda_1)F_{\gamma_2}(\lambda_2), \tag{2.18}$$

where

$$\Pr(\gamma_{2\to1} < \gamma_{th.1}) = \Pr\left(\left|\widehat{h}_2^{(\tau)}\right|^2 < \frac{\frac{\gamma_{th.1}}{\rho^2}\left(1+\gamma_0\left(\sigma_\kappa^2+\sigma_{f_d\tau}^2\right)\right)}{\gamma_0\left(\alpha_1-\alpha_2\gamma_{th.1}\right)}\right), \tag{2.19}$$

and

$$\Pr(\gamma_2 < \gamma_{th.2}) = \Pr\left(\left|\widehat{h}_2^{(\tau)}\right|^2 < \frac{\frac{\gamma_{th.2}}{\rho^2}\left(1+\gamma_0\left(\sigma_\kappa^2+\sigma_{f_d\tau}^2\right)\right)}{\gamma_0\left(\alpha_2-\alpha_1\xi\gamma_{th.2}\right)}\right). \tag{2.20}$$

We put $\lambda_1 = \frac{\frac{\gamma_{th.1}}{\rho^2}\left(1+\gamma_0\left(\sigma_\kappa^2+\sigma_{f_d\tau}^2\right)\right)}{\gamma_0(\alpha_1-\alpha_2\gamma_{th.1})}$ and $\lambda_2 = \frac{\frac{\gamma_{th.2}}{\rho^2}\left(1+\gamma_0\left(\sigma_\kappa^2+\sigma_{f_d\tau}^2\right)\right)}{\gamma_0(\alpha_2-\alpha_1\xi\gamma_{th.2})}$. Matching it with CDF definition in (2.14), we obtain:

$$F_{\gamma_{2\to1}}(\lambda_1) = 1 - \exp\left(\frac{-\left(\frac{\gamma_{th.1}}{\rho^2}\left(1+\gamma_0\left(\sigma_\kappa^2+\sigma_{f_d\tau}^2\right)\right)\right)}{\gamma_0\hat{\sigma}_2^2(\alpha_1-\alpha_2\gamma_{th.1})}\right), \tag{2.21}$$

and

$$F_{\gamma_2}(\lambda_2) = 1 - \exp\left(\frac{-\left(\frac{\gamma_{th.2}}{\rho^2}\left(1+\gamma_0\left(\sigma_\kappa^2+\sigma_{f_d\tau}^2\right)\right)\right)}{\gamma_0\hat{\sigma}_2^2(\alpha_2-\alpha_1\xi\gamma_{th.1})}\right). \tag{2.22}$$

Then, we expressed the OP of UE_2 as follows:

$$P_{out.2} = \left(1-\exp\left(\frac{\lambda_1}{\hat{\sigma}_2^2}\right)\right) + \left(1-\exp\left(\frac{\lambda_2}{\hat{\sigma}_2^2}\right)\right) - \left(1-\exp\left(\frac{\lambda_1}{\hat{\sigma}_2^2}\right)\right)\left(1-\exp\left(\frac{\lambda_2}{\hat{\sigma}_2^2}\right)\right). \tag{2.23}$$

With some algebraic manipulations, OP of UE_2 can simplified as:

$$P_{out.2} = 1 - \exp\left(\frac{-\left(\frac{\gamma_{th.1}}{\rho^2}\left(1+\gamma_0\left(\sigma_\kappa^2+\sigma_{f_d\tau}^2\right)\right)\right)}{\gamma_0\hat{\sigma}_2^2(\alpha_1-\alpha_2\gamma_{th.1})}\right)\exp\left(\frac{-\left(\frac{\gamma_{th.2}}{\rho^2}\left(1+\gamma_0\left(\sigma_\kappa^2+\sigma_{f_d\tau}^2\right)\right)\right)}{\gamma_0\hat{\sigma}_2^2(\alpha_2-\alpha_1\xi\gamma_{th.2})}\right). \tag{2.24}$$

Remark: It is important to note that, to establish a connection with UE_2, both conditions $\alpha_1 \geq \alpha_2\gamma_{th.1}$ and $\alpha_2 \geq \alpha_1\xi\gamma_{th.2}$ need to be satisfied.

2.3.3 Bit error rate analysis

In this section, we derive closed-form expressions for the BER at both the near and far users in the presence of practical impairments. Assuming BPSK modulation for both users.

2.3.3.1 Bit error rate at far user

The error probability at UE_1, when taking into account the maximum likelihood (ML) decision rule [86], can be expressed as follows:

$$P_1(e) = \frac{1}{2}\Pr\left(\left(\sqrt{\alpha_1 P_t}+\sqrt{\alpha_2 P_t}\right)\widehat{h}_1 < n_1 + \left(\sqrt{\alpha_1 P_t}+\sqrt{\alpha_2 P_t}\right)(\kappa_1+e_{1.fd})\right)$$

$$+\frac{1}{2}Pr\left(\left(\sqrt{\alpha_1 P_t}-\sqrt{\alpha_2 P_t}\right)\widehat{h}_1 < n_1 + \left(\sqrt{\alpha_1 P_t}-\sqrt{\alpha_2 P_t}\right)(\kappa_1+e_{1.fd})\right). \tag{2.25}$$

Next, utilizing the PDF and the Gaussian Q-function, we can express (2.25) as follows:

$$P_{UE_1}(e) = \frac{1}{2}\sum_{i=1}^{2} Q\left(\sqrt{\Gamma_i}\right), \tag{2.26}$$

where,

$$\Gamma_1 = \frac{\gamma_0\rho^2(\sqrt{\alpha_1}+\sqrt{\alpha_2})^2\left|\widehat{h}_1^{(\tau)}\right|^2}{\gamma_0(\sqrt{\alpha_1}+\sqrt{\alpha_2})^2\left(\sigma_\kappa^2+\sigma_{f_d\tau}^2\right)+1}, \qquad \Gamma_2 = \frac{\gamma_0\rho^2(\sqrt{\alpha_1}-\sqrt{\alpha_2})^2\left|\widehat{h}_1^{(\tau)}\right|^2}{\gamma_0(\sqrt{\alpha_1}-\sqrt{\alpha_2})^2\left(\sigma_\kappa^2+\sigma_{f_d\tau}^2\right)+1}.$$

By employing the alternative representation of the Q(.) function and the Moment Generating Function (MGF), we can express the average BER expression of UE_1 as follows:

$$\overline{P}_{UE_1}(e) = \frac{1}{4}\sum_{i=1}^{2}\left(1-\sqrt{\frac{\overline{\Gamma}_i}{2+\overline{\Gamma}_i}}\right), \tag{2.27}$$

where,

$$\overline{\Gamma}_1 = \frac{\gamma_0\rho^2(\sqrt{\alpha_1}+\sqrt{\alpha_2})^2E\left\{\left|\widehat{h}_1^{(\tau)}\right|^2\right\}}{\gamma_0(\sqrt{\alpha_1}+\sqrt{\alpha_2})^2\left(\sigma_\kappa^2+\sigma_{f_d\tau}^2\right)+1}, \qquad \overline{\Gamma}_2 = \frac{\gamma_0\rho^2(\sqrt{\alpha_1}-\sqrt{\alpha_2})^2E\left\{\left|\widehat{h}_1^{(\tau)}\right|^2\right\}}{\gamma_0(\sqrt{\alpha_1}-\sqrt{\alpha_2})^2\left(\sigma_\kappa^2+\sigma_{f_d\tau}^2\right)+1}.$$

Please see Appendix B for the proof.

2.3.3.2 Bit error rate at near user

The error probability of UE_2 is a combination of two cases involving the SIC process. Therefore, the BER UE_2 is expressed as follows:

$$P_{UE_2}(e) = P_{UE_2}(e|correct) + P_{UE_2}(e|error), \tag{2.28}$$

where, $P_{UE_2}(e|correct)$ and $P_{UE_2}(e|error)$ represent the error probability of UE_2 when UE_1 is decoding correctly and erroneously at UE_2, respectively [86].

$$P_{UE_2}(e|correct) = \frac{1}{4}\Pr\left[\left(\sqrt{\alpha_2 P_t}\right)\widehat{h}_2^{(\tau)} < n_2 + \left(\sqrt{\alpha_1 P_t}-\sqrt{\alpha_2 P_t}\right)(\kappa + e_{f_d\tau})\right] + \frac{1}{4}Pr$$

$$\left[\left(\sqrt{\alpha_2 P_t}\right)\widehat{h}_2^{(\tau)} < n_2 + \left(\sqrt{\alpha_1 P_t}+\sqrt{\alpha_2 P_t}\right)(\kappa + e_{f_d\tau}) < \left(\sqrt{\alpha_1 P_t}+\sqrt{\alpha_2 P_t}\right)\widehat{h}_2^{(\tau)}\right], \tag{2.29}$$

and

$$P_{UE_2}(e|error) = \frac{1}{4}\Pr\left[\left(2\sqrt{\alpha_1 P_t}+\sqrt{\alpha_2 P_t}\right)\widehat{h}_2^{(\tau)} < n_2 + \left(\sqrt{\alpha_1 P_t}+\sqrt{\alpha_2 P_t}\right)(\kappa + e_{f_d\tau})\right] + \frac{1}{4}Pr$$

$$\left[\left(\sqrt{\alpha_1 P_t}-\sqrt{\alpha_2 P_t}\right)\widehat{h}_2^{(\tau)} < n_2 + \left(\sqrt{\alpha_1 P_t}-\sqrt{\alpha_2 P_t}\right)(\kappa + e_{f_d\tau}) < \left(2\sqrt{\alpha_1 P_t}-\sqrt{\alpha_2 P_t}\right)\widehat{h}_2^{(\tau)}\right]. \tag{2.30}$$

Through, utilizing the PDF and the Gaussian Q-function, we can express (2.29) and (2.30) as follows:

$$P_{UE_2}(e) = \frac{1}{2}\sum_{i=3}^{8}\Phi Q\left(\sqrt{\Gamma_i}\right), \tag{2.31}$$

where, $\Phi = \{1, 1, -1, 1, 1, -1\}$,

$$\Gamma_3 = \frac{\alpha_2\gamma_0\rho^2\left|\widehat{h}_2^{(\tau)}\right|^2}{\gamma_0(\sqrt{\alpha_1}-\sqrt{\alpha_2})^2\left(\sigma_\kappa^2+\sigma_{f_d\tau}^2\right)+1}, \qquad \Gamma_4 = \frac{\alpha_2\gamma_0\rho^2\left|\widehat{h}_2^{(\tau)}\right|^2}{\gamma_0(\sqrt{\alpha_1}+\sqrt{\alpha_2})^2\left(\sigma_\kappa^2+\sigma_{f_d\tau}^2\right)+1},$$

$$\Gamma_5 = \frac{\gamma_0\rho^2(\sqrt{\alpha_1}+\sqrt{\alpha_2})^2\left|\widehat{h}_2^{(\tau)}\right|^2}{\gamma_0(\sqrt{\alpha_1}+\sqrt{\alpha_2})^2\left(\sigma_\kappa^2+\sigma_{f_d\tau}^2\right)+1}, \qquad \Gamma_6 = \frac{\gamma_0\rho^2(2\sqrt{\alpha_1}+\sqrt{\alpha_2})^2\left|\widehat{h}_2^{(\tau)}\right|^2}{\gamma_0(\sqrt{\alpha_1}+\sqrt{\alpha_2})^2\left(\sigma_\kappa^2+\sigma_{f_d\tau}^2\right)+1},$$

$$\Gamma_7 = \frac{\gamma_0\rho^2(\sqrt{\alpha_1}-\sqrt{\alpha_2})^2\left|\widehat{h}_2^{(\tau)}\right|^2}{\gamma_0(\sqrt{\alpha_1}-\sqrt{\alpha_2})^2\left(\sigma_\kappa^2+\sigma_{f_d\tau}^2\right)+1}, \qquad \Gamma_8 = \frac{\gamma_0\rho^2(2\sqrt{\alpha_1}-\sqrt{\alpha_2})^2\left|\widehat{h}_2^{(\tau)}\right|^2}{\gamma_0(\sqrt{\alpha_1}-\sqrt{\alpha_2})^2\left(\sigma_\kappa^2+\sigma_{f_d\tau}^2\right)+1}.$$

Finally, by employing the alternative representation of the Q(.) function and the MGF, we can express the average BER expression of UE_2 as follows:

$$\overline{P}_{UE_2}(e) = \frac{1}{4}\sum_{i=3}^{8}\Phi\left(1-\sqrt{\frac{\overline{\Gamma}_i}{2+\overline{\Gamma}_i}}\right), \tag{2.32}$$

where,

$$\overline{\Gamma}_3 = \frac{\alpha_2\gamma_0\rho^2 E\left\{\left|\widehat{h}_2^{(\tau)}\right|^2\right\}}{\gamma_0(\sqrt{\alpha_1}-\sqrt{\alpha_2})^2\left(\sigma_\kappa^2+\sigma_{f_d\tau}^2\right)+1}, \qquad \overline{\Gamma}_4 = \frac{\alpha_2\gamma_0\rho^2 E\left\{\left|\widehat{h}_2^{(\tau)}\right|^2\right\}}{\gamma_0(\sqrt{\alpha_1}+\sqrt{\alpha_2})^2\left(\sigma_\kappa^2+\sigma_{f_d\tau}^2\right)+1},$$

$$\overline{\Gamma}_5 = \frac{\gamma_0\rho^2(\sqrt{\alpha_1}+\sqrt{\alpha_2})^2 E\left\{\left|\widehat{h}_2^{(\tau)}\right|^2\right\}}{\gamma_0(\sqrt{\alpha_1}+\sqrt{\alpha_2})^2\left(\sigma_\kappa^2+\sigma_{f_d\tau}^2\right)+1}, \qquad \overline{\Gamma}_6 = \frac{\gamma_0\rho^2(2\sqrt{\alpha_1}+\sqrt{\alpha_2})^2 E\left\{\left|\widehat{h}_2^{(\tau)}\right|^2\right\}}{\gamma_0(\sqrt{\alpha_1}+\sqrt{\alpha_2})^2\left(\sigma_\kappa^2+\sigma_{f_d\tau}^2\right)+1},$$

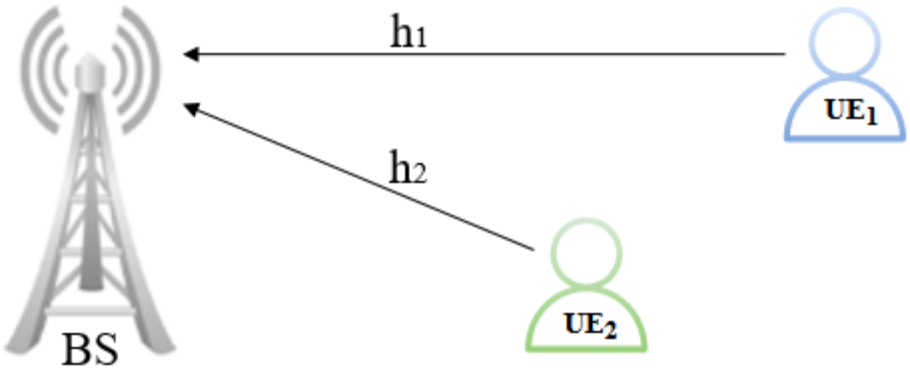

Figure 2.2: System model of uplink NOMA.

$$\overline{\Gamma}_7 = \frac{\gamma_0\rho^2(\sqrt{\alpha_1}-\sqrt{\alpha_2})^2 E\left\{\left|\widehat{h}_2^{(\tau)}\right|^2\right\}}{\gamma_0(\sqrt{\alpha_1}-\sqrt{\alpha_2})^2\left(\sigma_\kappa^2+\sigma_{f_d\tau}^2\right)+1}, \qquad \overline{\Gamma}_8 = \frac{\gamma_0\rho^2(2\sqrt{\alpha_1}-\sqrt{\alpha_2})^2 E\left\{\left|\widehat{h}_2^{(\tau)}\right|^2\right\}}{\gamma_0(\sqrt{\alpha_1}-\sqrt{\alpha_2})^2\left(\sigma_\kappa^2+\sigma_{f_d\tau}^2\right)+1}.$$

2.4 Modeling of SISO-NOMA uplink system

Similar to the downlink scenario, we examine the uplink NOMA network comprising a BS and two users: the far user UE_1 and the rear user UE_2 under the condition of imperfect SIC and CEE. As Shown in Figure 2.2, all nodes are fitted with a single antenna. Following the uplink NOMA protocol, the signal received at the BS is formulated as:

$$y = \sum_{j=1}^{J}\left(\widehat{h}_j + \sigma_{\kappa_j}^2\right)\sqrt{P_t\alpha_j}x_j + n, \tag{2.33}$$

where, $\widehat{h}_j$ is estimated channel fading coefficient between user j and BS, α_j is the power allocation coefficient for each user, and n is the AWGN follows $n \sim CN(0, N_o)$.

Using the received signal, the BS utilizes SIC to identify the symbols of the users. Because UE_2 has a better channel quality compared to UE_1, the BS decodes symbols from UE_2 while considering symbols from UE_1 as noise. Thus, the SINR of UE_2 is expressed as:

$$\gamma_2 = \frac{\alpha_2\gamma_0\left|\widehat{h}_2\right|^2}{\alpha_1\gamma_0\left|\widehat{h}_1\right|^2 + \gamma_0\sigma_\kappa^2 + 1}. \tag{2.34}$$

Following the decoding of UE_2, the BS applies SIC to detect the symbols of UE_1. So, the SINR of UE_1 is derived as:

$$\gamma_1 = \frac{\alpha_1 \gamma_0 \left|\widehat{h}_1\right|^2}{\alpha_2 \xi \gamma_0 \left|\widehat{h}_2\right|^2 + \gamma_0 \sigma_\kappa^2 + 1}. \tag{2.35}$$

2.5 Performance analysis of uplink SISO-NOMA

In this section, we formulate the mathematical expressions of the EC and OP for the uplink NOMA network with SIC and CSI imperfections, operating over a Rayleigh fading channel.

2.5.1 Ergodic capacity analysis

Similarly to the downlink NOMA, we derive the expression for the EC of the uplink NOMA system considering SIC and CEE imperfections over the Rayleigh fading channel.

2.5.1.1 Ergodic capacity at far user

The achievable rate of UE_1 is obtained by substituting (2.35) into (2.6), and after performing some algebraic simplifications, R_1 can be expressed as:

$$R_1 = \log_2 \left(\frac{1 + \gamma_0 \sigma_\kappa^2 + \alpha_1 \gamma_0 \left|\widehat{h}_1\right|^2 + \alpha_2 \xi \gamma_0 \left|\widehat{h}_2\right|^2}{1 + \gamma_0 \sigma_\kappa^2 + \alpha_2 \xi \gamma_0 \left|\widehat{h}_2\right|^2} \right). \tag{2.36}$$

In order to solve (2.36), we use $\log_2 \left(\frac{x}{y}\right) = \log_2 (x) - \log_2 (y)$. So, the rate of UE_1 can be written as:

$$R_1 = \log_2 \left(1 + \gamma_0 \sigma_\kappa^2 + \alpha_1 \gamma_0 \left|\widehat{h}_1\right|^2 + \alpha_2 \xi \gamma_0 \left|\widehat{h}_2\right|^2 \right) - \log_2 \left(1 + \gamma_0 \sigma_\kappa^2 + \alpha_2 \xi \gamma_0 \left|\widehat{h}_2\right|^2 \right). \tag{2.37}$$

To derive the ergodic rate, we put $\beta = 1 + \gamma_0 \sigma_\kappa^2$ and $\Delta = \alpha_1 \gamma_0 \delta_1 + \alpha_2 \xi \gamma_0 \delta_2$ where, $\delta_1 = \left|\widehat{h}_1\right|^2$ and $\delta_2 = \left|\widehat{h}_2\right|^2$. Then, using (2.7) the ergodic capacity of UE_1 is defined by:

$$C_{1,erg} = \int_0^\infty \log_2 (\beta + \Delta) f_\Delta (\Delta)\, d\Delta - \int_0^\infty \log_2 (\beta + \alpha_2 \xi \gamma_0 \delta_2) f_{\delta_2} (\delta_2)\, d\delta_2. \tag{2.38}$$

By using the integration by part $\int_0^\infty \log_2 (\beta + x)\, f_X (x)\, dx = \frac{1}{\ln(2)} \int_0^\infty \frac{1 - F_X(x)}{\beta + x} dx$ [95, eq. (11)]. (2.38) can be written in terms of CDF as:

$$C_{1,erg} = \underbrace{\frac{1}{\ln(2)} \int_0^\infty \frac{1 - F_\Delta(\Delta)}{\beta + \Delta} d\Delta}_{J_1} - \underbrace{\frac{1}{\ln(2)} \int_0^\infty \frac{1 - F_{\delta_2}(\delta_2)}{\beta + \delta_2} d\delta_2}_{J_2}. \tag{2.39}$$

Utilizing the CDF definition as outlined in equation (2.14), we acquire

$$F_{\delta_2}(\delta_2) = 1 - \exp\left(-\frac{\beta}{\alpha_2\xi\gamma_0\hat{\sigma}_2^2}\right), \tag{2.40}$$

and,

$$F_{\Delta}(\Delta) = 1 + \frac{\alpha_1\gamma_0\hat{\sigma}_1^2}{\alpha_1\gamma_0\hat{\sigma}_1^2 - \alpha_2\gamma_0\hat{\sigma}_2^2}\exp\left(\frac{\beta}{\alpha_1\gamma_0\hat{\sigma}_1^2}\right) - \frac{\alpha_2\xi\gamma_0\hat{\sigma}_2^2}{\alpha_1\gamma_0\hat{\sigma}_1^2 - \alpha_2\xi\gamma_0\hat{\sigma}_2^2}\exp\left(-\frac{\beta}{\alpha_2\xi\gamma_0\hat{\sigma}_2^2}\right). \tag{2.41}$$

Substituting (2.40) and (2.41) into (2.39) we obtain:

$$C_{1,erg} = \underbrace{\frac{1 + \frac{\alpha_2\xi\gamma_0\hat{\sigma}_2^2}{\alpha_1\gamma_0\hat{\sigma}_1^2 - \alpha_2\xi\gamma_0\hat{\sigma}_2^2}}{\ln(2)}\int_0^{\infty}\frac{\exp\left(-\frac{\beta}{\alpha_2\xi\gamma_0\hat{\sigma}_2^2}\right)}{\beta+\delta_2}d\Delta}_{J_1} - \underbrace{\frac{\frac{\alpha_1\gamma_0\hat{\sigma}_1^2}{\alpha_1\gamma_0\hat{\sigma}_1^2 - \alpha_2\xi\gamma_0\hat{\sigma}_2^2}}{\ln(2)}\int_0^{\infty}\frac{\exp\left(-\frac{\beta}{\alpha_1\gamma_0\hat{\sigma}_1^2}\right)}{\beta+\delta_1}d\delta_1}_{J_2}. \tag{2.42}$$

Finally, by employing $\int_0^{\infty}\frac{\exp(-\mu x)}{\beta+x}dx = -\exp(\mu\beta)\,Ei(-\mu\beta)$ [[93] eq(3.352.4)] and practice some algebraic manipulations, we obtained the closed-form expression for UE_1 as follows:

$$C_{1,erc}^{NOMA} = \frac{\alpha_1\gamma_0\hat{\sigma}_1^2}{(\alpha_1\gamma_0\hat{\sigma}_1^2 - \alpha_2\xi\gamma_0\hat{\sigma}_2^2)\times\ln(2)}\times\left(\exp\left(\frac{1+\gamma_0\sigma_\kappa^2}{\alpha_2\xi\gamma_0\hat{\sigma}_2^2}\right)\mathrm{Ei}\left(-\frac{1+\gamma_0\sigma_\kappa^2}{\alpha_2\xi\gamma_0\hat{\sigma}_2^2}\right)\right)$$

$$-\frac{\alpha_1\gamma_0\hat{\sigma}_1^2}{(\alpha_1\gamma_0\hat{\sigma}_1^2 - \alpha_2\xi\gamma_0\hat{\sigma}_2^2)\times\ln(2)}\times\left(\exp\left(\frac{1+\gamma_0\sigma_\kappa^2}{\alpha_1\gamma_0\hat{\sigma}_1^2}\right)\mathrm{Ei}\left(-\frac{1+\gamma_0\sigma_\kappa^2}{\alpha_1\gamma_0\hat{\sigma}_1^2}\right)\right). \tag{2.43}$$

2.5.1.2 Ergodic capacity at near user

Applying the same methodology and utilizing the algebraic equations employed earlier, it is easy to demonstrate that the closed-form expression of EC for UE_2 is

$$C_{2,erc}^{NOMA} = \frac{\alpha_2\gamma_0\hat{\sigma}_2^2}{(\alpha_2\gamma_0\hat{\sigma}_2^2 - \alpha_1\gamma_0\hat{\sigma}_1^2)\times\ln(2)}\times\left(\exp\left(\frac{1+\gamma_0\sigma_\kappa^2}{\alpha_1\gamma_0\hat{\sigma}_1^2}\right)\mathrm{Ei}\left(-\frac{1+\gamma_0\sigma_\kappa^2}{\alpha_1\gamma_0\hat{\sigma}_1^2}\right)\right)$$

$$-\frac{\alpha_2\gamma_0\hat{\sigma}_2^2}{(\alpha_2\gamma_0\hat{\sigma}_2^2 - \alpha_1\gamma_0\hat{\sigma}_1^2)\times\ln(2)}\times\left(\exp\left(\frac{1+\gamma_0\sigma_\kappa^2}{\alpha_2\gamma_0\hat{\sigma}_2^2}\right)\mathrm{Ei}\left(-\frac{1+\gamma_0\sigma_\kappa^2}{\alpha_2\gamma_0\hat{\sigma}_2^2}\right)\right). \tag{2.44}$$

2.5.2 Outage probability analysis

Similarly to the downlink NOMA, we derive the expression for the OP of the uplink NOMA system considering SIC and CEE imperfections over the Rayleigh fading channel.

2.5.2.1 Outage probability at near user

The OP of UE_2 can be determined by applying the definition of CDF:

$$P_{out.2} = F_{\gamma_2}(\gamma_{th.2}) = Pr(\gamma_2 \leq \gamma_{th,2}), \tag{2.45}$$

where $\gamma_{th,2}$ is the target of the UE_2 and F_{γ_2} is the CDF of γ_2.

$$F_{\gamma_2}(\gamma_{th.2}) = \Pr\left(\frac{\alpha_2\gamma_0\left|\widehat{h}_2\right|^2}{\alpha_1\gamma_0\left|\widehat{h}_1\right|^2 + \gamma_0\sigma_\kappa^2 + 1} \leq \gamma_{th.2}\right). \tag{2.46}$$

after some algebraic usages, we obtain the expression of the OP of UE_2 as follows:

$$P_{out.2} = 1 - \frac{\alpha_2\gamma_0\hat{\sigma}_2^2}{\alpha_2\gamma_0\hat{\sigma}_2^2 + \gamma_{th.2}\alpha_1\gamma_0\hat{\sigma}_1^2}\exp\left(-\frac{\gamma_{th.2}\left(1+\gamma_0\sigma_\kappa^2\right)}{\alpha_2\gamma_0\hat{\sigma}_2^2}\right). \tag{2.47}$$

2.5.2.2 Outage probability at far user

Similar to the near user, the OP of the far user can easily derived as:

$$P_{out.1} = 1 - \frac{\alpha_1\gamma_0\hat{\sigma}_1^2}{\alpha_1\gamma_0\hat{\sigma}_1^2 + \gamma_{th.1}\xi\alpha_2\gamma_0\hat{\sigma}_2^2}\exp\left(-\frac{\gamma_{th.1}\left(1+\gamma_0\sigma_\kappa^2\right)}{\alpha_1\gamma_0\hat{\sigma}_1^2}\right). \tag{2.48}$$

Nevertheless, the OP of UE_1 at the BS occurs when the decoding of both the UE_1 and UE_2 signals is unsuccessful. Therefore, the OP of UE_1 can be expressed as the union of these two events, as follows:

$$\begin{aligned}
P_{out.1} = &\left(1 - \frac{\alpha_2\gamma_0\hat{\sigma}_2^2}{\alpha_2\gamma_0\hat{\sigma}_2^2 + \gamma_{th.2}\alpha_1\gamma_0\hat{\sigma}_1^2}\exp\left(-\frac{\gamma_{th.2}\left(1+\gamma_0\sigma_\kappa^2\right)}{\alpha_2\gamma_0\hat{\sigma}_2^2}\right)\right) \\
&+ \left(1 - \frac{\alpha_1\gamma_0\hat{\sigma}_1^2}{\alpha_1\gamma_0\hat{\sigma}_1^2 + \gamma_{th.1}\xi\alpha_2\gamma_0\hat{\sigma}_2^2}\exp\left(-\frac{\gamma_{th.1}\left(1+\gamma_0\sigma_\kappa^2\right)}{\alpha_1\gamma_0\hat{\sigma}_1^2}\right)\right) \\
&- \left(1 - \frac{\alpha_2\gamma_0\hat{\sigma}_2^2}{\alpha_2\gamma_0\hat{\sigma}_2^2 + \gamma_{th.2}\alpha_1\gamma_0\hat{\sigma}_1^2}\exp\left(-\frac{\gamma_{th.2}\left(1+\gamma_0\sigma_\kappa^2\right)}{\alpha_2\gamma_0\hat{\sigma}_2^2}\right)\right) \\
&\times \left(1 - \frac{\alpha_1\gamma_0\hat{\sigma}_1^2}{\alpha_1\gamma_0\hat{\sigma}_1^2 + \gamma_{th.1}\xi\alpha_2\gamma_0\hat{\sigma}_2^2}\exp\left(-\frac{\gamma_{th.1}\left(1+\gamma_0\sigma_\kappa^2\right)}{\alpha_1\gamma_0\hat{\sigma}_1^2}\right)\right).
\end{aligned} \tag{2.49}$$

2.6 Numerical results

This section illustrates the effects of imperfect SIC, CEE, and feedback delay impairments on the performance of the SISO-NOMA network. Numerical results are presented over Rayleigh fading channel, with power coefficients allocated as $\alpha_1 = 0.8$ and $\alpha_2 = 0.2$, and distances set to $d_1 = 2m$ and $d_2 = 1m$. Additionally, we have $\xi = 0.01$, $\sigma_\kappa^2 = 0.001$, and $f_d\tau = 0.02$. In the plots, different lines and markers represent analytical and simulation curves, respectively. It is evident from all figures that both the analytical and simulated results are nearly identical, confirming the accuracy of the performance analysis.

In Figure 2.3, we can observe the comparative results of simulations and analytical proofs for the EC of UE_1 and UE_2 in the downlink NOMA system under different impairment scenarios. These scenarios include $\xi = 0.01$, $\sigma_\kappa^2 = 0.001$, and $f_d\tau = 0.02$. The EC for UE_2 tends to increase linearly with SNR. This is because perfect SIC effectively cancels interference, allowing for a significant capacity gain as SNR grows. Interestingly, the EC of UE_1 exhibits a slow increase with SNR and reaches saturation levels more rapidly, despite the fact that UE_1 receives a higher allocation of power. Further, in the presence of imperfect SIC, the EC growth for UE_2 is still positive, but it may increase at a slower rate compared to perfect SIC, while UE_1 remains unaffected by SIC imperfections. Additionally, with imperfect SIC at UE_2, CEE has a more pronounced negative impact on EC. Furthermore, feedback delay can result in an additional reduction in EC. However, UE_1 experiences a slight reduction in EC. However, particularly when perfect SIC is employed, figure 2.4 demonstrates advantages in EC at UE_2 even in the presence of CEE and feedback delay.

Figure 2.5 compares the sum EC performance between the NOMA system and the OMA system against the transmit SNR under various impairment scenarios. These scenarios involve parameters such as $\xi = 0.01$, $\sigma_\kappa^2 = 0.001$, and $f_d\tau = 0.02$. It's evident that under perfect SIC, NOMA generally outperforms OMA in sum EC. However, in the presence of imperfect SIC and CEE, NOMA's performance diminishes. This reduction is further exacerbated by feedback delay, making OMA more competitive under these conditions. While Figure 2.6 demonstrates the superior performance of NOMA in sum EC compared to OMA with perfect SIC, it underscores the pivotal role that SIC plays in mitigating the influence of CEE and feedback delay on sum EC. However, when SIC is imperfect, the effects of CEE and feedback delay become more pronounced, leading to a significant degradation in the performance of the NOMA system and ultimately leading to the superiority of OMA.

The OP of users in the downlink SISO-NOMA system under different impairment scenarios are presented in Figure 2.7 and Figure 2.8.

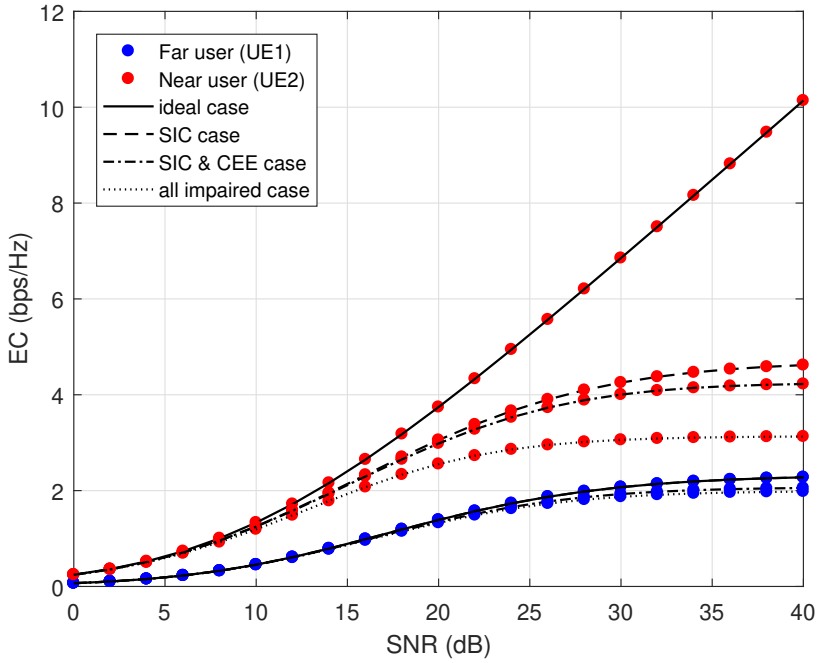

Figure 2.3: The EC of the downlink NOMA system in the presence of various impairments under imperfect SIC.

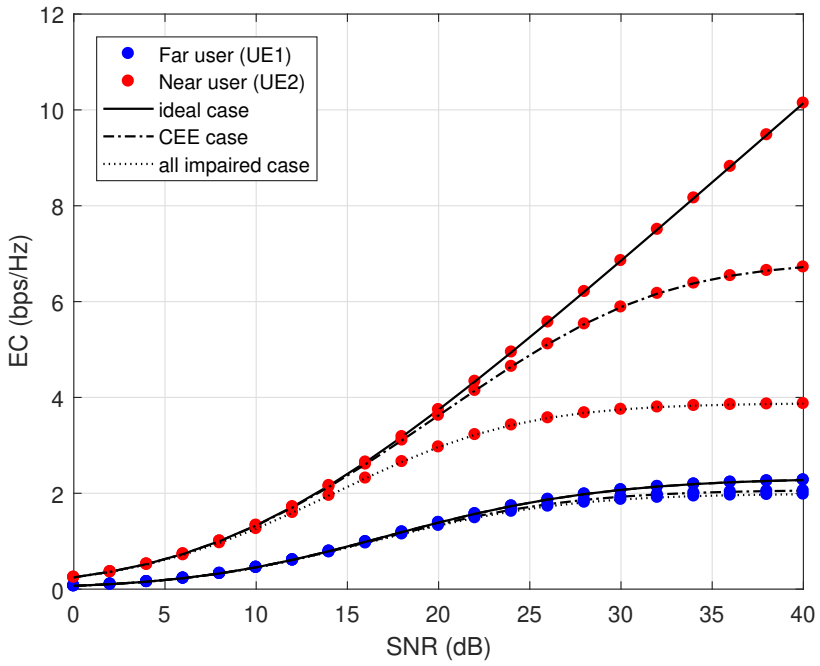

Figure 2.4: The EC of the downlink NOMA system in the presence of various impairments under perfect SIC.

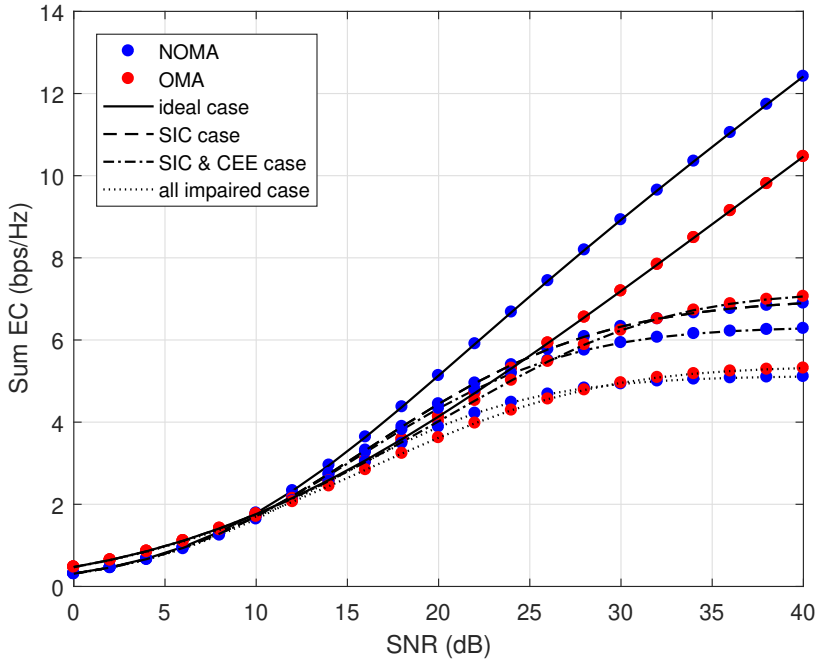

Figure 2.5: Comparison between sum EC of NOMA and OMA systems in the presence of various impairments under imperfect SIC.

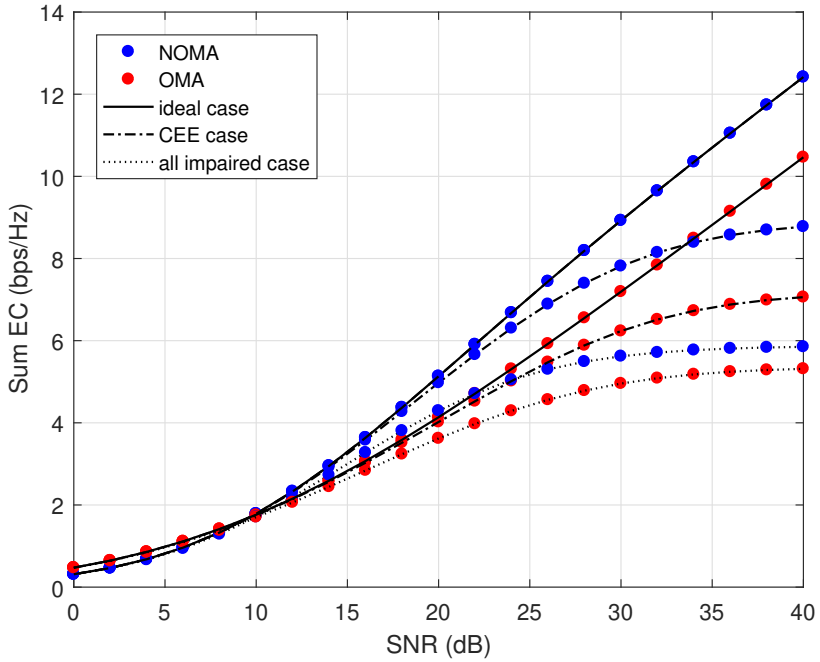

Figure 2.6: Comparison between sum EC of NOMA and OMA systems in the presence of various impairments under perfect SIC.

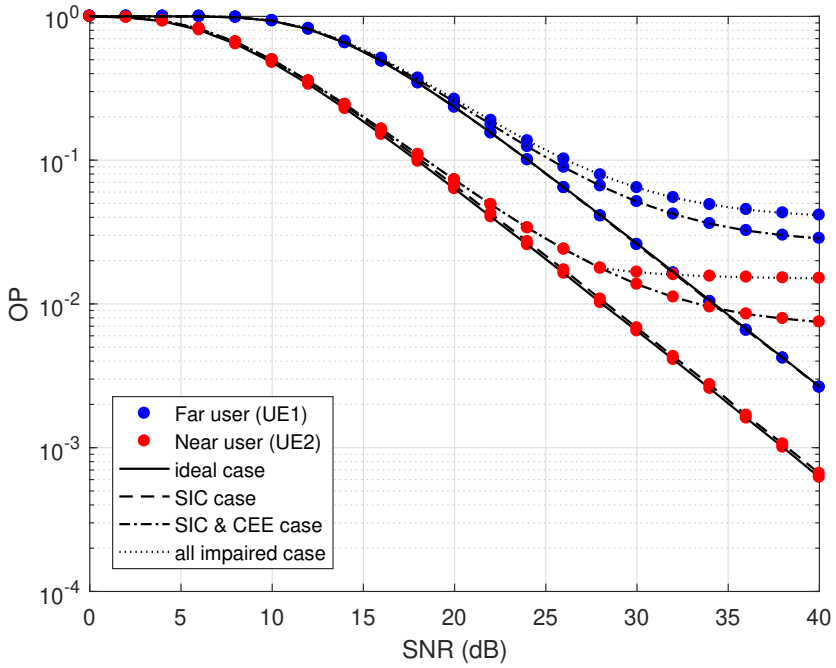

Figure 2.7: The OP of the downlink NOMA System in the presence of various impairments under imperfect SIC.

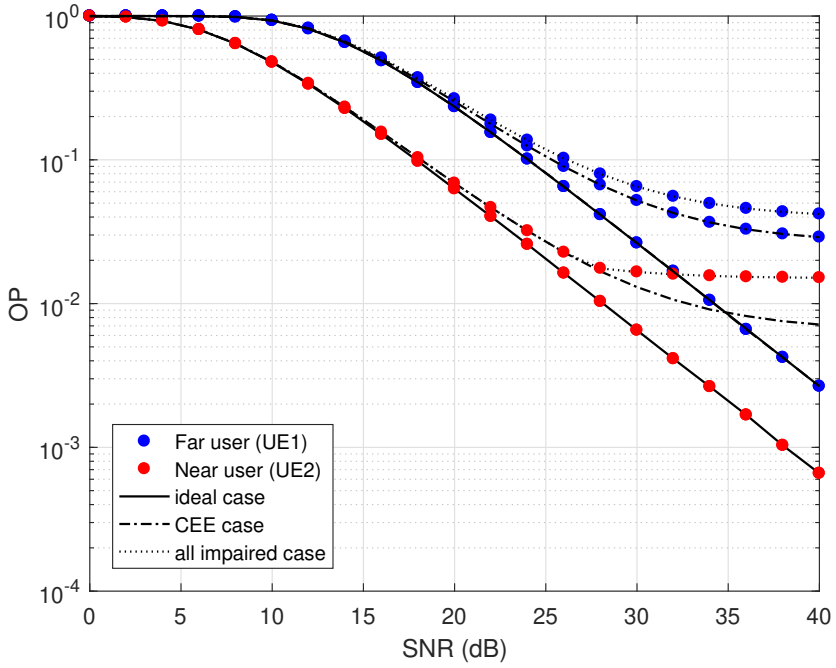

Figure 2.8: The OP of the downlink NOMA system in the presence of various impairments under perfect SIC.

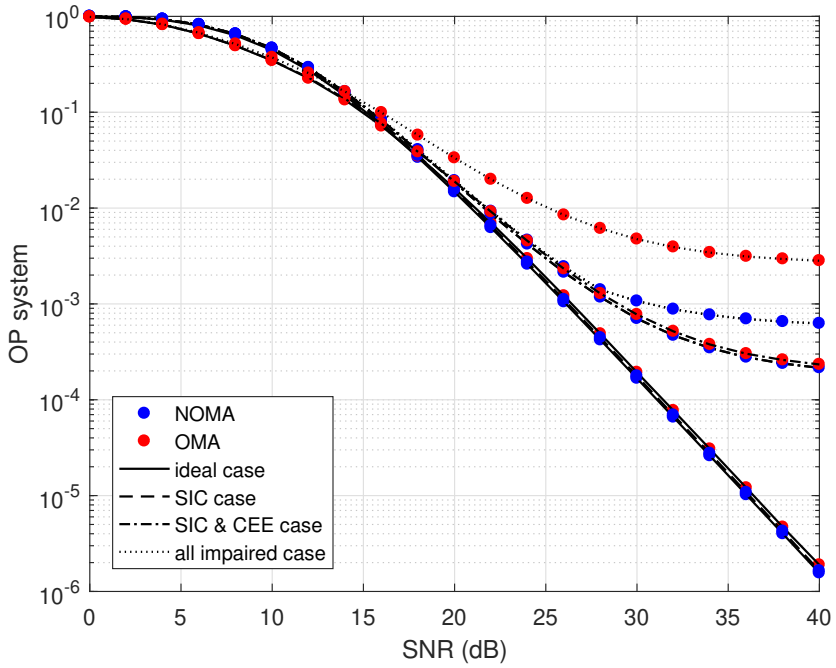

Figure 2.9: Comparison between OP system of NOMA and OMA systems in the presence of various impairments under imperfect SIC.

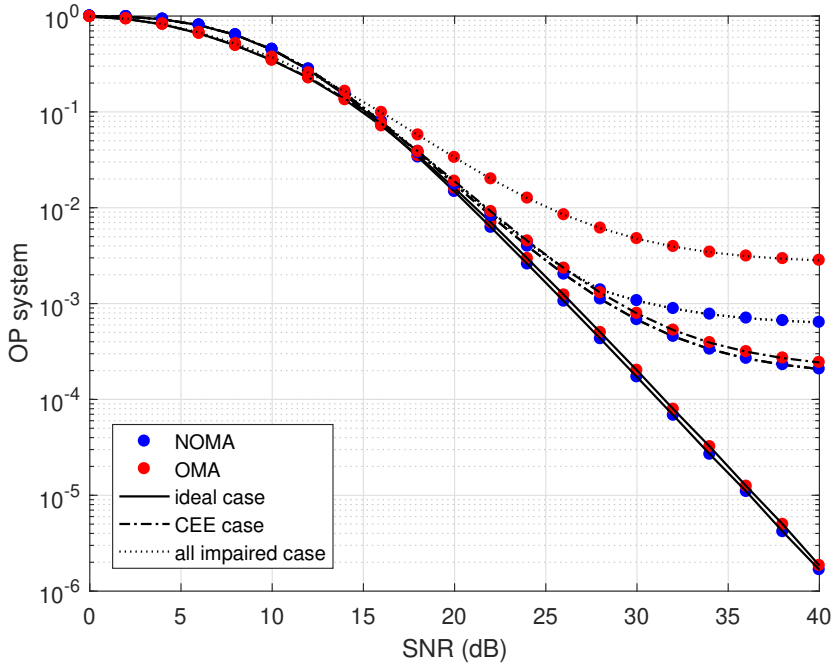

Figure 2.10: Comparison between OP system of NOMA and OMA systems in the presence of various impairments under perfect SIC.

These scenarios include $\xi = 0.01$, $\sigma_\kappa^2 = 0.001$, and $f_d\tau = 0.02$. As observed in the two figures, UE_2 outperforms UE_1 under perfect and imperfect SIC. Additionally, the statement suggests that CEE and feedback delay have a negative impact on the performance of the system. Simply put any errors in channel estimation or delays in providing feedback can greatly impair the overall performance of the system. These problems could potentially lead to an outage.

The comparison with OMA in terms of outage probability (OP) is depicted in Figure 1.9 and Figure 1.10. The key finding is that NOMA outperforms OMA in terms of Outage Probability. In other words, NOMA has a lower probability of experiencing communication outages or failures compared to OMA. What's noteworthy is that this superiority of NOMA is consistent regardless of the presence of impairments. So, even when there are challenges or issues, NOMA still performs better in terms of maintaining reliable connections with lower outage probabilities compared to OMA.

In addition to the previous discussions on EC and OP, we also need to consider the BER of the near and far users, as depicted in Figure 2.11 under the same impairments. It's evident that the average BER of UE_2 is superior to that of UE_1. However, with the introduction of CEE, this performance degrades.

This degradation persists with the application of feedback delay, eventually causing UE_2's performance to become inferior to UE_1. This phenomenon is primarily attributed to the impact of CEE and feedback delay impairments on the SIC process employed by UE_2. However, in the comparison between NOMA and OMA regarding BER as illustrated in Figure 2.12, NOMA is found to be inferior to OMA. This is because OMA is conceptually simpler, and the complexity of the SIC process employed by NOMA contributes to this difference.

Figure 2.13 offers valuable insights into the influence of CEE on the EC, OP and BER at both high and low SNRs. The findings unequivocally reveal that as the imperfection in CSI increases, there is a notable decline in EC performance in both ideal and impaired cases. Additionally, OP approaches an outage state for both users. These findings reaffirm the significant influence of CEE on the overall performance of the NOMA system.

Figure 2.14 illustrates the EC, OP and BER performance of the NOMA system in different SNRs, it highlights a crucial finding that suggests that as feedback delay increases, the system's performance, in terms of EC, OP and BER, deteriorates. In other words, longer feedback delays have a detrimental effect on the performance of the NOMA system.

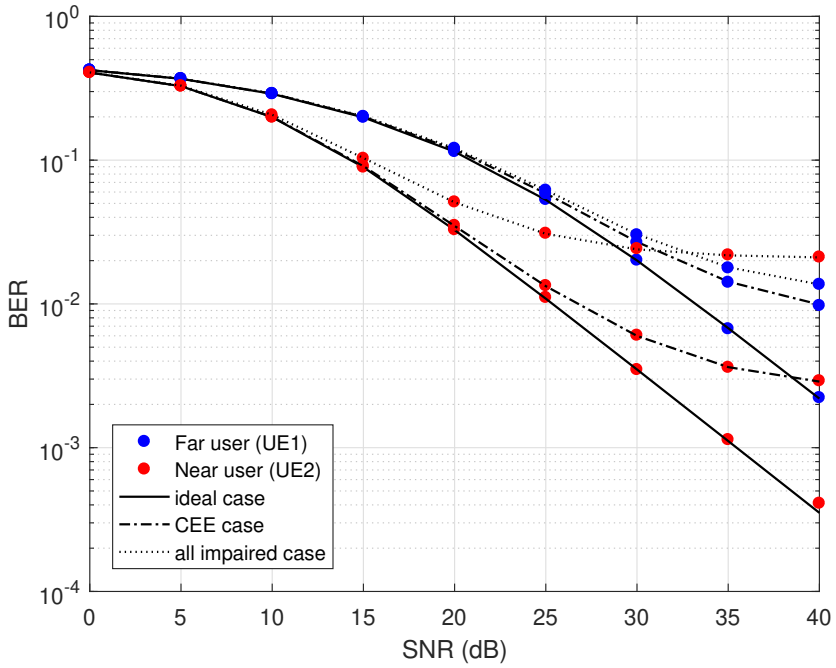

Figure 2.11: The BER of the downlink NOMA System in the presence of various impairments.

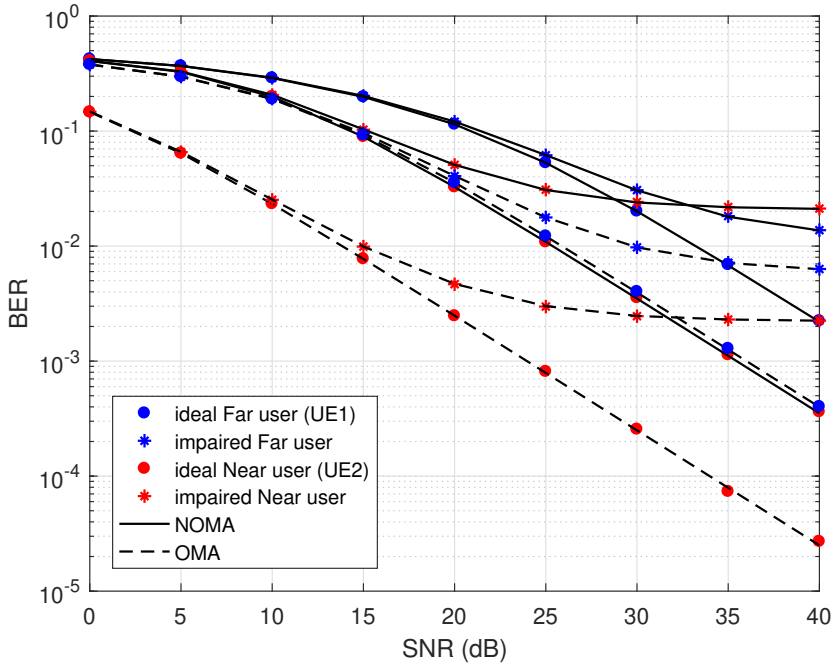

Figure 2.12: Comparison between BER of NOMA and OMA systems in the presence and absence of various impairments.

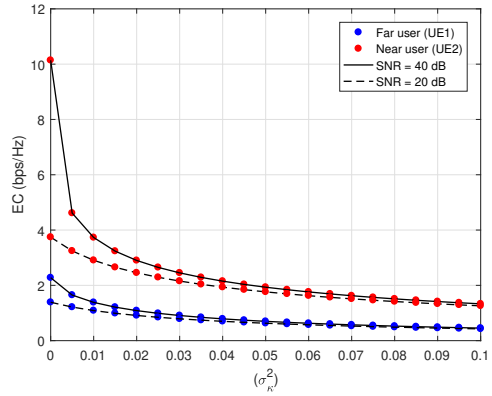

(a) Ideal case

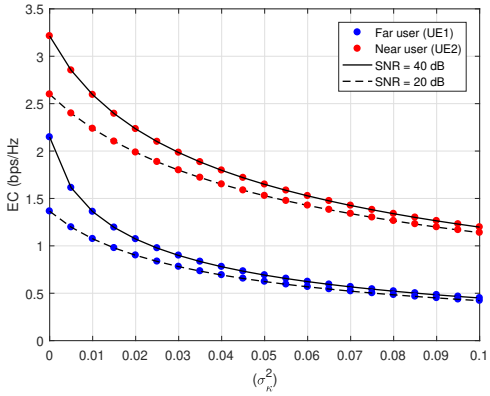

(b) Impaired case

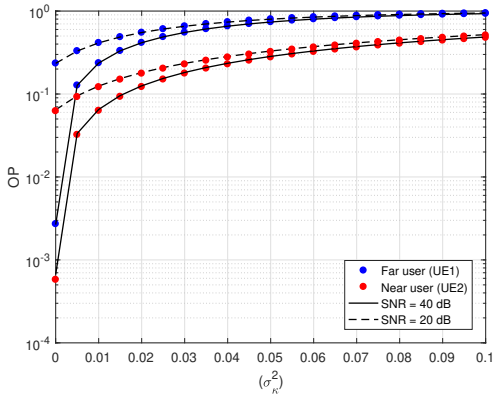

(c) Ideal case

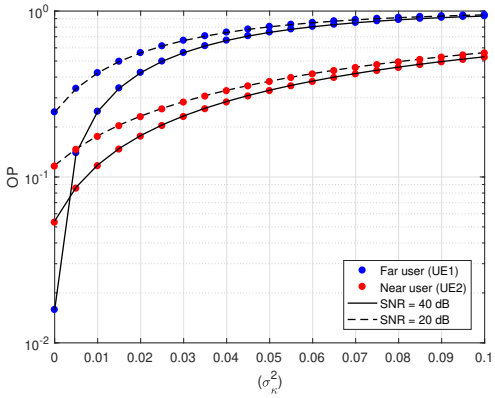

(d) Impaired case

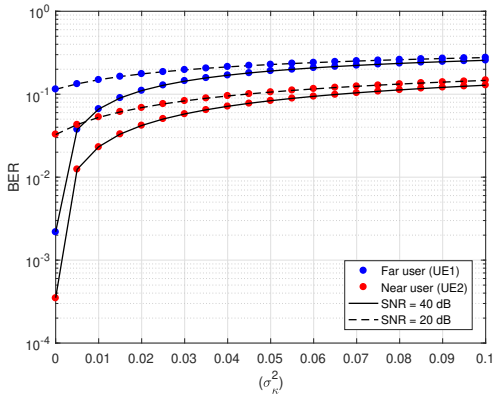

(e) Ideal case

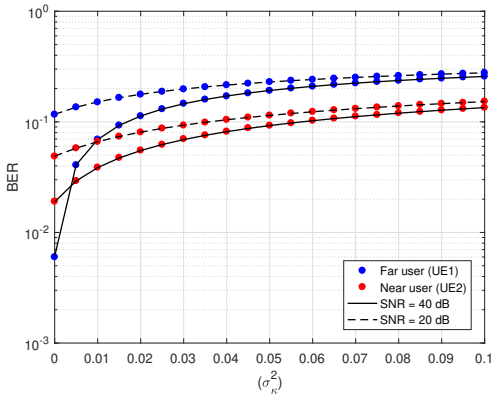

(f) Impaired case

Figure 2.13: The impact of CEE on the EC, OP & BER of the downlink NOMA system.

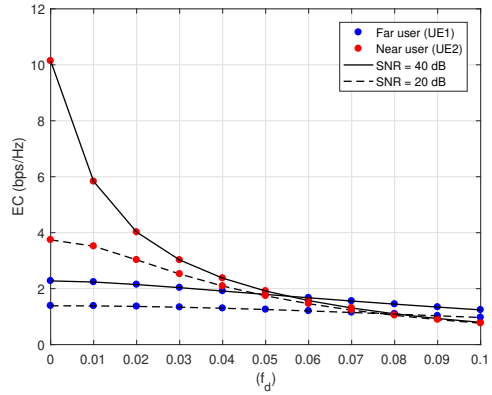

(a) Ideal case

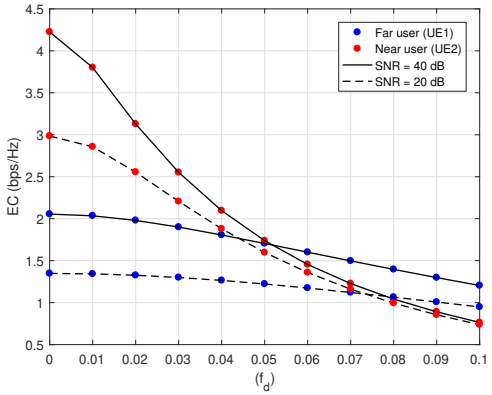

(b) Impaired case

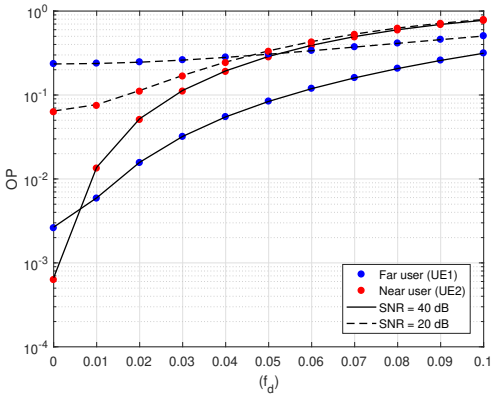

(c) Ideal case

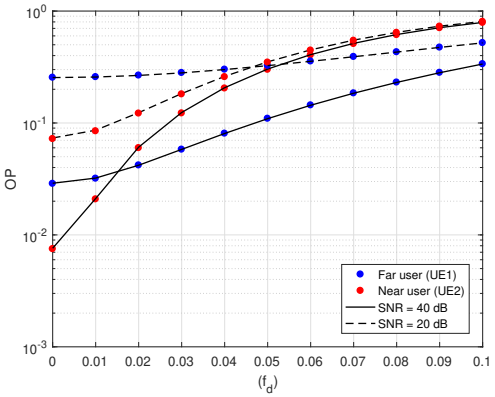

(d) Impaired case

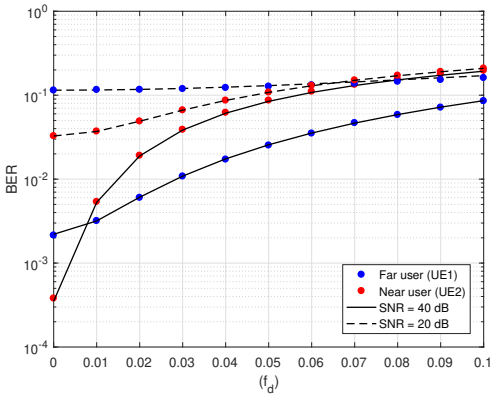

(e) Ideal case

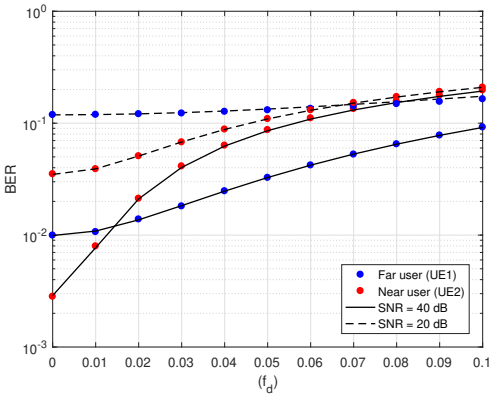

(f) Impaired case

Figure 2.14: The impact of f_d error on the EC, OP & BER of the downlink NOMA system.

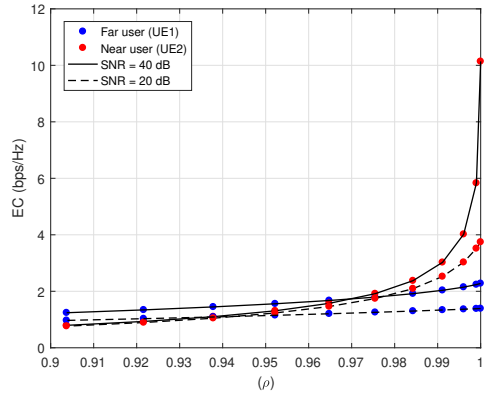

(a) Ideal case

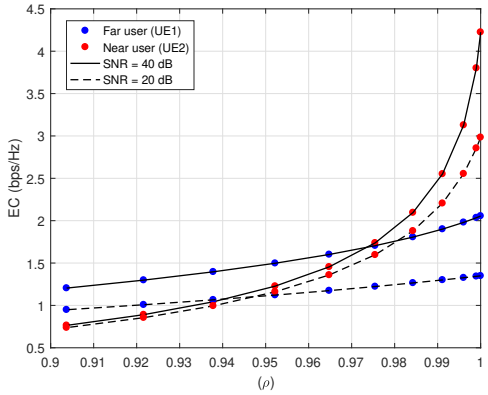

(b) Impaired case

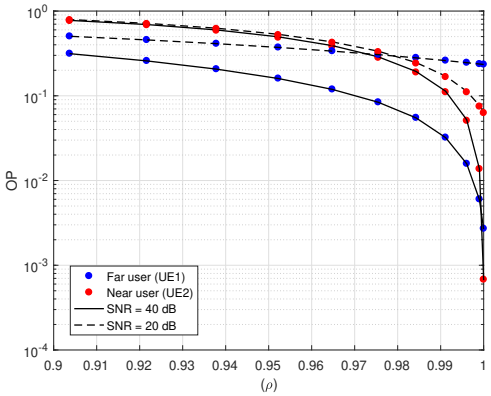

(c) Ideal case

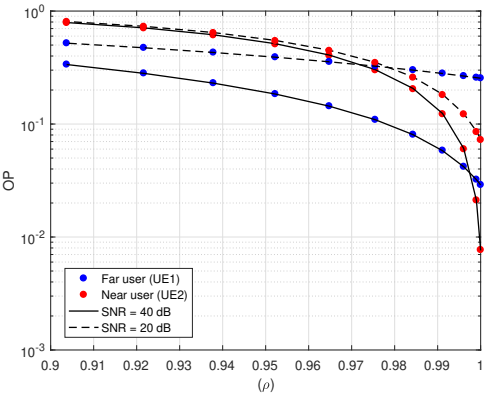

(d) Impaired case

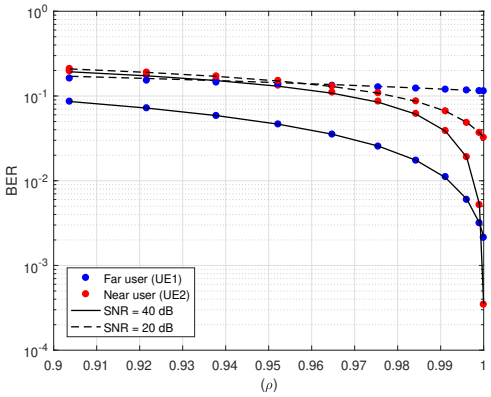

(e) Ideal case

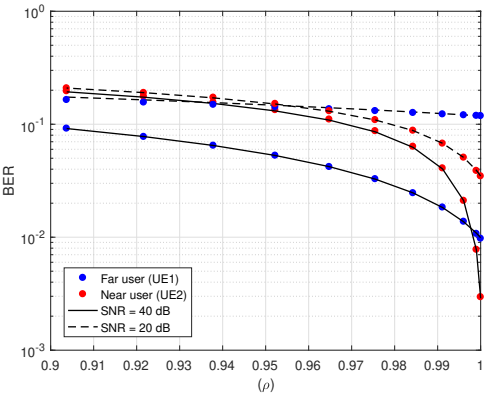

(f) Impaired case

Figure 2.15: The impact of ρ error on the EC, OP & BER of the downlink NOMA system.

Figure 2.13 compared to Figure 2.14 highlights an interesting observation about the system's performance sensitivity. It is evident that the system is more sensitive to CEE than to feedback delay.

The impact of the time correlation coefficient ρ, as depicted in Figure 2.15, clearly illustrates that higher values of ρ lead to enhanced EC, OP and BER performance. This holds for both ideal and impaired scenarios, providing a stronger guarantee of performance in the ideal case.

In the uplink NOMA system, similar to the downlink scenario, the near user exhibits better performance compared to the far user, as evidenced by the PA favoring the near user.

In Figure 2.16, we can see the comparison between simulation results and analytical evidence for the EC of UE_1 and UE_2 in the uplink NOMA system under various impairment conditions. These conditions encompass $\xi = 0.01$ and $\sigma_\kappa^2 = 0.01$. The EC for UE_1 shows a tendency to rise linearly with SNR. This occurs due to the effective interference cancellation facilitated by perfect SIC, resulting in a substantial EC increase as SNR increases. Interestingly, the EC of UE_2 displays rapid growth with SNR and reaches saturation at a substantial level, due to receiving a higher power allocation amount ($\alpha_2 = 0.8$). Moreover, when imperfect SIC is present, the EC for UE_1 decreases and quickly reaches a saturation point because of the imperfections in SIC and the reduced power allocation to UE_1 ($\alpha_1 = 0.2$).

In addition, the CEE has also a negative impact on the performance of the two users. The outage probability of users for the uplink SISO-NOMA system is presented in Figure 2.17 under $\xi = 0.01$ and $\sigma_\kappa^2 = 0.01$. As observed in the figure, UE_2 outperforms UE_1 under perfect and imperfect SIC, this is due to the amount of PA for each user. Additionally, The statement suggests that CEE has a negative impact on the performance of the system.

Figures 2.18 and 2.19 depict the impact of CEE on the Uplink NOMA system at high and low SNRs. The outcomes show a reduction in both the OP and EC performance for both users as the CEE rises. This finding emphasizes the importance of precise channel estimation for the NOMA system. Nevertheless, it's important to note that the system's performance can still be enhanced at higher SNR levels, despite the presence of imperfections.

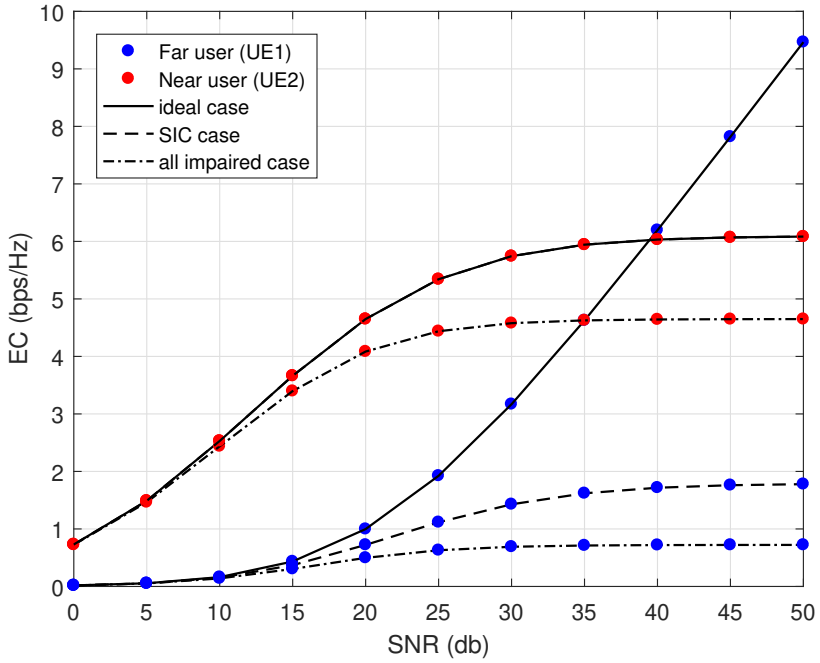

Figure 2.16: EC of the uplink NOMA system in the presence and absence of SIC and CEE imperfections.

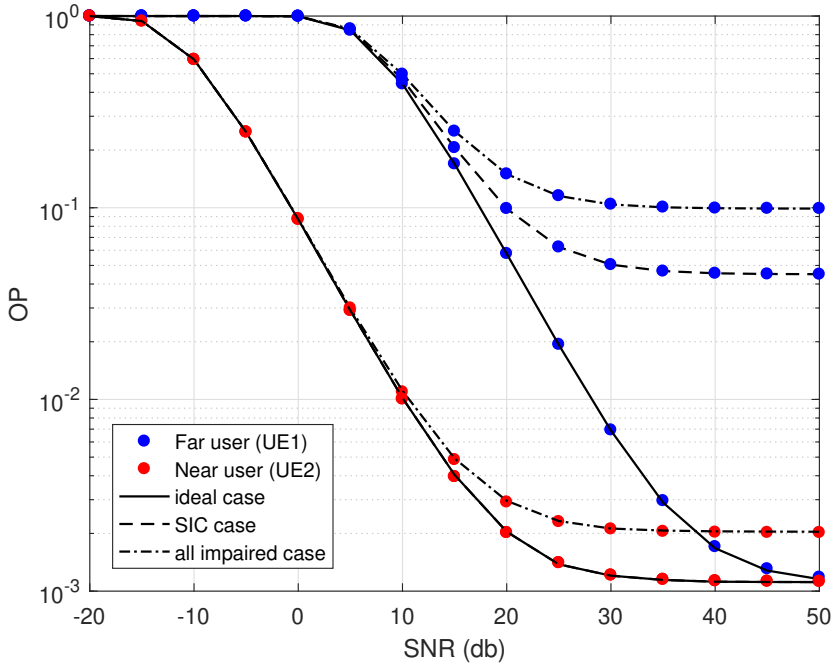

Figure 2.17: OP of the uplink NOMA system in the presence and absence of SIC and CEE imperfections.

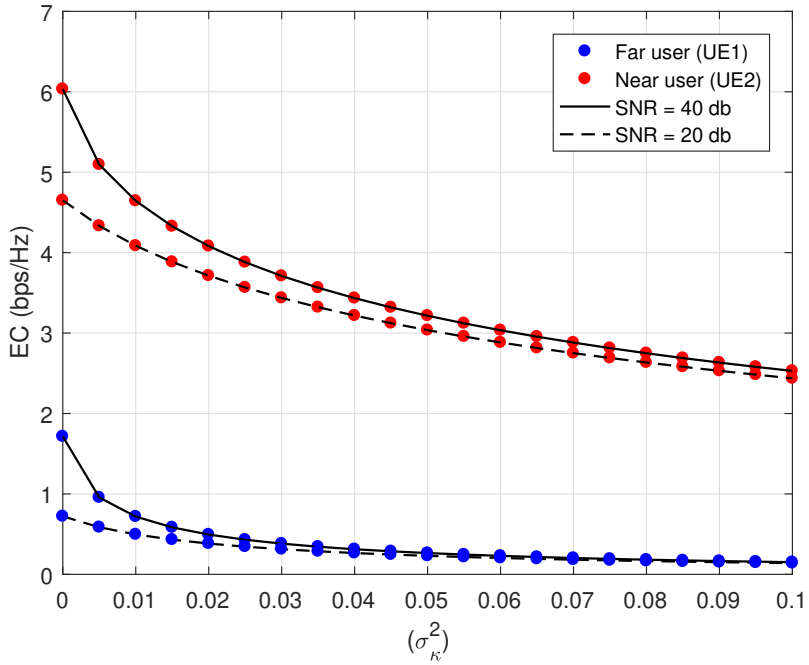

Figure 2.18: Impact of CEE error on the EC of the Uplink NOMA system.

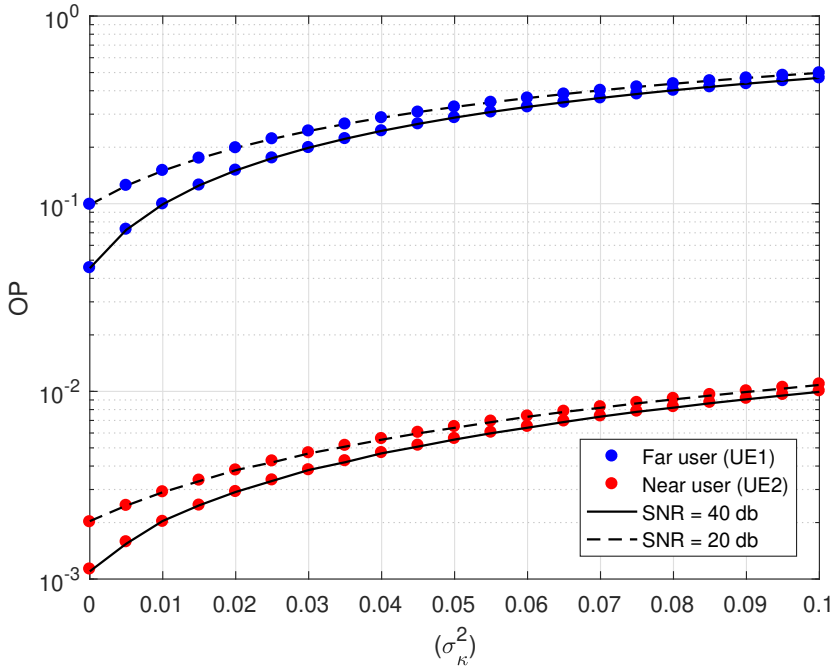

Figure 2.19: Impact of CEE error on the OP of the Uplink NOMA system.

2.7 Conclusion

This chapter has delved into an in-depth exploration of the SISO-NOMA system's performance, with a specific focus on a thorough analysis considering practical impairments. These impairments, including imperfect SIC, CEE, and feedback delay (f_d), significantly impact the system's performance over a Rayleigh fading channel.

Through our investigation, we have successfully derived closed-form expressions for key performance metrics, including EC, OP, and BER in the downlink scheme, as well as EC and OP in the uplink scheme. Our comprehensive findings highlighted the adverse effects of impairments such as SIC errors and CEE, with these effects being particularly pronounced in the near user due to the complexities of the SIC process.

Additionally, our study unveiled nuanced insights, demonstrating NOMA's superior performance in terms of EC and OP across various scenarios. However, a notable trade-off emerged: while NOMA generally excels in efficiency and capacity, OMA occasionally outperforms NOMA by achieving a lower BER in specific situations. This trade-off underscores the importance of context-specific analysis when choosing the appropriate multiple access technique for a given application.

Chapter 3

Ergodic Capacity Evaluation of MIMO-NOMA System with JTRAS Protocol

3.1 Introduction

Incorporating NOMA into long-term evolution (LTE) has provided several benefits for uplink and downlink performance. In particular, 3rd generation partnership project (3GPP) Release 13 focused on using multi-user superimposed transmission (MUST) as a standard mechanism for downlink scenarios. Subsequently, Release 14 included a work item to define the required mechanisms for LTE to support downlink MUST for data channels. Furthermore, Release 15 includes the incorporation of NOMA for use in fifth-generation new radio (5G NR). NOMA still to be a promising approach for the future beyond fifth-generation (B5G) and sixth-generation (6G) networks providing enhanced quality of service (QoS), significantly improved data rates, greater user fairness, increased connectivity, and ultra-high reliability [96, 97]. More specifically, authors [98, 99] provided some basics of NOMA systems where the NOMA technique can support multiple users within a single resource block (RB). In the power domain, NOMA employs superposition coding (SC) for multiple access techniques at the transmitters and uses successive interference cancellation (SIC) at the receivers to detect the required signals.

3.1.1 Related works

Many recent studies have highlighted the advantages of NOMA over conventional orthogonal multiple access (OMA) in terms of sum rate and ergodic capacity (EC) [100, 101, 102, 103, 104]. Authors [100] proposed NOMA for cooperative relaying power line communication systems with decode-and-forward (DF) to increase throughput and enhance user fairness. Authors [101] proposed a

fair-NOMA method, which can achieve capacity that is greater than or equal to the capacity of OMA in a single-input single-output (SISO) network. Authors [102, 103] investigated the EC performance of a cognitive radio NOMA (CR-NOMA) network under Rayleigh fading and with two imperfections SIC and channel estimation error (CEE). The proposed CR-NOMA system was found to improve the EC at high transmit signal-to-noise ratio (SNR) regions at the secondary source. Authors [104] investigated the ergodic sum capacity (ESC) analysis of simultaneous wireless information and power transfer (SWIPT) based NOMA, to get insight into the impact of the ESC on system performance. The authors concluded that power splitting (PS) relaying with NOMA is more energy efficient than time switching (TS) relaying. Authors [105] examined the EC of a full duplex NOMA (FD-NOMA) system with energy harvesting (EH) relays for supporting NOMA users at longer distances. Authors [106] discussed a NOMA scenario that supports multiple pairs of users, where a set of users can communicate with other users to achieve acceptable throughput in one of two modes, namely delay-limited mode or delay-tolerant mode. Authors [107, 108] proposed a cooperative relaying system (CRS) using NOMA to improve spectral efficiency and examined the performance of the achievable rate and outage probability (OP) in comparison to traditional CRS. Also, The exact and asymptotic capacity performance investigated for NOMA-based cooperative relaying over Fisher-Snedecor F composite fading [109]. The authors [110] investigated the effect of hardware impairments (HWI) on the bit error rate (BER) and OP performance using the cooperative-NOMA (CNOMA).

Previous studies have mostly focused on single antenna nodes. Besides that, other researchers have explored the potential of multi-antenna technology to improve the EC performance of NOMA systems. Authors of [111, 112] demonstrated that the interaction between NOMA and multi-input multi-output (MIMO) could achieve a higher ESC than OMA. Furthermore, authors of [113, 114] investigated the EC maximization problem for MIMO-NOMA systems with a total transmit power constraint and a weak user's minimum rate constraint. A downlink multiuser MIMO-NOMA relay system [115] proposed in which all users are divided into several clusters, the authors studied the EC in the presence of imperfect channel state information (CSI) over Nakagami-m fading channels, and also, imperfect SIC and CSI in [116].

3.1.2 Motivation and contribution

The use of multiple antennas can lead to heightened power consumption, complexity and hardware costs. To counter this, transmit antenna selection (TAS), receive antenna selection (RAS), and joint transmit and receive antenna selection (JTRAS) protocols have been implemented as viable solutions that reduce these costs while still capitalizing on the throughput advantages of multiple antennas. The interaction between MIMO with TAS protocol and NOMA has been introduced in [117]. In addition, the authors of [118] proposed an EH-based relay to develop a closed-form

expression of the OP for the TAS protocol that accounts for the impact of imperfect SIC and CSI. Authors of [119] proposed two modes for the selected antenna at the base station (BS) and demonstrated that increasing the number of transmit antennas improves EC. Also, authors of [120] investigated the EC of two robust transmit antenna strategies related to the BS, namely: TAS mode and two BS mode, as a result, the EC in the two BS (TBS) scheme performed better than the TAS scheme. The RAS protocol [76] is used to assess the performance of the OP in the downlink NOMA with amplify-and-forward (AF) relay over Nakagami-m fading channels. Besides that, the JTRAS protocol has been also added to the MIMO-NOMA network over Rayleigh [121] and Nakagami-m fading channels [122], where the authors examined the OP performance by using AF EH relaying. Also, the authors [123] proposed a hybrid antenna selection method involving MIMO-NOMA with TAS and maximal ratio combining (MRC), as well as MIMO-NOMA-based JTRAS, to analyze the OP. Additionally, the authors of [124] investigated the behavior of the BER for NOMA systems with a single antenna and attempted to improve it by utilizing multiple antennas, the impact of the practical impairments SIC, CSI and feedback delay on the BER also investigated [125].

Even though much has been said about the interaction between NOMA and MIMO under the JTRAS protocol, there is still more to explore. To our knowledge, the EC of a MIMO-NOMA system with JTRAS protocol, considering imperfect SIC and CEE over the Rayleigh fading channel, is still an open issue to study. With this in mind, our work presented the following contributions:

- We derive a novel closed-form expression of the EC for the MIMO-NOMA systems with JTRAS protocol in the presence of both imperfect SIC and CEE for the two-user scenario as well as for multi-user case.
- The asymptotic behavior of the EC at a high SNR regime for the suggested study scenarios is derived.
- We investigate and confirm that MIMO-NOMA with JTRAS outperforms traditional MIMO-OMA with JTRAS in terms of the sum EC.
- We compare the system under investigation to the MIMO-NOMA system with JTRAS protocol with perfect SIC and CEE.
- Additionally, we investigate the effect of CEE errors on EC to analyze the performance of users in high and low SNR regions.
- Finally, the effect of increasing the number of users and antennas on the EC is also considered.

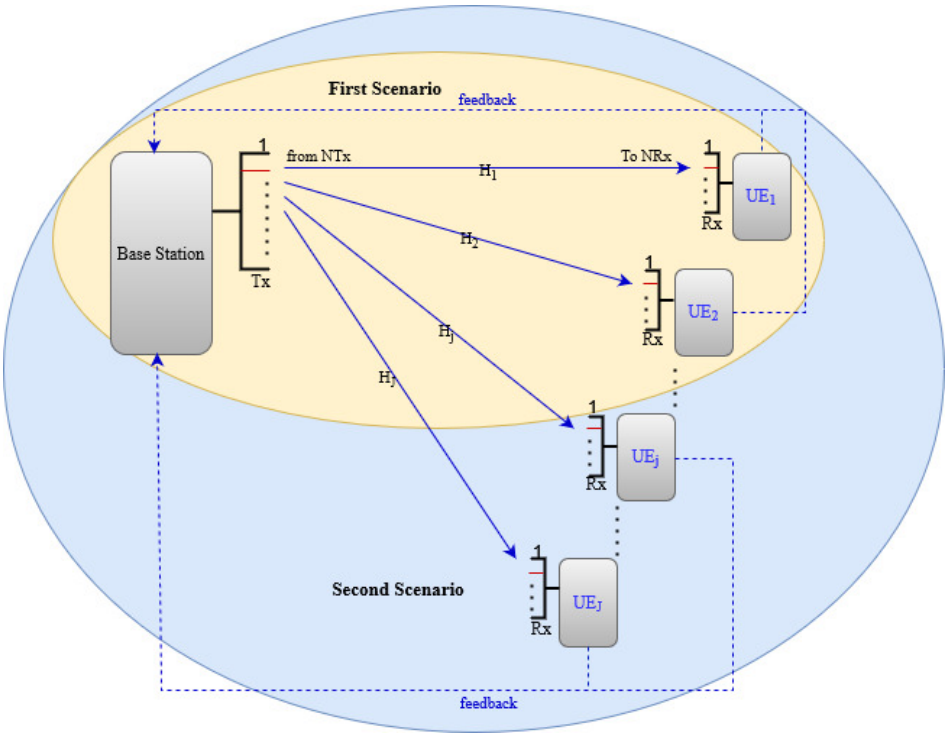

Figure 3.1: System model for MIMO-NOMA with JTRAS protocol.

3.2 System model

Our MIMO-NOMA downlink network has one base station and UE_J users, each with multiple antennas as shown in Figure 3.1.

The number of antennas on BS and UE_J is denoted respectively by $N_t > 1$ and $N_r > 1$. The NOMA network includes $N_t \times N_r$ channels from the N_t antennas at the BS to the N_r antennas at user UE_J is denoted by $H_j = \begin{bmatrix} {h_j}^{(1,1)} & \dots & {h_j}^{(1,N_r)} \\ \vdots & \ddots & \vdots \\ {h_j}^{(N_t,1)} & \dots & {h_j}^{(N_t,N_r)} \end{bmatrix}$, where $j = [1...J]$. The fading channel coefficients between the t^{th} transmit antenna $t = [1...N_t]$ and the r^{th} receive antenna $r = [1...N_r]$ of the user UE_j are denoted by ${h_j}^{(t.r)} \in H_j$, where ${h_j}^{(t.r)} \sim CN\left(0, \sigma_j^2\right)$ assumed as a complex Gaussian random variable with zero mean and variance $\sigma_j^2 = d_j^{-\mu}$, μ and d_j are the path loss exponent factor and the distance between the BS and UE_j, respectively. We assume that the CSI between the BS and UE_j is imperfect; thus, the estimated channel coefficients of ${h_j}^{(t.r)}$ given by $\hat{h}_j^{(t,r)} = h_j^{(t,r)} - \kappa_j^{(t,r)}$ modelled as a complex Gaussian random variable $\widehat{h}_j^{(t,r)} \sim CN\left(0, \widehat{\sigma}_j^2 = \sigma_j^2 - \sigma_\kappa^2\right)$. The CEE factor κ is assumed to be the same for all antennas at the transmitter and receiver and is assumed to have a complex Gaussian random variable $\kappa \sim CN\left(0, \sigma_\kappa^2\right)$, which we assume to be the same for all antennas at the transmitter and receiver, to simplify the calculation [89].

The JTRAS protocol is applied to find the most suitable pairing of antennas (one at the BS and the other at UE_j) for transmission and receiving. During the training phase, the BS obtains knowledge about the necessary CSI by sending pilot symbols from all users to the BS. Next, the channel coefficients are estimated in the BS, the best links between transmit antennas and user-receive antennas are identified, and the transmit antenna is chosen. Subsequently, the BS sends the selected receive antenna indices back to the users via a feedback channel. So, the selected transmit-receive antenna pair defined through
$\left(\widetilde{t},\widetilde{r}\right) = \underset{1\leq t\leq N_t, 1\leq r\leq N_r}{\arg\max} \left|\hat{h}_j^{(t,r)}\right|^2$.

In the power domain, according to the NOMA principle, the BS broadcasts a superimposed signal to each user simultaneously as follows:

$$x = \sum_{j=1}^{J} \sqrt{P_t \alpha_j} x_j, \tag{3.1}$$

where x_j are the messages of UE_j, P_t denotes the total transmit power and the power allocation coefficients α_j satisfy the condition $\sum\limits_{j=1}^{J} \alpha_j = 1$. Also NOMA implies that the power coefficients of the different users must be ordered in such a way that consider the order statistics among the selected channels $\left|\widetilde{h}_1\right|^2 < \left|\widetilde{h}_2\right|^2 < \left|\widetilde{h}_3\right|^2 < ... < \left|\widetilde{h}_J\right|^2$, where $\widetilde{h}_j$ satisfies $\widetilde{h}_j = \max(H_j)$ leading to $\alpha_1 > \alpha_2 > \alpha_3 > \ldots > \alpha_J$. And while, performing this power allocation for j^{th} user, we also should ensure that $\alpha_j > \alpha_{j+1} + \alpha_{j+2} + \ldots + \alpha_J$.

On the other hand, NOMA performs SIC at the UE_j receivers to decode the received signal defined as:

$$y_j = \left(\widehat{\widetilde{h}}_j^{(t.r)} + \kappa\right) \sum_{j=1}^{J} \sqrt{P_t \alpha_j} x_j + n_j, \tag{3.2}$$

where $\widehat{\widetilde{h}}_j^{(t.r)}$ is the estimated fading channel coefficient between the selected antenna of the BS and UE_j and n_j is the additive white Gaussian noise (AWGN) with zero mean and N_0 variance.
By substituting (3.1) into (3.2), and after some algebra simplification, the received signals for each user can be written as follows:

$$y_j = \left(\widehat{\widetilde{h}}_j^{(t.r)} + \kappa\right) \left(\sqrt{P_t \alpha_j} x_j + \sum_{u=j+1}^{J} \sqrt{P_t \alpha_u} x_u + \xi \sum_{s=1}^{j-1} \sqrt{P_t \alpha_s} x_s\right) + n_j, \tag{3.3}$$

where the desired signal of j user denoted by the term $\left(\widehat{\widetilde{h}}_j^{(t.r)} + \kappa\right) \sqrt{P_t \alpha_j} x_j$, the term $\left(\widehat{\widetilde{h}}_j^{(t.r)} + \kappa\right) \sum\limits_{u=j+1}^{J} \sqrt{P_t \alpha_u} x_u$ denotes the interference from the other users and the term

$\left(\widehat{\widetilde{h}}_j^{(t.r)} + \kappa\right) \xi \sum_{s=1}^{j-1} \sqrt{P_t \alpha_s} x_s$ due to the imperfect SIC is equal zero in the case of perfect SIC.

- In the first scenario, the system model includes a BS as a transmitter and two receivers, denoted by UE_1 and UE_2. Taking into account the power allocation conditions mentioned above and since α_1 is greater than α_2, directly decoding y_1 will result in the recovery of x_1, while treating x_2 as interference. The signal-to-interference-plus-noise ratio (SINR) for the distant user UE_1 can be calculated using equation (3.3).

$$\gamma_1 = \frac{\left|\widehat{\widetilde{h}}_1^{(t.r)}\right|^2 \gamma_0 \alpha_1}{\left|\widehat{\widetilde{h}}_1^{(t.r)}\right|^2 \gamma_0 \alpha_2 + \gamma_0 \sigma_\kappa^2 + 1}. \tag{3.4}$$

  Also, by using SIC to cancel the signal of x_1 from (3.3), the SINR for UE_2 is given as:

$$\gamma_2 = \frac{\left|\widehat{\widetilde{h}}_2^{(t.r)}\right|^2 \gamma_0 \alpha_2}{\left|\widehat{\widetilde{h}}_2^{(t.r)}\right|^2 \xi \gamma_0 \alpha_1 + \gamma_0 \sigma_\kappa^2 + 1}, \tag{3.5}$$

  where $\gamma_0 = \frac{P_t}{N_0}$ is the transmit SNR and ξ defines the imperfect SIC effect coefficient.

- In the second scenario, we expanded the scope of the system model by adding more users. By using (3.3), the SINR for all users γ_j is obtained as:

$$\gamma_j = \frac{\left|\widehat{\widetilde{h}}_j^{(t.r)}\right|^2 \gamma_0 \alpha_j}{\left|\widehat{\widetilde{h}}_j^{(t.r)}\right|^2 \left(\sum_{u=j+1}^{J} \alpha_u + \xi \sum_{s=1}^{j-1} \alpha_s\right) \gamma_0 + \gamma_0 \sigma_\kappa^2 + 1}. \tag{3.6}$$

3.3 Ergodic capacity analysis

In this section, we derive the closed form of exact and asymptotic EC for the MIMO-NOMA system with JTRAS in the presence of imperfect SIC and CEE over the Rayleigh fading channel. The EC of UE_j for $j = [1...J]$ is obtained by averaging the achievable rates over instantaneous channel coefficients.

The achievable rates for the MIMO-NOMA system can be expressed as follows:

$$R_j = \log_2 (1 + \gamma_j). \tag{3.7}$$

3.3.1 Exact ergodic capacity for the first scenario

In this subsection, we first derive the exact closed-form expressions of EC for MIMO-NOMA with JTRAS of UE_1 and UE_2, respectively.

3.3.1.1 Ergodic capacity at far user

The achievable rates of UE_1 is given by substituting (3.4) into (3.7), and with some algebraic simplifications, R_1 can be given as:

$$R_1 = \log_2 \left(\frac{1 + \gamma_0 \sigma_\kappa^2 + \left| \widehat{\widetilde{h}}_1^{(t.r)} \right|^2 \gamma_0}{1 + \gamma_0 \sigma_\kappa^2 + \left| \widehat{\widetilde{h}}_1^{(t.r)} \right|^2 \gamma_0 \alpha_2} \right). \tag{3.8}$$

Then, by using $\log_2 \left(\frac{x}{y} \right) = \log_2 (x) - \log_2 (y)$, (3.8) becames

$$R_1 = \log_2 \left(\beta + \left| \widehat{\widetilde{h}}_1^{(t.r)} \right|^2 \gamma_0 \right) - \log_2 \left(\beta + \left| \widehat{\widetilde{h}}_1^{(t.r)} \right|^2 \gamma_0 \alpha_2 \right), \tag{3.9}$$

where $\beta = 1 + \gamma_0 \sigma_\kappa^2$.
Let us assume $X_1 = \left| \widehat{\widetilde{h}}_1^{(t.r)} \right|^2 \gamma_0$, and $Y_1 = \left| \widehat{\widetilde{h}}_1^{(t.r)} \right|^2 \gamma_0 \alpha_2$, as exponential random variables [120], therefore, the EC of UE_1 is obtained by averaging the achievable rates expressed in (3.8) as:

$$C_1^{erg} = E[R_1] = \int_0^\infty \log_2 (\beta + x) f_{X_1}(x) \, \mathrm{dx} - \int_0^\infty \log_2 (\beta + y) f_{Y_1}(y) \, \mathrm{dy}. \tag{3.10}$$

By using the integration by part [95, eq. (11)], (3.10) can be written in terms of CDF as:

$$C_1^{erg} = \underbrace{\frac{1}{\ln(2)} \int_0^\infty \frac{1 - F_{X_1}(x)}{\beta + x} \mathrm{dx}}_{J_1} - \underbrace{\frac{1}{\ln(2)} \int_0^\infty \frac{1 - F_{Y_1}(y)}{\beta + y} \mathrm{dy}}_{J_2}. \tag{3.11}$$

To complete the analysis, we define also the CDF of the estimated channel power gain of $X_j = \left| \widehat{h}_j \right|^2$ as:

$$F_{X_j}(x) = 1 - \exp \left(-\frac{x}{\hat{\sigma}_j^2} \right), \tag{3.12}$$

where $\hat{\sigma}_j^2 = E\{X_j\}$ is the estimated channel mean power of the Rayleigh fading channel. Using (3.12), [119, eq. (31)] and the binomial theorem [93, eq. (1.111)] to calculate the CDF of each

component of X_1 and Y_1, followed by some mathematical simplification, the CDF of X_1 can be calculated as:

$$F_{X_1}^{jtras}(x) = \left(1 - \exp\left(-\frac{x}{\gamma_0 \widehat{\sigma}_1^2}\right)\right)^I = \sum_{i=0}^{I} \binom{I}{i} (-1)^i \exp\left(-\frac{ix}{\gamma_0 \widehat{\sigma}_1^2}\right)$$
$$= 1 - \sum_{i=1}^{I} (-1)^i \frac{I!}{i!\,(I-i)!} \exp\left(-\frac{ix}{\gamma_0 \widehat{\sigma}_1^2}\right). \tag{3.13}$$

Similarly, the CDF of Y_1 can be expressed as:

$$F_{Y_1}^{jtras}(y) = \left(1 - \exp\left(-\frac{y}{\gamma_0 \alpha_2 \widehat{\sigma}_1^2}\right)\right)^I = \sum_{i=0}^{I} \binom{I}{i} (-1)^i \exp\left(-\frac{ix}{\gamma_0 \alpha_2 \widehat{\sigma}_1^2}\right)$$
$$= 1 - \sum_{i=1}^{I} (-1)^i \frac{I!}{i!\,(I-i)!} \exp\left(-\frac{ix}{\gamma_0 \alpha_2 \widehat{\sigma}_1^2}\right). \tag{3.14}$$

Substituting (3.13) and (3.14) in J_1 and J_2, and then after applying [93, eq. (3.352.4)], we obtain the two components of (3.12) as:

$$J_1 = \frac{1}{\ln(2)} \sum_{i=1}^{I} (-1)^i \frac{I!}{i!\,(I-i)!} \left(\exp\left(\frac{i\beta}{\gamma_0 \hat{\sigma}_1^2}\right) \mathrm{Ei}\left(-\frac{i\beta}{\gamma_0 \hat{\sigma}_1^2}\right)\right), \tag{3.15}$$

and

$$J_2 = \frac{1}{\ln(2)} \sum_{i=1}^{I} (-1)^i \frac{I!}{i!\,(I-i)!} \left(\exp\left(\frac{i\beta}{\gamma_0 \alpha_2 \hat{\sigma}_1^2}\right) \mathrm{Ei}\left(-\frac{i\beta}{\gamma_0 \alpha_2 \hat{\sigma}_1^2}\right)\right). \tag{3.16}$$

Finally, substituting (3.15) and (3.16) into (3.11), we obtain the closed-form expression of EC for UE_1 as:

$$C_{1,erc}^{MIMO-NOMA} = \frac{1}{\ln(2)} \sum_{i=1}^{I} (-1)^i \frac{I!}{i!\,(I-i)!}$$
$$\times \left(\exp\left(\frac{i\beta}{k}\right) \mathrm{Ei}\left(-\frac{i\beta}{k}\right) - \exp\left(\frac{i\beta}{l}\right) \mathrm{Ei}\left(-\frac{i\beta}{l}\right)\right), \tag{3.17}$$

where $I = N_r \times N_t$, $\beta = 1 + \gamma_0 \sigma_\kappa^2$, $k = \gamma_0 \alpha_2 \hat{\sigma}_1^2$, $l = \gamma_0 \hat{\sigma}_1^2$.

3.3.1.2 Ergodic Capacity at near user

Following the same steps and the algebraic equations used previously, it is straightforward to show that the closed-form expression of EC for UE_2 is:

$$C_{2,erc}^{MIMO-NOMA} = \frac{1}{\ln(2)} \sum_{i=1}^{I} (-1)^i \frac{I!}{i!\,(I-i)!} \times \left(\exp\left(\frac{i\beta}{K}\right) \mathrm{Ei}\left(-\frac{i\beta}{K}\right) - \exp\left(\frac{i\beta}{L}\right) \mathrm{Ei}\left(-\frac{i\beta}{L}\right) \right), \quad (3.18)$$

where $I = N_r \times N_t$, $\beta = 1 + \gamma_0 \sigma_\kappa^2$, $K = \xi \gamma_0 \alpha_1 \hat{\sigma}_2^2$, $L = (\alpha_2 + \alpha_1 \xi)\, \gamma_0 \hat{\sigma}_2^2$ and Ei(.) denotes the exponential integral function.

3.3.2 Exact ergodic capacity for the second scenario

The achievable rate for the MIMO-NOMA system with the JTRAS system for multi-user in (3.19) is obtained by substituting the equation (3.6) into (3.7). That is

$$R_j = \log_2 \left(1 + \frac{\left| \widehat{\widetilde{h}}_j^{(t.r)} \right|^2 \gamma_0 \alpha_j}{\left| \widehat{\widetilde{h}}_j^{(t.r)} \right|^2 \left(\sum_{u=j+1}^{J} \alpha_u + \xi \sum_{s=1}^{j-1} \alpha_s \right) \gamma_0 + \gamma_0 \sigma_\kappa^2 + 1} \right). \quad (3.19)$$

To simplify (3.19), let's put $\beta = 1 + \gamma_0 \sigma_\kappa^2$, $\lambda_1 = \alpha_j + \left(\sum_{u=j+1}^{J} \alpha_u + \xi \sum_{s=1}^{j-1} \alpha_s \right)$ and $\lambda_2 = \left(\sum_{u=j+1}^{J} \alpha_u + \xi \sum_{s=1}^{j-1} \alpha_s \right)$.

After some algebraic manipulations, the achievable rate of UE_j for $j = [1...J]$ in (3.19) is rewritten as follows:

$$R_j = \log_2 \left(\frac{\beta + \left| \widehat{\widetilde{h}}_j^{(t.r)} \right|^2 \gamma_0 \lambda_1}{\beta + \left| \widehat{\widetilde{h}}_j^{(t.r)} \right|^2 \gamma_0 \lambda_2} \right). \quad (3.20)$$

Let's assume $Z_1 = \left| \widehat{\widetilde{h}}_j^{(t.r)} \right|^2 \gamma_0 \lambda_1$ and $Z_2 = \left| \widehat{\widetilde{h}}_j^{(t.r)} \right|^2 \gamma_0 \lambda_2$, as exponential random variables, therefore, the EC of UE_j is obtained by averaging the achievable rate expressed in (3.20). Therefore, in terms of CDF, the EC of UE_j can be written as:

$$C^{erg} = \underbrace{\frac{1}{\ln(2)} \int_0^{\infty} \frac{1 - F_{Z_1}(z)}{\beta + z} \mathrm{dx}}_{\Xi_1} - \underbrace{\frac{1}{\ln(2)} \int_0^{\infty} \frac{1 - F_{Z_2}(z)}{\beta + z} \mathrm{dy}}_{\Xi_2}. \tag{3.21}$$

By using (3.12), [119, eq. (31)] and the binomial theorem [93, eq. (1.111)], followed by some mathematical simplification, the CDF of Z_v can be given as:

$$F_{Z_v}^{jtras}(z) = 1 - \sum_{i=1}^{I} (-1)^i \frac{I!}{i!\,(I-i)!} \exp\left(-\frac{iz}{\gamma_0 \hat{\sigma}_j^2}\right), \tag{3.22}$$

where $v = \{1, 2\}$.

Then substituting (3.24) into Ξ_v for $v = \{1, 2\}$, and after applying [93, eq. (3.352.4)], we obtain the two components of (3.23) as follows:

$$\Xi_v = \frac{1}{\ln(2)} \sum_{i=1}^{I} (-1)^i \frac{I!}{i!\,(I-i)!} \left(-\exp\left(\frac{i\beta}{L_v}\right) \mathrm{Ei}\left(-\frac{i\beta}{L_v}\right)\right), \tag{3.23}$$

where $v = \{1, 2\}$, $I = N_r \times N_t$, $\beta = 1 + \gamma_0 \sigma_\kappa^2$, $L_2 = \left(\sum_{u=j+1}^{J} \alpha_u + \xi \sum_{s=1}^{j-1} \alpha_s\right) \gamma_0 \hat{\sigma}_j^2$ and $L_1 = \left(\alpha_j + \left(\sum_{u=j+1}^{J} \alpha_u + \xi \sum_{s=1}^{j-1} \alpha_s\right)\right) \gamma_0 \hat{\sigma}_j^2$.

Finally, we obtain the closed-form expression of EC for the MIMO-NOMA system with JTRAS under both imperfect SIC and CSI for multi-user scenarios, as follows:

$$C_{j,erc}^{MIMO-NOMA} = \frac{1}{\ln(2)} \sum_{i=1}^{I} (-1)^i \frac{I!}{i!\,(I-i)!} \times \left(\exp\left(\frac{i\beta}{L_2}\right) \mathrm{Ei}\left(-\frac{i\beta}{L_2}\right) - \exp\left(\frac{i\beta}{L_1}\right) \mathrm{Ei}\left(-\frac{i\beta}{L_1}\right)\right). \tag{3.24}$$

3.3.3 Exact ergodic capacity of MIMO-OMA

For the sake of comparison, the UE_j users of MIMO-OMA with JTRAS protocol receive equal power allocation coefficients, where $\alpha_1 = \alpha_2 = ... = \alpha_j$. Therefore, by using the same procedures and the same algebraic equations that were previously utilized, it is easy to prove that the closed-form expression of EC for MIMO-OMA with JTRAS protocol can written as follows:

$$C_{j,erc}^{MIMO-OMA} = \frac{1}{J\ln(2)} \sum_{i=1}^{I} (-1)^i \frac{I!}{i!\,(I-i)!} \left(\exp\left(\frac{i\beta}{\gamma_0 \hat{\sigma}_j^2}\right) - \mathrm{Ei}\left(-\frac{i\beta}{\gamma_0 \hat{\sigma}_j^2}\right)\right), \tag{3.25}$$

where $j = [1...J]$ and J denotes the number of users.

The sum EC achieved for MIMO-NOMA and MIMO-OMA systems with JTRAS protocol can be expressed, respectively, as:

$$C_{erc}^{MIMO-NOMA} = \sum_{j=1}^{J} C_{j,erc}^{MIMO-NOMA}, \tag{3.26}$$

and

$$C_{erc}^{MIMO-OMA} = \sum_{j=1}^{J} C_{j,erc}^{MIMO-OMA}. \tag{3.27}$$

3.3.4 Asymptotic ergodic capacity analysis

In this subsection, we derive the asymptotic expressions for EC of the MIMO-NOMA system with JTRAS protocol, to know further about the system performance, the asymptotic analysis is focused on obtaining expressions in higher SNR regimes. Then, through the subsequent corollaries, we study certain asymptotic cases.

Corollary 3.1: In the high-SNR regime, the asymptotic expressions of the closed-form EC expressions are derived as:

- MIMO-NOMA based JTRAS under both perfect SIC and CSI:

$$c_{j,asym}^{MIMO-NOMA} = \log_2 \left(1 + \frac{\alpha_j}{\sum\limits_{u=j+1}^{J} \alpha_u} \right), \tag{3.28}$$

  and

$$C_{J,asym}^{MIMO-NOMA} = \log_2 \left(\alpha_J \gamma_0 \hat{\sigma}_J^2 \right) - \frac{Ec}{\ln(2)} + \sum_{i=1}^{I} (-1)^i \frac{I!}{i!\,(I-i)!} \log_2(i), \tag{3.29}$$

  where $E_c \approx 0.57721$ is the Euler constant, $j = [1...J-1]$, and J is the nearest user.

- MIMO-NOMA based JTRAS under imperfect SIC and perfect CSI:

$$c_{j,asym}^{MIMO-NOMA} = \log_2\left(1 + \frac{\alpha_j}{\sum\limits_{u=j+1}^{J} \alpha_u + \xi \sum\limits_{s=1}^{j-1} \alpha_s}\right). \tag{3.30}$$

- MIMO-OMA based JTRAS under perfect CSI:

$$C_{j,asym}^{MIMO-OMA} = \frac{1}{J}\left(\log_2\left(\gamma_0 \hat{\sigma}_j^2\right) - \frac{Ec}{\ln(2)} + \sum_{i=1}^{I} (-1)^i \frac{I!}{i!\,(I-i)!} \log_2(i)\right). \tag{3.31}$$

Proof: When $\gamma_0 \to \infty$, the following mathematical approximations $\exp(x) \approx 1 + x$ where $x \to 0$ [93, eq. (8.212.1)] and $\mathrm{Ei}(-x) \approx E_c + \ln(x)$ [93, eq. (1.211.1)] can be applied on (3.26), after some mathematical simplifications.

Corollary 3.2: When $\gamma_0 \to \infty$ the asymptotic expression of the closed-form EC for MIMO-NOMA based JTRAS and MIMO-OMA based JTRAS protocol are derived, respectively, as

- MIMO-NOMA based JTRAS under both imperfect SIC and CSI:

$$C_{j,asym}^{MIMO-NOMA} = \frac{1}{\ln(2)} \sum_{i=1}^{I} (-1)^i \frac{I!}{i!\,(I-i)!} \times \left(\exp\left(\frac{i\sigma_\kappa^2}{K_2}\right) \mathrm{Ei}\left(-\frac{i\sigma_\kappa^2}{K_2}\right) - \exp\left(\frac{i\sigma_\kappa^2}{K_1}\right) \mathrm{Ei}\left(-\frac{i\sigma_\kappa^2}{K_1}\right)\right), \tag{3.32}$$

where $j = [1...J]$, $I = N_r \times N_t$, $K_2 = \left(\sum\limits_{u=j+1}^{J} \alpha_u + \xi \sum\limits_{s=1}^{j-1} \alpha_s\right) \hat{\sigma}_j^2$,

and $K_1 = \left(\alpha_j + \left(\sum\limits_{u=j+1}^{J} \alpha_u + \xi \sum\limits_{s=1}^{j-1} \alpha_s\right)\right) \hat{\sigma}_j^2$.

- MIMO-OMA based JTRAS under imperfect CSI:

$$C_{j,asym}^{MIMO-OMA} = \frac{1}{J\ln(2)} \sum_{i=1}^{I} (-1)^i \frac{I!}{i!\,(I-i)!} \left(\exp\left(\frac{i\sigma_\kappa^2}{\hat{\sigma}_j^2}\right) - \mathrm{Ei}\left(-\frac{i\sigma_\kappa^2}{\hat{\sigma}_j^2}\right)\right). \tag{3.33}$$

Proof: In high SNR regime, the asymptotic ergodic capacity obtained via the yielding $1 + \gamma_0\sigma_\kappa^2 \to \gamma_0\sigma_\kappa^2$, after that, substituting it in (3.26) and (3.27).

Table 3.1: Simulation parameters.

Symbols and Description	Values
• path loss exponent μ	4
• imperfect SIC coefficient ξ	0.01
• number of antennas (N_t, N_r)	(2, 2)
• distance between BS and 02 users	$d_1 = 2$ m and $d_2 = 1$ m
• distance between BS and 03 users	$d_1 = 4$ m, $d_2 = 2$ m and $d_1 = 1$ m
• distance between BS and 04 users	$d_1 = 5$ m, $d_2 = 3$ m $d_3 = 2$ m and $d_4 = 1$ m
• power allocation factor for 02 users	$\alpha_1 = 0.8$ and $\alpha_2 = 0.2$
• power allocation factor for 03 users	$\alpha_1 = 0.8$, $\alpha_2 = 0.15$ and $\alpha_3 = 0.05$
• power allocation factor for 02 users	$\alpha_1 = 0.75$, $\alpha_2 = 0.15$, $\alpha_3 = 0.08$ and $\alpha_4 = 0.02$

3.4 Numerical results

In this section, the analytical, asymptotic, and simulation results of EC for MIMO-NOMA systems with JTRAS are presented and discussed along with two constraints: imperfect SIC and CEE. It is clear from all figures that both analytical and simulated results are identical which proves the correctness of the performance analysis. The fact that these results are identical proves the accuracy of the presented performance analysis. In addition, the EC of this system is compared in the presence and absence of imperfect SIC using different parameters as shown in Table 3.1.

Figure 3.2 compares the sum EC performance between the MIMO-NOMA system with JTRAS protocol and the MIMO-OMA system with JTRAS protocol versus transmit SNR, we can observe at high SNR the sum EC performance is better in MIMO-NOMA system with JTRAS protocol than MIMO-OMA system with JTRAS protocol plotted with straight lines.

In contrast, at low SNR, the sum EC of MIMO-OMA-JTRAS performs somewhat better than MIMO-NOMA-JTRAS, and this is due to simultaneous transmission used in NOMA systems. Also, the results shown with dashed lines show a deterioration in the sum EC performance for the MIMO-NOMA system with JTRAS protocol; and this is caused by the influence of the imperfectness of SIC applied to the NOMA system, which has an adverse effect on the sum EC performance whenever its value is increased. For example, when the value of ξ reaches 0.01 this leads to a significant deterioration compared to the MIMO-OMA system with JTRAS protocol. Moreover, the asymptotic curves are in full agreement with the exact results of EC in the high SNR region, confirming the accuracy of the derived asymptotic EC expressions obtained in (3.30) - (3.33) for the system under study.

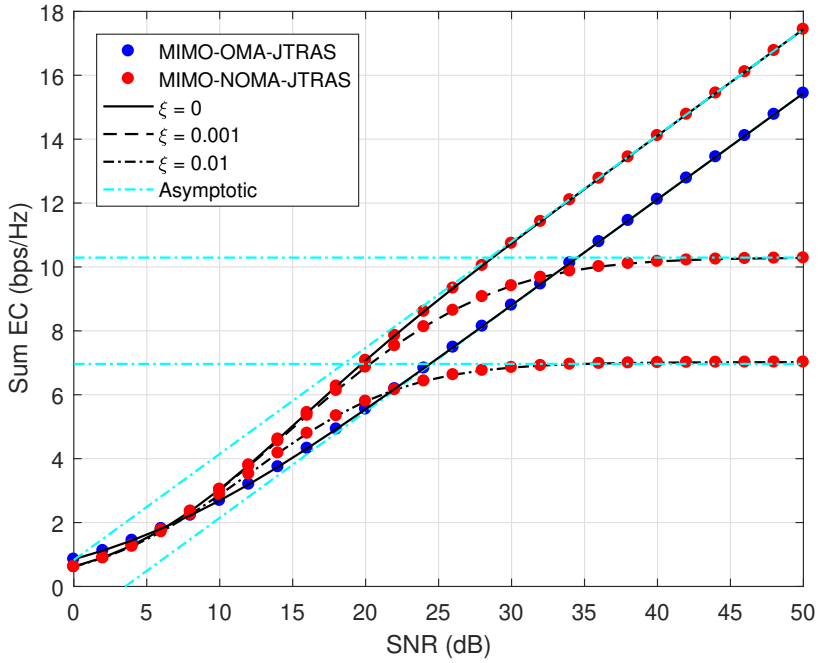

Figure 3.2: Comparison between sum EC of MIMO-NOMA and MIMO-OMA systems with JTRAS protocol.

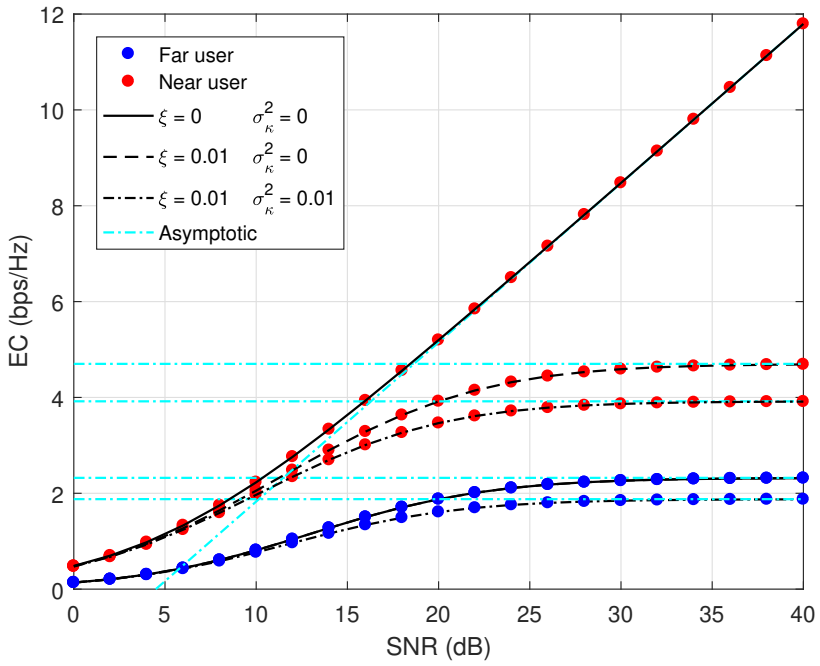

Figure 3.3: Exact and asymptotic EC at UE_1 and UE_2 of MIMO-NOMA system with JTRAS under perfect and imperfect SIC and CSI.

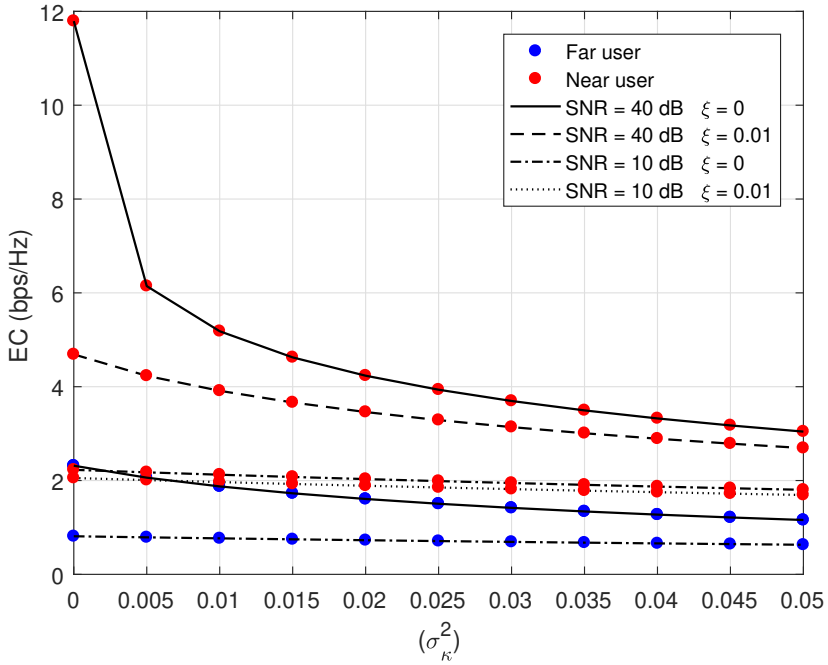

Figure 3.4: The impact of CEE on EC at UE_1 and UE_2 for MIMO-NOMA system with JTRAS protocol.

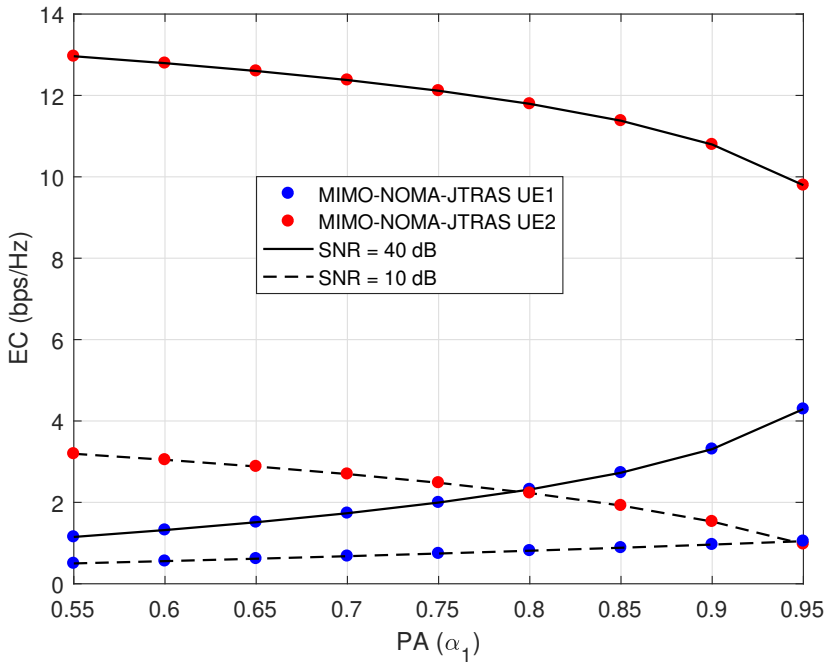

Figure 3.5: The impact of power allocation on EC at UE_1 and UE_2 of MIMO-NOMA system with JTRAS protocol.

Figure 3.3 plots the simulation, asymptotic and exact EC results at UE_1 and UE_2 in the presence and absence of imperfect SIC and CEE. Based on the results, at $\xi = \sigma_\kappa^2 = 0$, we can clearly see that the EC of UE_2 increases while the transmit SNR increases. While, the EC of UE_1 for the NOMA system reaches saturation values faster even though power allocation is higher for UE1, and this is because a power residual still exists as an interference in the denominator of the derivative expression for γ_1 in (3.4).

For $\xi = 0.01$ and $\sigma_\kappa^2 = 0$, we can see that SIC affects performance by decreasing EC of UE_2. In contrast, UE_1 is not affected by imperfections of SIC, because it does not require the SIC algorithm to decode its signal. In addition to the imperfect SIC, the CEE slightly reduces the EC for both users. Due to the combination of these two error factors, the EC of the MIMO-NOMA system under the JTRAS protocol suffers significantly. Also, It should be noted that in the high SNR region, our analytical and simulation results for UE_1 and UE_2 match the asymptotic results, which depend on the ratios $\frac{\alpha_j}{\sum_{u=j+1}^{J} \alpha_u}$ and $\frac{\alpha_j}{\sum_{u=j+1}^{J} \alpha_u + \xi \sum_{s=1}^{j-1} \alpha_s}$ defined in (3.30) and (3.32), respectively.

Figure 3.4 depicts the effect of CEE on the EC at UE_2 and UE_1, through the MIMO-NOMA using JTRAS protocol with $\xi = 0$ and $\xi = 0.01$ at high and low SNR values. And for the sake of clarity at high SNR, when σ_κ^2 varies from 0 to 0.02 the EC of UE_2 rapidly decreases, when σ_κ^2 is increased from 0.02 to 0.05 the EC gradually decreases. But UE_1 known a slight decrease in EC for all σ_κ^2 values. At low SNR, on the contrary, we see a slight degradation of EC for UE_2 and UE_1 at all σ_κ^2 values. This leads us to the fact that the CEE error affects the SIC process to detect the signal.

Figure 3.5, evaluates the impact of the power allocation factor at UE_1 and UE_2 for a MIMO-NOMA system with JTRAS protocol at high and low SNR, and we see that for SNR = 40 dB or 10 dB the EC of UE_2 is higher than UE_1. That is because NOMA depends entirely on power allocation to ensure optimal performance, which leads to the conclusion that to simultaneously retain their capacity, UE_1 needs to be provided with a power substantially higher than UE_2.
In addition to considering two users, we discussed the sum EC of the system under investigation in greater detail, considering the effect of SIC and CSI imperfection by increasing the number of users.

In addition to the aforementioned analyses, Figure 3.6 illustrates the impact of the number of antennas on the EC of the MIMO-NOMA system with the JTRAS protocol. It is evident that increasing the number of antennas using the JTRAS protocol results in a slight improvement in the EC for UE_1 and UE_2.

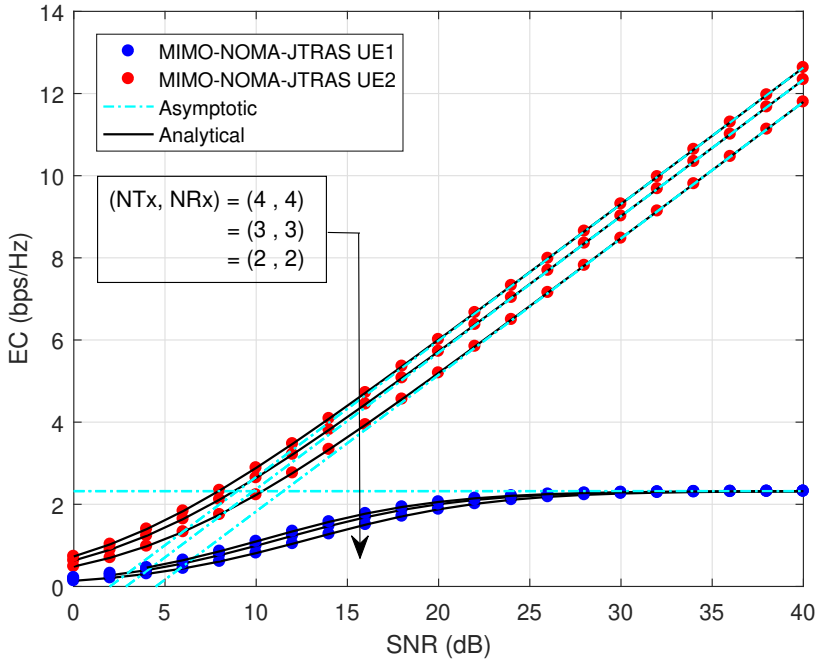

Figure 3.6: The impact of antennas on EC for MIMO-NOMA system with JTRAS protocol.

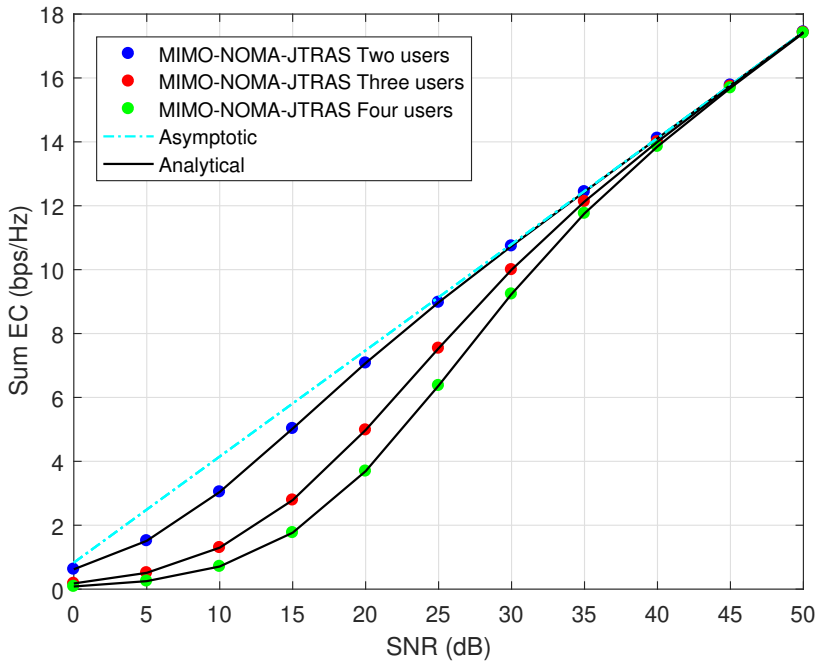

Figure 3.7: The impact of users on EC for MIMO-NOMA system with JTRAS protocol under $\xi = \sigma_{\kappa}^2 = 0$.

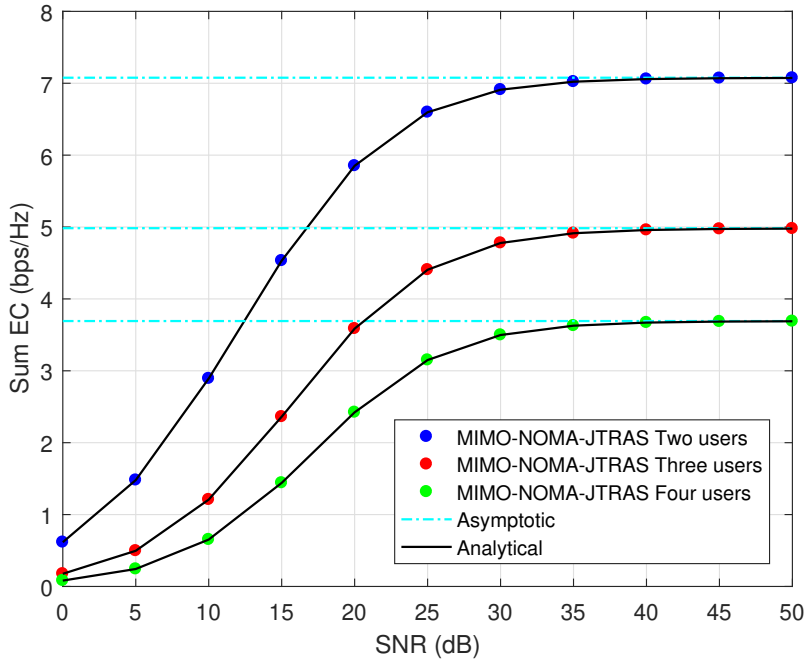

Figure 3.8: The impact of users on EC for MIMO-NOMA system with JTRAS protocol under $\xi = 0$ and $\sigma_\kappa^2 = 0.01$.

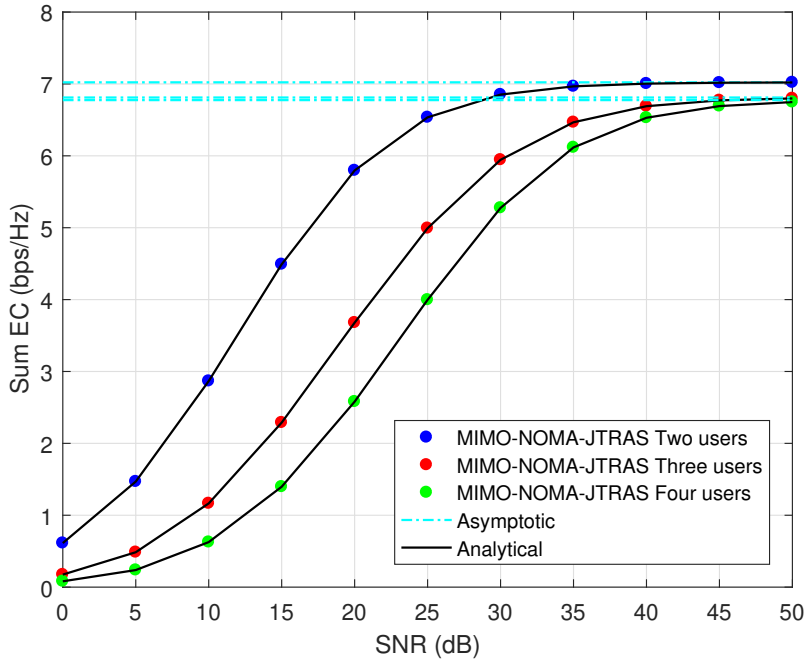

Figure 3.9: The impact of users on EC for MIMO-NOMA system with JTRAS protocol Under $\xi = 0.01$ and $\sigma_\kappa^2 = 0$.

In Figure 3.7, we can easily conclude that increasing the number of users has a negative impact on NOMA systems anyway. However, the three curves converge to the same value, which is supported by the asymptotic EC results. Also, in Figure 3.8, the CSI error greatly affects the sum EC, particularly as the number of users increases to 3 and 4. Similarly, in Figure 3.9, the imperfect SIC significantly affects the sum EC, due to the sequential application of the SIC algorithm to multiple users as the equation demonstrates in (3.32). Also, we can see that the CSI has a more significant impact than SIC and this is because the latter influences the overall NOMA system but the SIC excludes the farthest user.

3.5 Conclusion

This chapter has investigated the performance of the MIMO-NOMA system with JTRAS protocol to develop a closed-form expression for the exact and asymptotic EC for two scenarios: two-user scenario and multi-user scenario. We have considered two imperfections, namely, imperfect SIC and CEE. Moreover, the model under investigation was compared with the conventional MIMO-OMA system with JTRAS in terms of sum EC.

According to the findings, MIMO-NOMA with JTRAS outperforms MIMO-OMA with JTRAS in the scenario of a perfect SIC. However, this performance is negatively impacted by the SIC imperfectness. Also, we have compared the EC of the proposed MIMO-NOMA with JTRAS under imperfect SIC and CEE to MIMO-NOMA with JTRAS under perfect SIC and CEE. The results revealed that the imperfection in both SIC and CEE leads to capacity degradation. In addition, the increase in user numbers has adversely affected the EC.

Finally, the good agreement between the analytical, asymptotic, and simulated results indicates the accuracy of the presented analysis.

Chapter 4

Performnce Analysis of MIMO-CNOMA System with TAS Protocol

4.1 Introduction

The upcoming generations of wireless networks are poised to initiate a transformative revolution in wireless communications. Adhering to stringent requirements is paramount, encompassing exceptionally high data throughput, minimal latency, and the efficient utilization of energy and spectrum resources. This evolution is critical to support the extensive array of connected devices and innovative services emerging from paradigms like the Internet of Things (IoT) [126, 127]. Non-orthogonal multiple access (NOMA) positions itself as a transformative technology with the potential to shape the landscape of B5G and 6G networks due to its capacity to significantly boost network capacity by optimizing the utilization of scarce spectrum resources [128, 129]. In power-domain NOMA, multiple users are served on the same time-frequency resources [130]. For that, downlink information is efficiently broadcasted using superposition coding (SC) at the base station (BS). Subsequently, successive interference cancellation (SIC) is employed at the users to eliminate multiuser interference [131].

4.1.1 Related works

In recent times, there has been a significant uptick in interest regarding the utilization of NOMA in cooperative communication for 5G and Beyond deployment scenarios [132, 133]. This increased attention is driven by the inherent advantages of cooperative relaying strategies, which include expanded coverage, improved reliability, and effective mitigation of challenges arising from multipath propagation [134, 135]. In relay communication, two widely recognized protocols are employed:

the decode-and-forward (DF) protocol, in which the relay decodes and re-encodes the information signal before forwarding, and the amplify-and-forward (AF) protocol, where the relay amplifies the received signal from the source and transmits it directly to the destination [136].

Therefore, to enhance the performance of the NOMA system, some studies have explored the combined utilization of NOMA and cooperative communication. In [137, 138], the authors examined a downlink NOMA system with cooperative full-duplex (FD) relaying, employing the near user as a relay for the far user. They derived closed-form expressions for the OP and ergodic sum rate (ESR), considering both fixed power allocations and optimal power allocations aimed at minimizing the outage probability, as well as the OP performance in a downlink CNOMA with an AF relay [139]. The authors in [140] developed a novel closed-form expression for the bit error rates (BER) of full-duplex cooperative NOMA (FD-CNOMA) systems in the presence of imperfect SIC and residual self-interference (RSI). The authors have investigated a hybrid relaying scheme, that switches between full and half duplex (FD/HD) to improve the performance of the DF CNOMA system for two-user [141], and multi-user [142]. In addition, the investigation in [143], focuses on evaluating the OP and ESR of an FD/HD coordinated direct and DF-based relay scheme in a NOMA system. This analysis specifically considers scenarios with imperfections in CSI and SIC. To enhance the coverage and performance for the far user, a proposed scheme [89] involves utilizing a multi-hop DF relay-aided NOMA (MH-DF-R-NOMA). This scheme includes deriving closed-form expressions for BER and OP in the presence of imperfect SIC and CSI.

The impact of the relay selection (RS) strategy on the performance of cooperative NOMA is examined to reach the minimal OP across all possible RS schemes and meet the Quality of Service (QoS) criteria for both users [144, 145, 146]. The authors in [136, 147], delve into the performance analysis of OP and the sum rate of NOMA schemes within AF relay systems considering partial relay selection (PRS). Furthermore, the best relay selection (BRS) considered in [148, 149], the authors analyzed the OP of the optimal RS schemes for cooperative downlink NOMA, considering both fixed and adaptive power allocations (PAs) at the relays, respectively. The OP performance of a dual-hop multi-relay NOMA system using a DF scheme over Nakagami-m fading channels is investigated in [150]. In [151], the authors analyzed the secrecy outage performance for a NOMA network assisted by multiple relays operating over Nakagami-m fading channels, utilizing relay selection. The authors in [152], investigate the analysis of BER performance for both AF and DF relay selection in cooperative NOMA systems over Rayleigh fading channels. Notably, the AF-assisted Max-Min relay selection method exhibits superior performance for the far user compared to the DF relay. The implementation of BRS in the downlink scenario of NOMA-based Cognitive Relay Networks (NCRNs) is investigated under the assumption of Rayleigh fading channels in [153].

4.1.2 Motivation and contribution

Beyond the contribution of cooperative communications to enhancing NOMA system performance, researchers suggest the implementation of multiple-input multiple-output (MIMO) techniques to ensure these improvements. Considering that MIMO techniques entail higher complexity and power consumption, the strategy of antenna selection (AS) is deemed a robust option to ensure the desired performance [16, 154]. According to AS techniques, three main protocols are widely known, namely: transmit antenna selection (TAS) [155], receive antenna selection (RAS) [156], and joint transmit and receive antenna selection (JTRAS) [19]. The authors in [157] investigated three NOMA downlink models, including a single-input-single-output (SISO) scenario featuring a single antenna, a multi-input-single-output (MISO) scenario, and a MIMO scenario. The transmit antenna selection (TAS) protocol was employed in all scenarios. The authors conducted a comparison of the OP and system throughput, considering all users over the Rayleigh fading channel. In [158], the researchers introduced AS for an FD-CNOMA system intending to maximize the end-to-end signal-to-interference-noise ratio (SINR) for both the near and far users. This involved employing TAS/RAS protocols at the relay. The performance was characterized in terms of OP and ESR. A comprehensive analysis of the OP performance for two hybrid AS schemes, namely TAS and maximal ratio combining (MRC) at the first hop, as well as JTRAS at the second hop, in a MIMO-NOMA-based downlink AF relaying network. The analysis considers the impact of channel estimation error (CEE) and feedback delay (f_d) over Nakagami-m fading channels [159]. In addition, new combined antenna selection strategies, such as max-max-max and max-min-max, have been developed in [160, 161]. Nevertheless, the max-max-max and max-min-max schemes have the common goal of enhancing the stronger and weaker user, respectively. Furthermore, the impact of hardware impairments (HWI) on the uplink SIMO CNOMA (SIMO-CNOMA) using BRS under SIC and CSI imperfections is examined in terms of OP and system throughput in [162]

Drawing from the aforementioned literature, CNOMA studies have predominantly focused on single-relay scenarios, often overlooking factors like imperfect SIC, CEE, and feedback delay (f_d). Moreover, investigations rarely delve into the joint application of RS and TAS within CNOMA frameworks. Consequently, the integration of RS and TAS protocols into CNOMA systems while addressing practical challenges such as SIC, CEE, and feedback delay remains largely unexplored. This chapter fills this gap by evaluating and analyzing the performance of CNOMA systems using schemes that combine best relay selection with TAS (BRS-TAS CNOMA) and partial relay selection with TAS (PRS-TAS CNOMA), with a focus on OP and throughput performances. Therefore, the primary contributions of this study are outlined as follows:

- We investigate a realistic downlink CNOMA scheme influenced by SIC, CEE, and feedback delay. Our study includes different scenarios with multiple relays and antennas, employing

the RS technique and the integration of the TAS protocol to improve performance. The transmitting base station (BS) and relays are equipped with multiple antennas, while single antennas are employed at the reception.

- The exact integral expressions for the OP and throughput of all scenarios are derived, considering SIC, CEE, and feedback delay imperfections. These expressions are validated through both asymptotic analysis using the McLaurin series expansion and simulations carried out with Matlab.

- The impact of key system parameters on the OP and throughput performance was evaluated based on the obtained analytical expressions. These parameters include the number of relays and antennas, the distance between the relay and the base station, the power allocation factor, and practical impairments.

- Furthermore, we provide a performance comparison between the analyzed schemes and their HD relay-aided NOMA system counterpart.

- Finally, numerical results show that the systems under study in the high SNR region are limited by practical constraints, as indicated by the presence of an error floor (EF). Increasing the number of antennas and relays helps reduce these effects.

4.2 System model

We examine the downlink CNOMA system comprising a base station (BS), N relays and two users: a far user UE_1 and a near user UE_2. As shown in Figure 4.1, the BS and relays are equipped with N_t transmit antennas, while each user and relay use a single receiving antenna, resulting in a two-hop communication setup using the TAS scheme. In the two hops, the TAS scheme is applied, ensuring that N_t at both the BS and relay offer the highest SNR, respectively. To represent this system under the influence of imperfect SIC and imperfect CSI, including channel estimation error (CEE) and feedback delay, we first introduce

some notations and definitions:

- $h_{j.SR_i}$ and $h_{j.R_iD}$: are the $N_t \times 1$ fading channel coefficients vector of both hops, between the BS - R and R - UE_j, respectively, modeled as a complex Gaussian random variable $h_{j.SR_i} \sim CN\left(0, \sigma^2_{j.I}\right)$ and $h_{j.R_iD} \sim CN\left(0, \sigma^2_{j.II}\right)$. The variances are defined as $\sigma^2_{j.SR_i} = E\left\{|h_{j.SR_i}|^2\right\}$ and $\sigma^2_{j.R_iD} = E\left\{|h_{j.R_iD}|^2\right\}$, respectively, with $j = 1, 2$.

- $\hat{h}_{j.SR_i}$ and $\hat{h}_{j.R_iD}$: are the $N_t \times 1$ estimated channel coefficients vector of the two-hops can expressed by $\hat{h}_{j.SR_i} = h_{j.SR_i} - \kappa_{j.I}$ and $\hat{h}_{j.R_iD} = h_{j.R_iD} - \kappa_{j.II}$, where $\kappa_{j.I}$ and $\kappa_{j.II}$

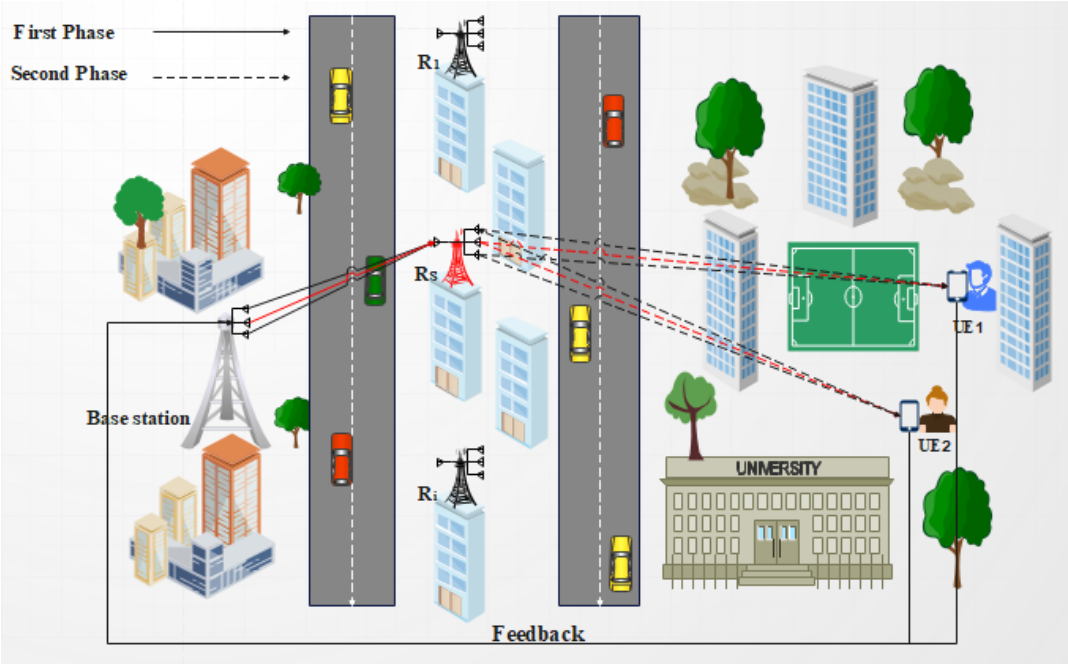

Figure 4.1: System model of the proposed Downlink CNOMA.

are the CEE independent of $\hat{h}_{j.SR_i}$ and $\hat{h}_{j.R_iD}$ and modelled as $\kappa_{j.I} \sim CN\left(0, \sigma^2_{\kappa_{j.I}}\right)$ and $\kappa_{j.II} \sim CN\left(0, \sigma^2_{\kappa_{j.II}}\right)$, respectively. The variances are defined as $\sigma^2_{\kappa_{j.I}} = \sigma^2_{j.SR_i} - \widehat{\sigma}^2_{j.SR_i}$ and $\sigma^2_{\kappa_{j.II}} = \sigma^2_{j.R_iD} - \widehat{\sigma}^2_{j.R_iD}$, where $\widehat{\sigma}^2_{j.SR_i} = E\left\{\left|\widehat{h}_{j.SR_i}\right|^2\right\}$ and $\widehat{\sigma}^2_{j.R_iD} = E\left\{\left|\widehat{h}_{j.R_iD}\right|^2\right\}$ are the variances of $\widehat{h}_{j.SR_i}$ and $\widehat{h}_{j.R_iD}$, respectively, with $j = 1, 2$.

- $\widehat{h}^{(\tau)}_{j.SR_i}$ and $\widehat{h}^{(\tau)}_{j.R_iD}$: are the $N_t \times 1$ feedback delayed of the estimated channels vector of $\hat{h}_{j.SR_i}$ and $\hat{h}_{j.R_iD}$ for the two-hops are defined as $\hat{h}_{j.SR_i} = \rho\widehat{h}^{(\tau)}_{j.SR_i} + e_{fd_{j.I}}$ and $\hat{h}_{j.R_iD} = \rho\widehat{h}^{(\tau)}_{j.R_iD} + e_{fd_{j.II}}$, where, $e_{fd_{j.I}}$ and $e_{fd_{j.II}}$ are the feedback error of the two-hops modelled as $e_{fd_{j.I}} \sim CN\left(0, \sigma^2_{fd_{j.I}}\right)$ and $e_{fd_{j.II}} \sim CN\left(0, \sigma^2_{fd_{j.II}}\right)$, which $\sigma^2_{fd_{j.I}} = (1 - \rho_{j.I})\,\widehat{\sigma}^2_{j.SR_i}$ and $\sigma^2_{fd_{j.II}} = (1 - \rho_{j.II})\,\widehat{\sigma}^2_{j.R_iD}$ and $\rho = J_0(2\pi f_d\tau)$ $0 < \rho < 1$, ρ and $f_d\tau$ represent the time correlation coefficient and the normalized Doppler frequency, respectively. We assume $e_{j.fd}$ and κ_j of the two hops are independent random variables, we define a new error for both hops $e_{j.I} = \kappa_{j.I} + e_{fd_{j.I}}$ and $e_{j.II} = \kappa_{j.II} + e_{fd_{j.II}}$, then $e_{j.I} \sim CN\left(0, \sigma^2_{e_{j.I}}\right)$ and $e_{j.II} \sim CN\left(0, \sigma^2_{e_{j.II}}\right)$, where $\sigma^2_{e_{j.I}} = \sigma^2_{\kappa_{j.I}} + \sigma^2_{fd_{j.I}}$ and $\sigma^2_{e_{j.II}} = \sigma^2_{\kappa_{j.II}} + \sigma^2_{fd_{j.II}}$ are the variances of each element in the error term $e_{j.I}$ and $e_{j.II}$, respectively. To simplify the calculation, we make the assumption, $\sigma^2_{\kappa_I} = \sigma^2_{\kappa_{j.I}}$, $\sigma^2_{\kappa_{II}} = \sigma^2_{\kappa_{j.II}}$, $\sigma^2_{fd_I} = \sigma^2_{fd_{j.I}}$ and $\sigma^2_{fd_{II}} = \sigma^2_{fd_{j.II}}$.

- Applying the TAS scheme in the two hops, a transmit antenna, denoted as $\widetilde{t}$, is selected at both the BS and relay. This selection is based on having the maximum sum of squared channel

gains between the receiver antennas of the relay and the users. So, the selected transmit antenna criteria for the two-hop given by:

$$\widetilde{t} = \underset{1<t<N_t}{\arg\max} |h_t|^2. \tag{4.1}$$

- Best relay selection (BRS): In the BRS scheme, the optimal relay is selected based on maximizing the minimum signal-to-interference-noise ratios (SINRs) between the source-to-relay link $(S - R_i)$ and the relay-to-UE$_j$ link. This selection criteria is expressed as:

$$R_s = \underset{1<l<L}{\arg\max} \left\{ \min \left(\gamma_{SR_i}, \gamma_{R_i D} \right) \right\}. \tag{4.2}$$

- Partial relay selection (PRS): In the PRS scheme, a partial relay selection is performed for one hop only, wherein the relay is chosen based on the CSI of each hop. The selection criteria is given as:

$$R_s = \underset{1<l<L}{\arg\max} \left\{ \left(\gamma_{SR_i} \right) \right\}, \tag{4.3}$$

and

$$R_s = \underset{1<l<L}{\arg\max} \left\{ \left(\gamma_{R_i D} \right) \right\}. \tag{4.4}$$

In the first hop of communication, the BS transmits a superimposed signal $x = \sum_{j=1}^{2} \sqrt{P_t \alpha_j} x_j$ to the relay, where x_j are the messages of UE$_j$, P_t denotes the BS transmit power and the coefficients α_j satisfy the conditions $\sum_{j=1}^{2} \alpha_j = 1$ and $\alpha_1 > \alpha_2$ leading to $|h_{1.SR_i}|^2 < |h_{2.SR_i}|^2$.
The received signal by the relay is given as:

$$y_r = \left(\rho \widehat{\widetilde{h}}^{(\tau)}_{j.SR_i} + e_I \right) \sum_{j=1}^{2} \sqrt{P_t \alpha_j} x_j + n_r, \tag{4.5}$$

where P_t denotes the BS transmit power. n_r is the additive white Gaussian noise (AWGN) $n_r \sim CN\left(0, N_o\right)$.
The received SINRs for x_1 and x_2 at the relay are given, respectively by:

$$\gamma_1^{SR_i} = \frac{\alpha_1 \gamma_0 \left| \widehat{\widetilde{h}}^{(\tau)}_{1.SR_i} \right|^2}{\alpha_2 \gamma_0 \left| \widehat{\widetilde{h}}^{(\tau)}_{1.SR_i} \right|^2 + \frac{\gamma_0}{\rho_I^2} \left(\sigma_{\kappa_I}^2 + \sigma_{fd_I}^2 \right) + \frac{1}{\rho_I^2}}, \tag{4.6}$$

and

$$\gamma_2^{SR_i} = \frac{\alpha_2\gamma_0\left|\widehat{\widetilde{h}}^{(\tau)}_{2.SR_i}\right|^2}{\alpha_1\gamma_0\xi\left|\widehat{\widetilde{h}}^{(\tau)}_{2.SR_i}\right|^2 + \frac{\gamma_0}{\rho_I^2}\left(\sigma^2_{\kappa_I} + \sigma^2_{fd_I}\right) + \frac{1}{\rho_I^2}}, \tag{4.7}$$

where ξ denotes the residual SIC factor and $\gamma_0 = \frac{P_r}{N_0}$ is the transmit SNR.

In the second hop of communication, the RS transmits a superimposed signal $x = \sum_{j=1}^{2}\sqrt{P_r\alpha_j}x_j$ to the users, where x_j are the messages of UE$_j$, P_r denotes the relay transmit power and the coefficients α_j satisfy the conditions $\sum_{j=1}^{2}\alpha_j = 1$ and $\alpha_1 > \alpha_2$ leading to $|h_{1.R_iD}|^2 < |h_{2.R_iD}|^2$.
So, the signal received by the UE$_j$ users can be expressed as follows:

$$y_j = \left(\rho\widehat{\widetilde{h}}^{(\tau)}_{j.R_iD} + e_{II}\right)\sum_{j=1}^{2}\sqrt{P_r\alpha_j}x_j + n_j, \tag{4.8}$$

where P_r denotes the relay transmit power. n_j is the additive white Gaussian Noise (AWGN) $n_j \sim CN(0, N_o)$.
The received SINRs for x_1 and x_2 at UE$_j$ are defined as:

$$\gamma_1^{R_iD} = \frac{\alpha_1\gamma_0\left|\widehat{\widetilde{h}}^{(\tau)}_{1.R_iD}\right|^2}{\alpha_2\gamma_0\left|\widehat{\widetilde{h}}^{(\tau)}_{1.R_iD}\right|^2 + \frac{\gamma_0}{\rho_{II}^2}\left(\sigma^2_{\kappa_{II}} + \sigma^2_{fd_{II}}\right) + \frac{1}{\rho_{II}^2}}, \tag{4.9}$$

$$\gamma_{2\to1}^{R_iD} = \frac{\alpha_1\gamma_0\left|\widehat{\widetilde{h}}^{(\tau)}_{2.R_iD}\right|^2}{\alpha_2\gamma_0\left|\widehat{\widetilde{h}}^{(\tau)}_{2.R_iD}\right|^2 + \frac{\gamma_0}{\rho_{II}^2}\left(\sigma^2_{\kappa_{II}} + \sigma^2_{fd_{II}}\right) + \frac{1}{\rho_{II}^2}}, \tag{4.10}$$

and

$$\gamma_2^{R_iD} = \frac{\alpha_2\gamma_0\left|\widehat{\widetilde{h}}^{(\tau)}_{2.R_iD}\right|^2}{\alpha_1\gamma_0\xi\left|\widehat{\widetilde{h}}^{(\tau)}_{2.R_iD}\right|^2 + \frac{\gamma_0}{\rho_{II}^2}\left(\sigma^2_{\kappa_{II}} + \sigma^2_{fd_{II}}\right) + \frac{1}{\rho_{II}^2}}, \tag{4.11}$$

where $\gamma_0 = \frac{P_r}{N_0}$ is the transmit SNR.

4.3 Performance analysis

In this section, we derive the OP and throughput expressions of the CNOMA-based RS and TAS protocol in the presence of practical impairments; SIC, CEE, and feedback delay over the Rayleigh

fading channel.

4.3.1 Outage probability analysis

In this subsection, we present the expressions of OP for various CNOMA schemes; BRS-TAS-CNOMA and PRS-TAS-CNOMA over the Rayleigh fading channel. The e2e OP of the CNOMA can be obtained as:

$$P_{e2e.j} = 1 - \left(1 - P_{out.j.I}\right)\left(1 - P_{out.j.II}\right), \tag{4.12}$$

where, $P_{out.j.I}$ and $P_{out.j.II}$ are the OP for the first and second hops, respectively, for each user.

4.3.1.1 Outage probability at far user

The end-2-end (e2e) OP of UE_1 is expressed as follows:

$$P_{e2e.1} = 1 - \left(1 - \Pr\left(\gamma_1^{SR} < \gamma_{th,1}\right)\right)\left(1 - \Pr\left(\gamma_1^{RD} < \gamma_{th,1}\right)\right). \tag{4.13}$$

Best relay selection : The e2e OP for the far user in CNOMA considering both BRS and TAS schemes, is expressed as:

$$P_{e2e.1}^{BRS} = \prod_{i=1}^{N}\left(1 - \left(1 - \prod_{t=1}^{N_t}\Pr\left(\gamma_1^{SR_i} < \gamma_{th,1}\right)\right)\left(1 - \prod_{t=1}^{N_t}\Pr\left(\gamma_1^{R_iD} < \gamma_{th,1}\right)\right)\right). \tag{4.14}$$

The OP for the first and second hops for UE_1 can be calculated, respectively as:

$$\begin{aligned}\prod_{t=1}^{N_t}\Pr\left(\gamma_1^{SR_i} < \gamma_{th,1}\right) &= \prod_{t=1}^{N_t}\left(1 - \exp\left(\frac{\frac{\gamma_{th,1}}{\rho_I^2}\left(1 + \gamma_0\left(\sigma_{\kappa_I}^2 + \sigma_{fd_I}^2\right)\right)}{\sigma_{1.SR_i}^2\gamma_0\left(\alpha_1 - \alpha_2\gamma_{th,1}\right)}\right)\right) \\ &= \prod_{t=1}^{N_t}\left(1 - \exp\left(\frac{\lambda_1^{SR_i}}{\sigma_{1.SR_i}^2}\right)\right),\end{aligned} \tag{4.15}$$

and

$$\begin{aligned}\prod_{t=1}^{N_t}\Pr\left(\gamma_1^{R_iD} < \gamma_{th,1}\right) &= \prod_{t=1}^{N_t}\left(1 - \exp\left(\frac{\frac{\gamma_{th,1}}{\rho_I^2}\left(1 + \gamma_0\left(\sigma_{\kappa_{II}}^2 + \sigma_{fd_{II}}^2\right)\right)}{\sigma_{1.R_iD}^2\gamma_0\left(\alpha_1 - \alpha_2\gamma_{th,1}\right)}\right)\right) \\ &= \prod_{t=1}^{N_t}\left(1 - \exp\left(\frac{\lambda_1^{R_iD}}{\sigma_{1.R_iD}^2}\right)\right),\end{aligned} \tag{4.16}$$

where, $\lambda_1^{SR_i} = \frac{\frac{\gamma_{th,1}}{\rho_I^2}\left(1+\gamma_0\left(\sigma_{\kappa_I}^2+\sigma_{fd_I}^2\right)\right)}{\gamma_0\left(\alpha_1-\alpha_2\gamma_{th,1}\right)}$, and $\lambda_1^{R_iD} = \frac{\frac{\gamma_{th,1}}{\rho_I^2}\left(1+\gamma_0\left(\sigma_{\kappa_{II}}^2+\sigma_{fd_{II}}^2\right)\right)}{\gamma_0\left(\alpha_1-\alpha_2\gamma_{th,1}\right)}$.

Finally, by substituting equations (4.15) and (4.16) into (4.14), the end-to-end OP of the far user can be expressed as:

$$P_{e2e.1}^{BRS} = \prod_{i=1}^{N}\left(1-\left(1-\prod_{t=1}^{N_t}\left(1-\exp\left(\frac{\lambda_1^{SR_i}}{\sigma_{1.r}^2}\right)\right)\right)\left(1-\prod_{t=1}^{N_t}\left(1-\exp\left(\frac{\lambda_1^{R_iD}}{\sigma_1^2}\right)\right)\right)\right). \tag{4.17}$$

Partial relay selection : The e2e OP for the far user in CNOMA incorporating both PRS at first hop and TAS schemes, is formulated as:

$$P_{e2e.1}^{PRS} = 1-\left(1-\prod_{i=1}^{N}\prod_{t=1}^{N_t}\Pr\left(\gamma_1^{SR_i}<\gamma_{th.1}\right)\right)\left(1-\prod_{t=1}^{N_t}\Pr\left(\gamma_1^{R_sD}<\gamma_{th.1}\right)\right). \tag{4.18}$$

Next, by substituting $\lambda_1^{SR_i}$ and $\lambda_1^{R_sD}$ into equation (4.18), the end-to-end OP for the far user, considering TAS and PRS, can be represented as:

$$P_{e2e.1}^{PRS} = 1-\left(1-\prod_{i=1}^{N}\prod_{t=1}^{N_t}\left(1-\exp\left(\frac{\lambda_1^{SR_i}}{\sigma_{1.SR_i}^2}\right)\right)\right)\left(1-\prod_{t=1}^{N_t}\left(1-\exp\left(\frac{\lambda_1^{R_sD}}{\sigma_{1.R_sD}^2}\right)\right)\right). \tag{4.19}$$

4.3.1.2 Outage probability at near user

We recall that the e2e OP of CNOMA for the near user is as follows:

$$P_{e2e.2} = 1-\left(1-\Pr\left(\gamma_2^{SR}<\gamma_{th,2}\right)\right)\left(1-\Pr\left(\gamma_2^{RD}<\gamma_{th,2}\right)\right). \tag{4.20}$$

Best relay selection: The e2e OP for the near user in CNOMA considering both BRS and TAS schemes, is expressed as

$$P_{e2e.2}^{BRS} = \prod_{i=1}^{N}\left(1-\left(\left(1-\underbrace{\prod_{t=1}^{N_t}P_{out.2}^{SR_i}}_{trerm\ I}\right)\left(1-\underbrace{\prod_{t=1}^{N_t}P_{out.2}^{R_iD}}_{term\ II}\right)\right)\right), \tag{4.21}$$

In this context, terms I and II denote the OP of the near user utilizing the TAS protocol in the first and second hops, respectively. So, the OP of of the term I for UE_2, can be expressed as follows:

$$\prod_{t=1}^{N_t}P_{out.2}^{SR_i} = \prod_{t=1}^{N_t}Pr\left(\gamma_{2\to1}^{SR_i}<\gamma_{th.1}\right)+\left[\prod_{t=1}^{N_t}Pr\left(\gamma_{2\to1}^{SR_i}\geq\gamma_{th.1}\right)\prod_{t=1}^{N_t}Pr\left(\gamma_2^{SR_i}<\gamma_{th.2}\right)\right]. \tag{4.22}$$

Each probability condition is calculated as follows:

$$\prod_{t=1}^{N_t} P\left(\gamma_{2\to1}^{SR_i} < \gamma_{th.1}\right) = \prod_{t=1}^{N_t}\left(1-\exp\left(-\frac{\frac{\gamma_{th_1}}{\rho_I^2}\left(1+\gamma_0\left(\sigma_{\kappa_I}^2+\sigma_{fd_I}^2\right)\right)}{\sigma_{2,SR_i}^2\gamma_0\left(\alpha_1-\alpha_2\gamma_{th_1}\right)}\right)\right) \tag{4.23}$$

$$= \prod_{t=1}^{N_t}\left(1-\exp\left(-\frac{\lambda_2^{SR_i}}{\sigma_{2,SR_i}^2}\right)\right),$$

and

$$\prod_{t=1}^{N_t} P\left(\gamma_{2}^{SR_i} < \gamma_{th.2}\right) = \prod_{t=1}^{N_t}\left(1-\exp\left(-\frac{\frac{\gamma_{th_2}}{\rho_I^2}\left(1+\gamma_0\left(\sigma_{\kappa_I}^2+\sigma_{fd_I}^2\right)\right)}{\sigma_{2,SR_i}^2\gamma_0\left(\alpha_2-\alpha_1\xi\gamma_{th_2}\right)}\right)\right) \tag{4.24}$$

$$= \prod_{t=1}^{N_t}\left(1-\exp\left(-\frac{\lambda_3^{SR_i}}{\sigma_{2,SR_i}^2}\right)\right),$$

where, $\lambda_2^{SR_i} = \frac{\frac{\gamma_{th_1}}{\rho_I^2}\left(1+\gamma_0\left(\sigma_{\kappa_I}^2+\sigma_{fd_I}^2\right)\right)}{\gamma_0\left(\alpha_1-\alpha_2\gamma_{th_1}\right)}$, and $\lambda_3^{SR_i} = \frac{\frac{\gamma_{th_2}}{\rho_I^2}\left(1+\gamma_0\left(\sigma_{\kappa_I}^2+\sigma_{fd_I}^2\right)\right)}{\gamma_0\left(\alpha_2-\alpha_1\xi\gamma_{th_2}\right)}$.

After substituting (4.23) and (4.24) into (4.22), term I can be written as:

$$\prod_{t=1}^{N_t} P_{out.2}^{SR_i} = \prod_{t=1}^{N_t}\left(1-\exp\left(-\frac{\lambda_2^{SR_i}}{\sigma_{2,SR_i}^2}\right)\right)$$

$$+\left[\left(1-\prod_{t=1}^{N_t}\left(1-\exp\left(-\frac{\lambda_2^{SR_i}}{\sigma_{2,SR_i}^2}\right)\right)\right)\times\prod_{t=1}^{N_t}\left(1-\exp\left(-\frac{\lambda_3^{SR_i}}{\sigma_{2,SR_i}^2}\right)\right)\right]. \tag{4.25}$$

Similar to the first hop, the OP of the second hop for UE_2, can be expressed as follows:

$$\prod_{t=1}^{N_t} P_{out.2}^{R_iD} = \prod_{t=1}^{N_t} Pr\left(\gamma_{2\to1}^{R_iD} < \gamma_{th.1}\right) + \left[\prod_{t=1}^{N_t} Pr\left(\gamma_{2\to1}^{R_iD} \geq \gamma_{th.1}\right)\prod_{t=1}^{N_t} Pr\left(\gamma_{2}^{R_iD} < \gamma_{th.2}\right)\right] \tag{4.26}$$

The calculation of each probability condition proceeds as follows:

$$\prod_{t=1}^{N_t} P\left(\gamma_{2\to1}^{R_iD} < \gamma_{th.1}\right) = \prod_{t=1}^{N_t}\left(1-\exp\left(-\frac{\frac{\gamma_{th_1}}{\rho_{II}^2}\left(1+\gamma_0\left(\sigma_{\kappa_{II}}^2+\sigma_{fd_{II}}^2\right)\right)}{\sigma_{2,R_iD}^2\gamma_0\left(\alpha_1-\alpha_2\gamma_{th_1}\right)}\right)\right) \tag{4.27}$$

$$= \prod_{t=1}^{N_t}\left(1-\exp\left(-\frac{\lambda_2^{R_iD}}{\sigma_{2,R_iD}^2}\right)\right),$$

and

$$\prod_{t=1}^{N_t} P\left(\gamma_2^{R_iD} < \gamma_{th.2}\right) = \prod_{t=1}^{N_t}\left(1 - \exp\left(-\frac{\frac{\gamma_{th_2}}{\rho_{II}^2}\left(1+\gamma_0\left(\sigma_{\kappa_{II}}^2+\sigma_{fd_{II}}^2\right)\right)}{\sigma_{2,R_iD}^2\gamma_0\left(\alpha_2-\alpha_1\xi\gamma_{th_2}\right)}\right)\right) \tag{4.28}$$

$$= \prod_{t=1}^{N_t}\left(1 - \exp\left(-\frac{\lambda_3^{R_iD}}{\sigma_{2,R_iD}^2}\right)\right),$$

where, $\lambda_2^{R_iD} = \frac{\frac{\gamma_{th_1}}{\rho_{II}^2}\left(1+\gamma_0\left(\sigma_{\kappa_{II}}^2+\sigma_{fd_{II}}^2\right)\right)}{\gamma_0\left(\alpha_1-\alpha_2\gamma_{th_1}\right)}$, and $\lambda_3^{R_iD} = \frac{\frac{\gamma_{th_2}}{\rho_{II}^2}\left(1+\gamma_0\left(\sigma_{\kappa_{II}}^2+\sigma_{fd_{II}}^2\right)\right)}{\gamma_0\left(\alpha_2-\alpha_1\xi\gamma_{th_2}\right)}$.

Now, by substituting (4.27) and (4.28) into (4.26), the term II can be obtained as

$$\prod_{t=1}^{N_t} P_{out.2}^{R_iD} = \prod_{t=1}^{N_t}\left(1 - \exp\left(-\frac{\lambda_2^{R_iD}}{\sigma_{2,R_iD}^2}\right)\right)$$

$$+\left[\left(1-\prod_{t=1}^{N_t}\left(1-\exp\left(-\frac{\lambda_2^{R_iD}}{\sigma_{2,R_iD}^2}\right)\right)\right)\times\prod_{t=1}^{N_t}\left(1-\exp\left(-\frac{\lambda_3^{R_iD}}{\sigma_{2,R_iD}^2}\right)\right)\right]. \tag{4.29}$$

Finally, the e2e OP of the UE_2 using TAS and BRS is obtained by substituting (4.25) and (4.29) into (4.21).

Partial relay selection: In line with the proofs presented previously, the e2e OP for the near user in CNOMA using both PRS and TAS schemes is obtained as:

$$P_{e2e.2}^{PRS} = 1 - \left(1 - \prod_{i=1}^{N}\prod_{t=1}^{N_t} P_{out.2}^{SR_i}\right)\left(1 - \prod_{t=1}^{N_t} P_{out.2}^{R_sD}\right), \tag{4.30}$$

where,

$$\prod_{t=1}^{N_t} P_{out.2}^{R_sD} = \prod_{t=1}^{N_t} P\left(\gamma_{2\to1}^{R_sD} < \gamma_{th.1}\right) + \left[\prod_{t=1}^{N_t} P\left(\gamma_{2\to1}^{R_sD} \geq \gamma_{th.1}\right)\prod_{t=1}^{N_t} P\left(\gamma_2^{R_sD} < \gamma_{th.2}\right)\right]. \tag{4.31}$$

Following the same mathematical proofs

$$\prod_{t=1}^{N_t} P_{out.2}^{R_sD} = \prod_{t=1}^{N_t}\left(1 - \exp\left(-\frac{\lambda_2^{R_sD}}{\sigma_{2,R_sD}^2}\right)\right)$$

$$+\left[\left(1-\prod_{t=1}^{N_t}\left(1-\exp\left(-\frac{\lambda_2^{R_sD}}{\sigma_{2,R_sD}^2}\right)\right)\right)\times\prod_{t=1}^{N_t}\left(1-\exp\left(-\frac{\lambda_3^{R_sD}}{\sigma_{2,R_sD}^2}\right)\right)\right]. \tag{4.32}$$

Finally, the e2e OP of the UE_2 using TAS and PRS is obtained by substituting (4.25) and (4.32) into (4.30).

4.3.2 Asymptotic outage probability

In this subsection, we delve into the performance of asymptotic OP in scenarios marked by high SNR, aiming to gain a more profound understanding of the considered situations. Hence, the asymptotic OP is defined in conditions of high SNR (i.e., as $\gamma_0 \to \infty$), employing the McLaurin series expansion $\exp(-x) \approx 1 - x$ [147].

4.3.2.1 Asymptotic OP of far user:

The asymptotic expression for the OP of UE_1, at high SNR regime, is given for BRS and PRS scenarios, respectively, as:

$$P_{e2e.1}^{BRS,asy} \approx \prod_{i=1}^{N} \left(1 - \left(1 - \prod_{t=1}^{N_t} \left(\frac{\lambda_1^{SR_i}}{\sigma_{1.SR_i}^2}\right)\right)\left(1 - \prod_{t=1}^{N_t} \left(\frac{\lambda_1^{R_iD}}{\sigma_{1.R_iD}^2}\right)\right)\right), \tag{4.33}$$

and

$$P_{e2e.1}^{PRS,asy} \approx 1 - \left(1 - \prod_{i=1}^{N}\prod_{t=1}^{N_t} \left(\frac{\lambda_1^{SR_i}}{\sigma_{1.SR_i}^2}\right)\right)\left(1 - \prod_{t=1}^{N_t} \left(\frac{\lambda_1^{R_sD}}{\sigma_{1.R_sD}^2}\right)\right). \tag{4.34}$$

4.3.2.2 Asymptotic OP of near user:

Similarly, the asymptotic expression for the OP of UE_2, at high SNR regime, is given for BRS and PRS scenarios, respectively, as follows:

$$\prod_{t=1}^{N_t} P_{out.2}^{SR_i,asy} \approx \prod_{t=1}^{N_t} \left(\frac{\lambda_2^{SR_i}}{\sigma_{2,SR_i}^2}\right) + \left[\left(1 - \prod_{t=1}^{N_t} \left(\frac{\lambda_2^{SR_i}}{\sigma_{2,SR_i}^2}\right)\right) \times \prod_{t=1}^{N_t} \left(\frac{\lambda_3^{SR_i}}{\sigma_{2,SR_i}^2}\right)\right], \tag{4.35}$$

$$\prod_{t=1}^{N_t} P_{out.2}^{R_iD,asy} \approx \prod_{t=1}^{N_t} \left(\frac{\lambda_2^{R_iD}}{\sigma_{2,R_iD}^2}\right) + \left[\left(1 - \prod_{t=1}^{N_t} \left(\frac{\lambda_2^{R_iD}}{\sigma_{2,R_iD}^2}\right)\right) \times \prod_{t=1}^{N_t} \left(\frac{\lambda_3^{R_iD}}{\sigma_{2,R_iD}^2}\right)\right], \tag{4.36}$$

and

$$\prod_{t=1}^{N_t} P_{out.2}^{R_sD,asy} \approx \prod_{t=1}^{N_t} \left(\frac{\lambda_2^{R_sD}}{\sigma_{2,R_sD}^2}\right) + \left[\left(1 - \prod_{t=1}^{N_t} \left(\frac{\lambda_2^{R_sD}}{\sigma_{2,R_sD}^2}\right)\right) \times \prod_{t=1}^{N_t} \left(\frac{\lambda_3^{R_sD}}{\sigma_{2,R_sD}^2}\right)\right]. \tag{4.37}$$

4.3.3 System throughput analysis

The system throughput is the sum of the achievable received bit rates at UE_1 and UE_2. As a result, the system throughput can be calculated as follows:

$$Tp_{sys} = Tp_1 + Tp_2 = (1 - P_{out.1})\, R_1^* + (1 - P_{out.2})\, R_2^*, \tag{4.38}$$

where, R_1^* and R_2^* are the threshold rates of UE_1 and UE_2, respectively.

4.4 Numerical results

In this section, we present a validation of the analysis for cooperative NOMA scenarios provided in the previous sections. The practical impairments, SIC, CEE, and feedback delay, are taken into account to evaluate OP and throughput over the Rayleigh fading channels. with power coefficients allocated as $\alpha_1 = 0.8$ and $\alpha_2 = 0.2$, The Distance between the BS and relays set to $dsr = 1m$ and distances between the users and relays set to $dr_1 = 2m$ and $dr_2 = 1m$. Additionally, we have $\xi = 0.01$, $\sigma_\kappa^2 = 0.01$, and $f_d\tau = 0.02$. In the plots, different lines and markers represent analytical, simulation, and asymptotic curves. The figures demonstrate a close alignment among the analytical, asymptotic, and simulated results, providing strong confirmation of the validity of the performance analysis.

The analytical and simulation results in Figures 4.2 to 4.5 compare multiple scenarios inside the downlink CNOMA system, examining the OP of UE_1 and UE_2, separately. These scenarios include the use of AS and RS to CNOMA while taking into account the presence and absence of certain impairments: $\xi = 0.01$, $\sigma_\kappa^2 = 0.01$, and $f_d\tau = 0.02$.

Figures 4.2 and 4.3 depict the OP outcomes at UE_1 for various scenarios, including CNOMA using a single antenna as a benchmark, CNOMA with partial and best RS, and TAS integration into CNOMA-based PRS and BRS. Through analysis and simulation, it becomes evident that the performance of the CNOMA system gradually improves with the addition of more RS. Moreover, employing the TAS protocol at both the BS and relays yields better performance than relying only on CNOMA-based RS. This underscores the significance of antenna configurations at the BS and relays for enhancing CNOMA system performance. However, as depicted in Figure 4.3, there is a decline in performance attributed to the presence of imperfections in SIC, CEE and feedback delay, leading to an error floor at high SNR.

Likewise, Figures 4.4 and 4.5 provide insights into the OP of UE_2. Notably, the CNOMA-based BRS-TAS scenario demonstrates superior performance compared to other scenarios. This enhancement is achieved by incorporating TAS at both the BS and relays, confirming the critical

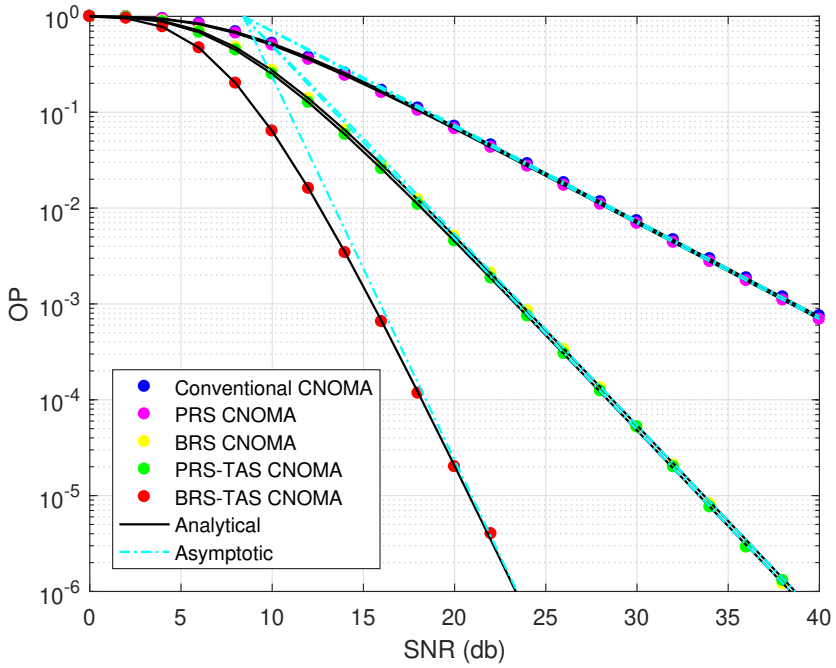

Figure 4.2: The OP of UE_1 in the downlink CNOMA scenarios under ideal conditions.

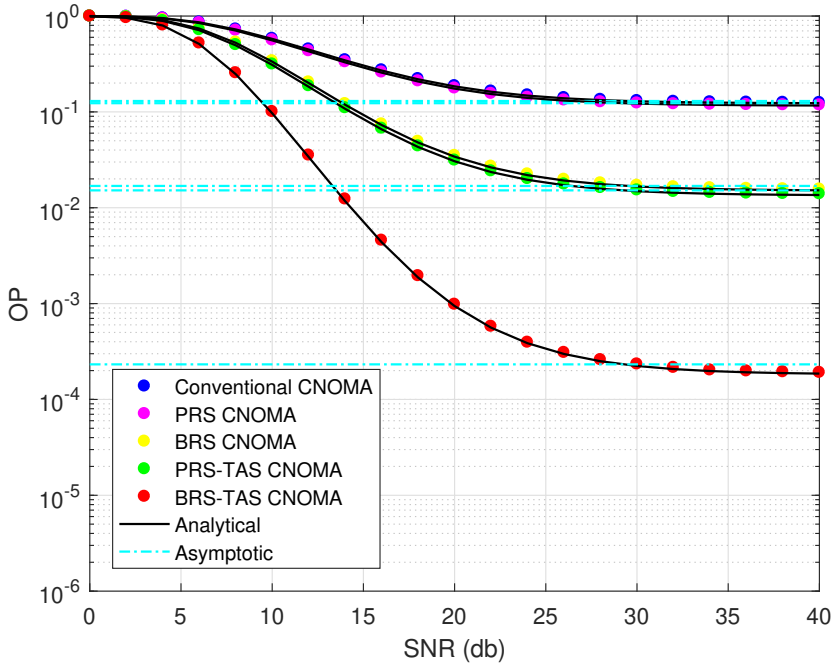

Figure 4.3: The OP of UE_1 in the downlink CNOMA scenarios under impaired conditions.

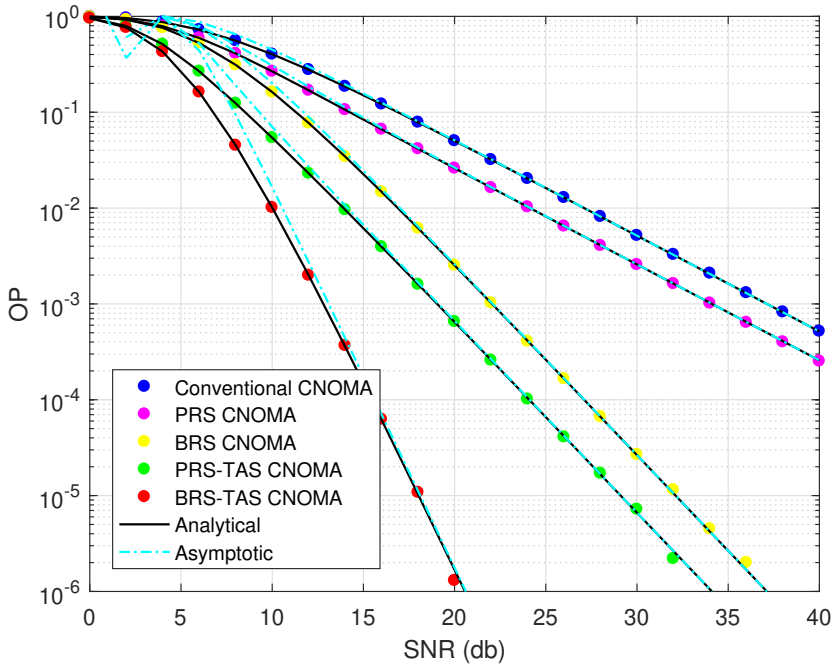

Figure 4.4: The OP of UE_2 in the downlink CNOMA scenarios under ideal conditions.

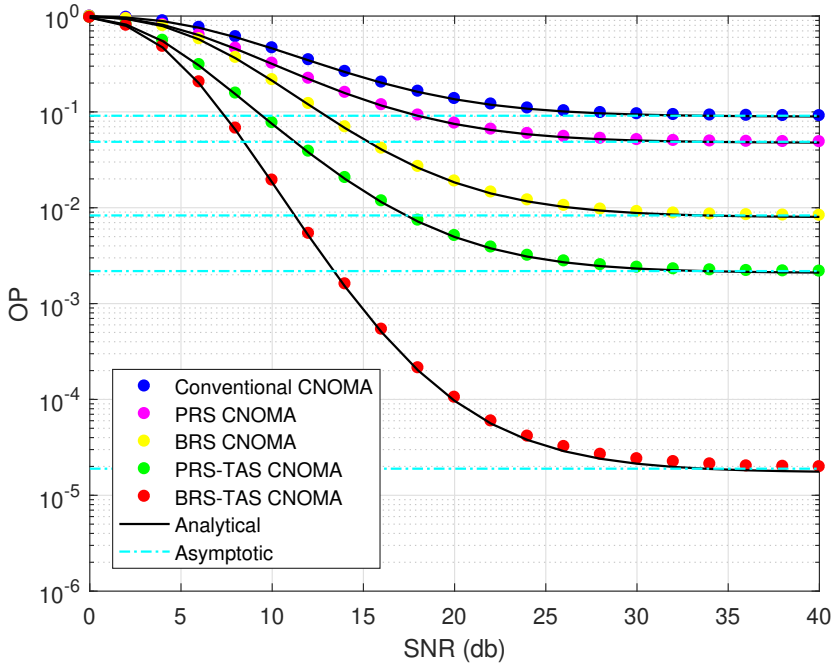

Figure 4.5: The OP of UE_2 in the downlink CNOMA scenarios under impaired conditions.

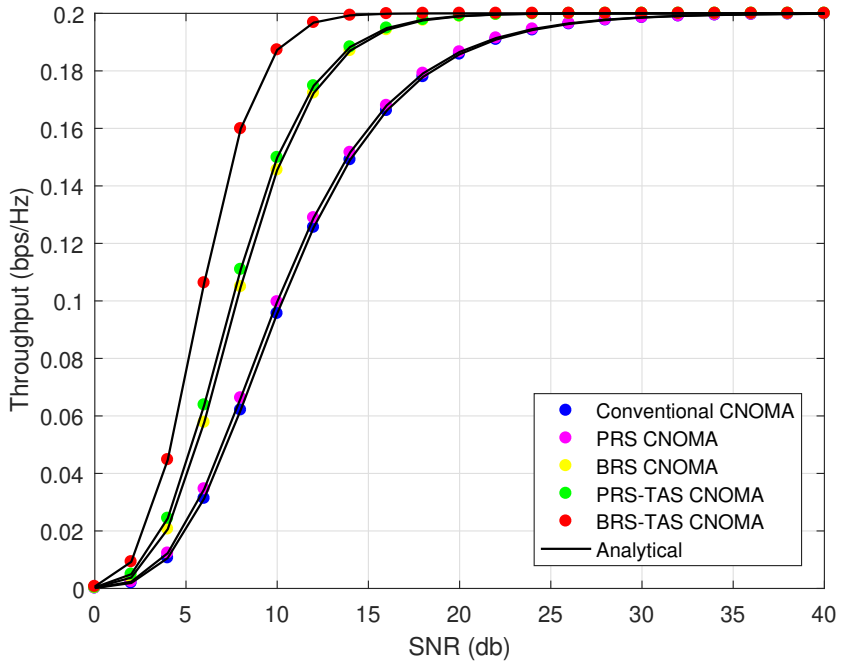

Figure 4.6: The Throughput of UE_1 in the downlink CNOMA scenarios under ideal conditions.

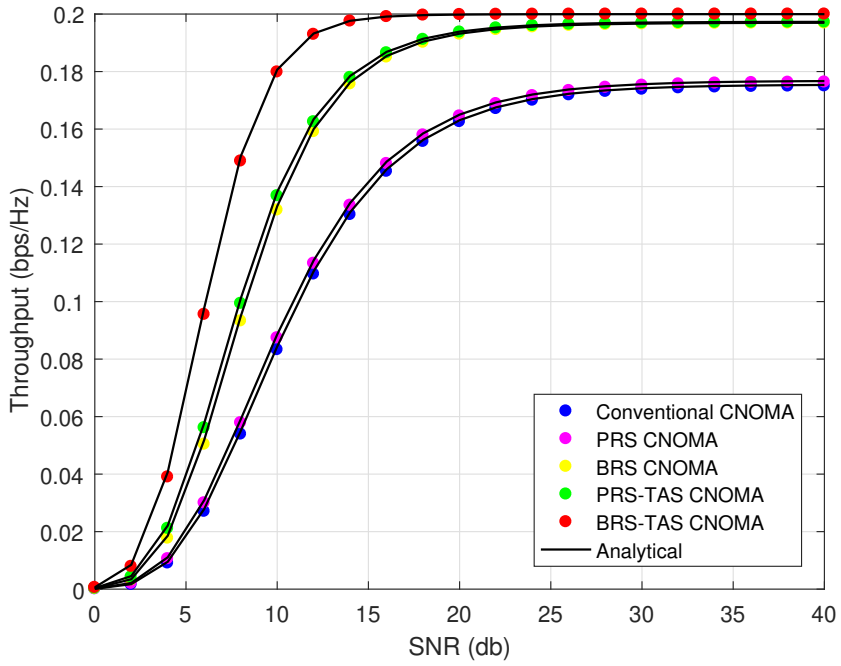

Figure 4.7: The Throughput of UE_1 in the downlink CNOMA scenarios under impaired conditions.

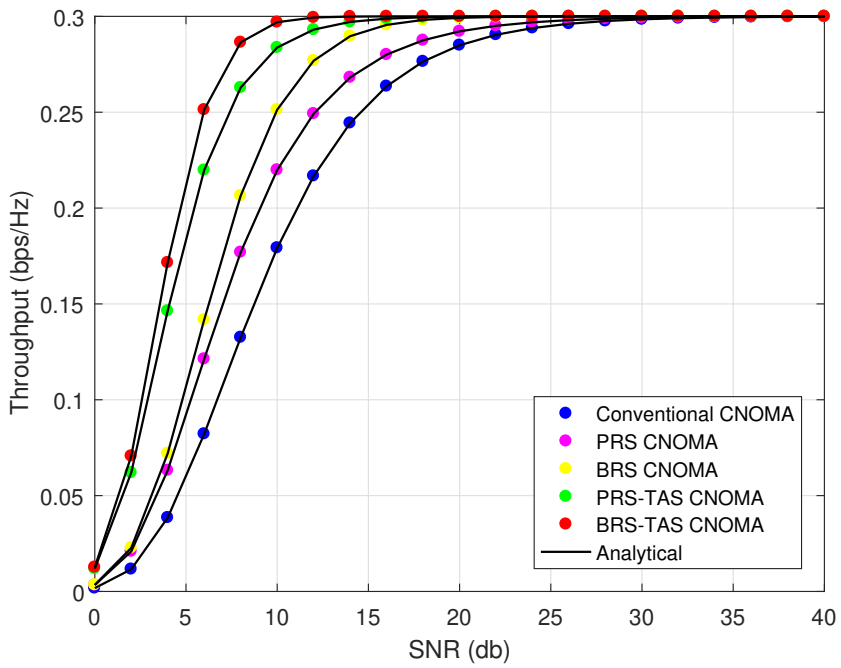

Figure 4.8: The Throughput of UE_2 in the downlink CNOMA scenarios under ideal conditions.

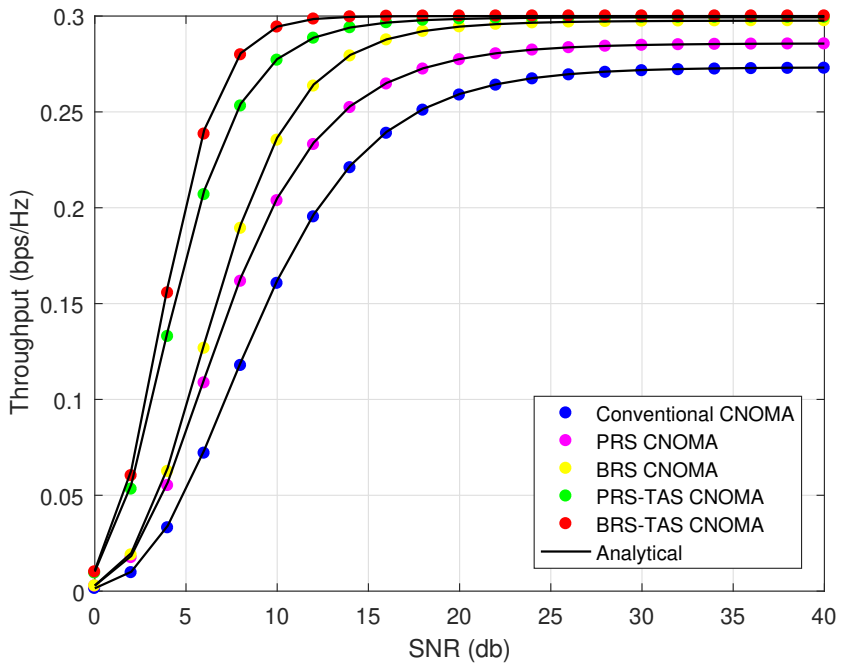

Figure 4.9: The Throughput of UE_2 in the downlink CNOMA scenarios under impaired conditions.

role of leveraging multiple antennas for improved UE_2 performance. In addition, the asymptotic results corroborate the analytical findings, affirming the accuracy of our analysis.

In Figures 4.6 to 4.9, we present the throughput performance comparison of the studied scenarios versus SNR, considering the presence and absence of imperfections in SIC, CEE, and feedback delay. As we can see, the CNOMA-based RS outperforms conventional CNOMA. Additionally, the use of the TAS protocol has a positive impact on both BRS and PRS schemes. The simulation plots are well-matched with the analytical results, validating the accuracy of our analysis.

Figures 4.10 and 4.11 depict the OP and throughput of the CNOMA system relative to the distance dr, assuming an SNR of 25 dB. Specifically, we compare the performance of CNOMA with BRS-TAS against conventional CNOMA. Noteworthy observations lead to several conclusions: at $dr = 1m$, UE_2 exhibits superior OP performance compared to the far user UE_1. However, at distances $dr = 2m$ and beyond, the performance of UE_1 surpasses that of UE_2. Furthermore, as the distance increases, UE_2 experiences outage more rapidly than UE_1.

The assessment of the influence of power allocation (α_1) on CNOMA is conducted by examining the OP and Throughput in Figures 4.12 and 4.13, respectively. With a fixed SNR of 25 dB, it is evident that the performance of UE_1 improves proportionally with the increased power allocated to it. However, this improvement comes at the expense of deteriorating performance for UE_2. Furthermore, it is notable that, across varying values of (α_1), the CNOMA-based BRS-TAS consistently ensures superior performance in terms of both OP and throughput.

The presence of channel estimation error (${\sigma_\kappa}^2$) detrimentally affects the OP and throughput in all evaluated CNOMA scenarios. The negative impact of these errors is clearly observable in the performance metrics, and it intensifies as the magnitude of the estimation error increases. As illustrated in Figures 4.14 and 4.15, the escalation of channel estimation error results in a more substantial decline in both OP and throughput. This trend underscores the essential role of precise channel estimation in maintaining and optimizing the performance of CNOMA systems.

Figures 4.16 and 4.17 illustrate the impact of Feedback Delay and the Time Correlation Coefficient (ρ) on the OP and throughput of the CNOMA system. With the SNR held constant at 25 dB, the figures demonstrate that increasing feedback delay leads to a noticeable decline in system performance, affecting both OP and throughput negatively. On the other hand, higher values of ρ, which indicate stronger time correlation in the channel, result in improved performance metrics. This dual effect highlights the critical balance between feedback timeliness and channel stability in optimizing CNOMA system efficiency.

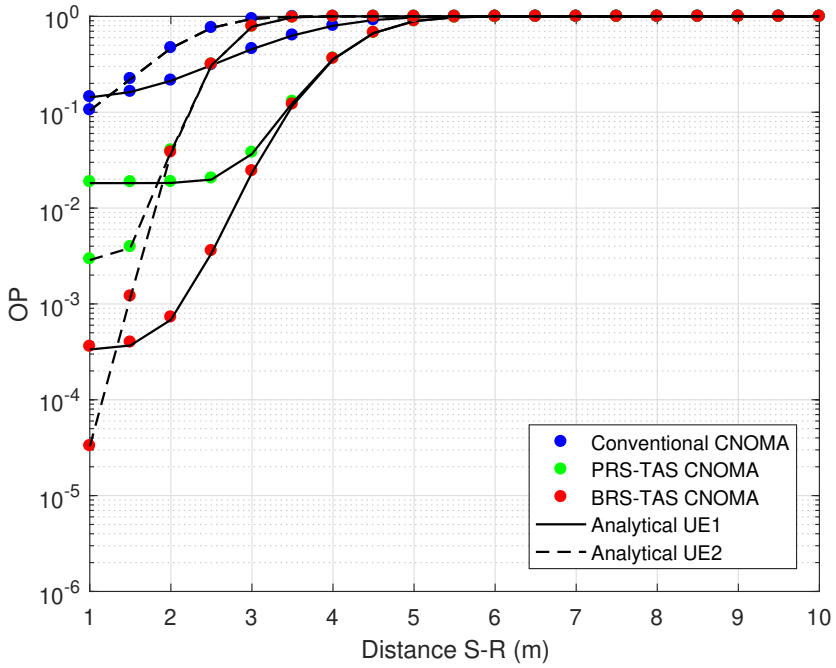

Figure 4.10: The impact of distance on the OP of the downlink CNOMA under various impairments.

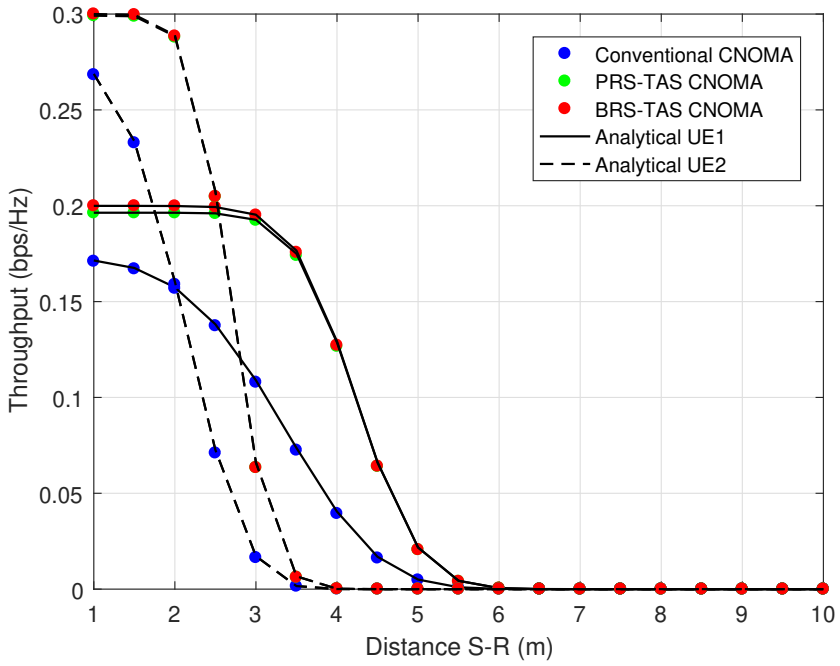

Figure 4.11: The impact of distance on the Throughput of the downlink CNOMA under various impairments.

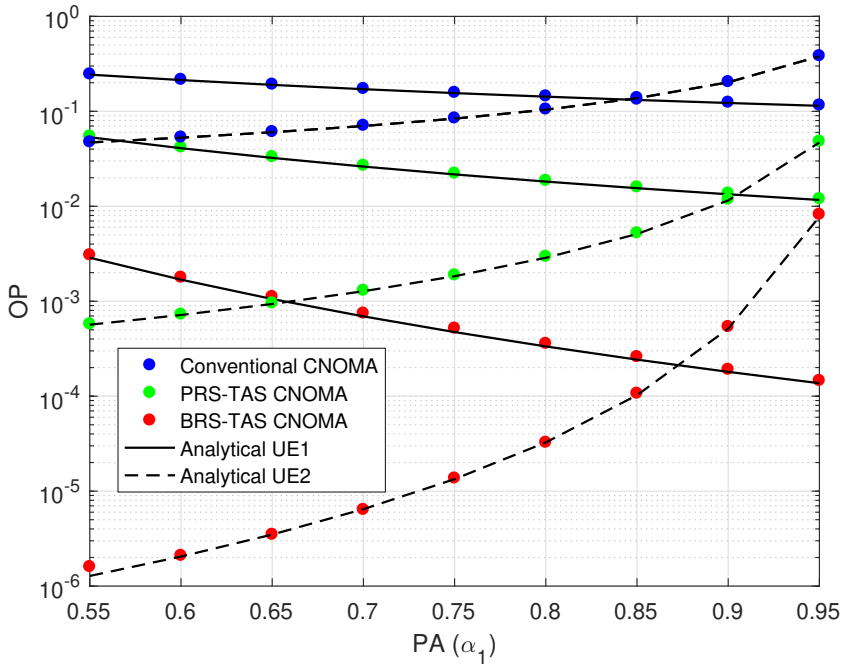

Figure 4.12: The impact of PA on the OP of the downlink CNOMA under various impairments.

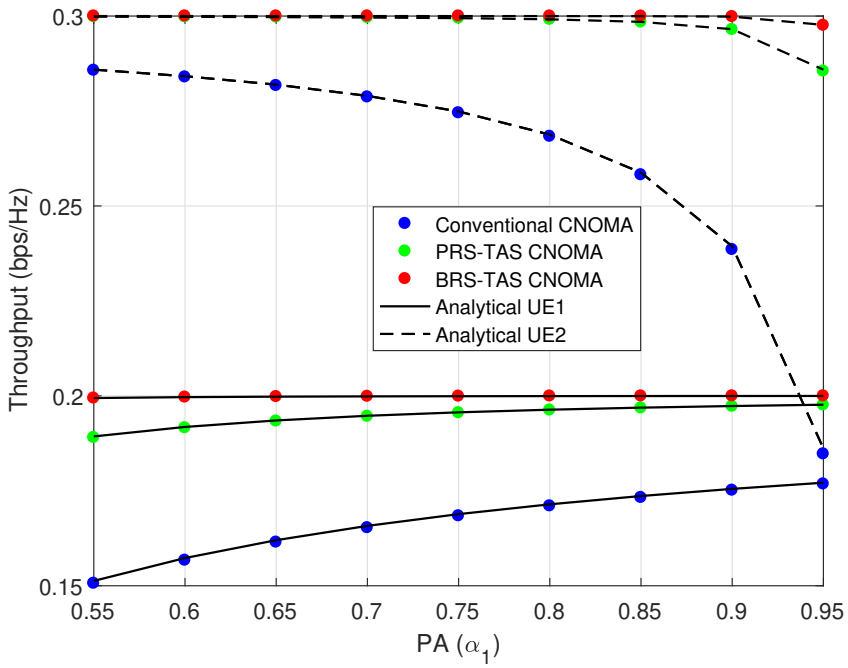

Figure 4.13: The impact of PA on the Throughput of the downlink CNOMA under various impairments.

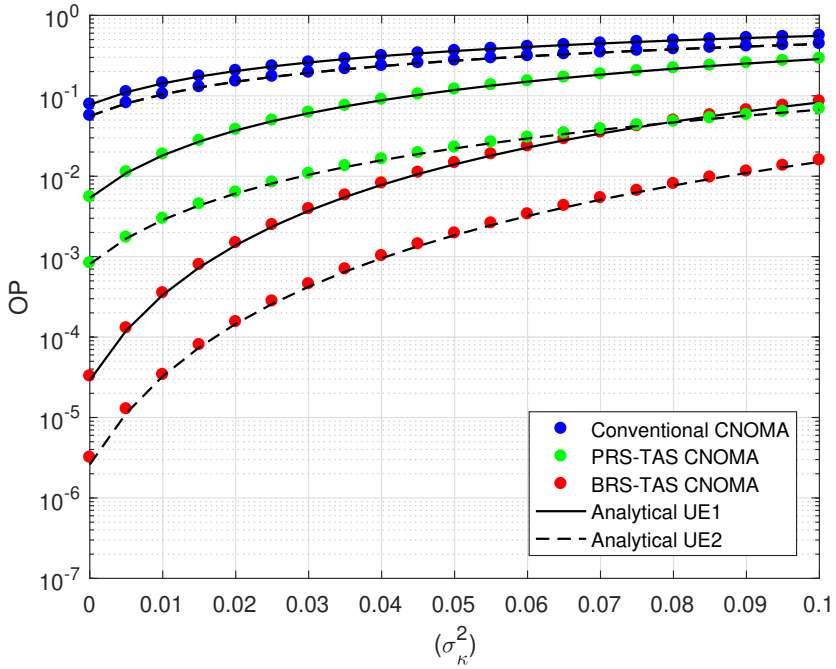

Figure 4.14: The impact of CEE on the OP of the downlink CNOMA under various impairments.

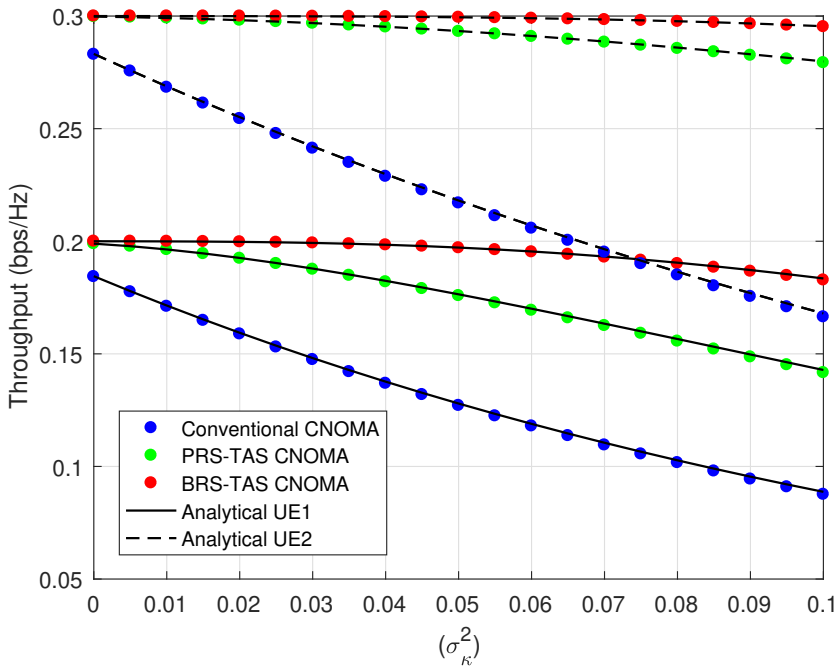

Figure 4.15: The impact of CEE on the throughput of the downlink CNOMA under various impairments.

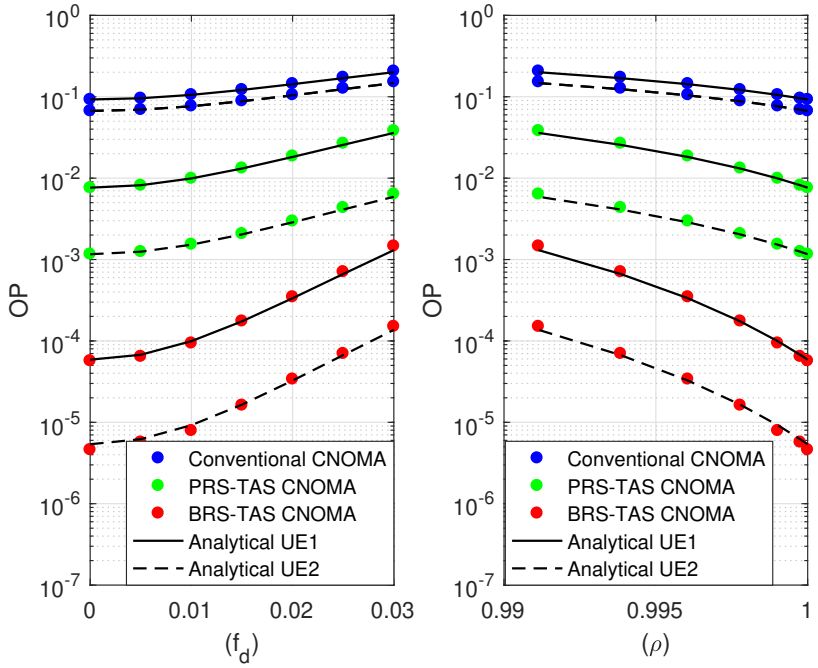

Figure 4.16: The impact of ρ and f_d error on the OP of the downlink CNOMA under various impairments.

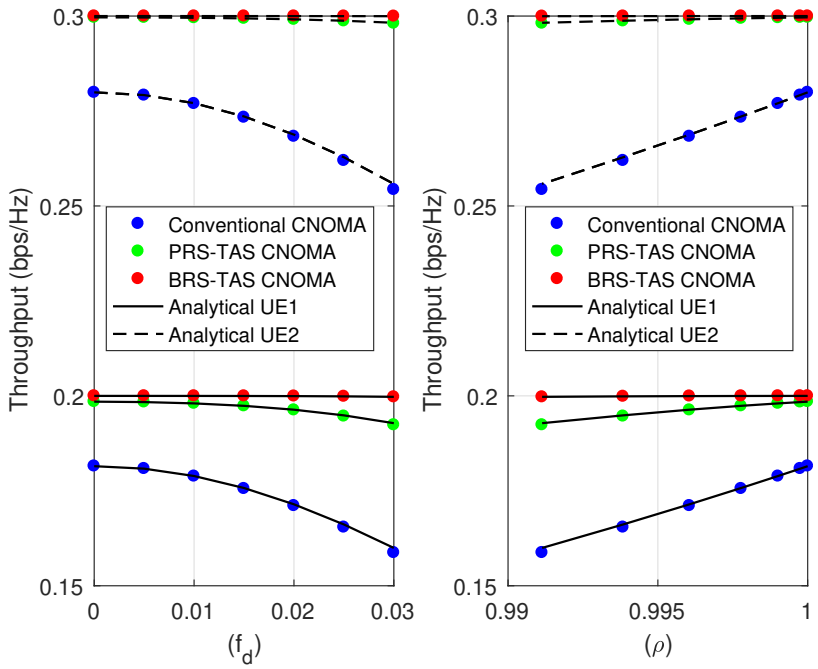

Figure 4.17: The impact of ρ and f_d error on the Throughput of the downlink CNOMA under various impairments.

4.5 Conclusion

In conclusion, this chapter systematically explored and compared CNOMA with TAS against the conventional CNOMA approach. The investigation considered both BRS and PRS paradigm selection among multiple relays, resulting in the formulation of BRS-TAS CNOMA and PRS-TAS CNOMA schemes. Practical impairments such as SIC error, CEE, and feedback delay were comprehensively considered in both scenarios. Exact expressions for OP and throughput over Rayleigh fading channels were derived and validated through simulations and asymptotic proofs.

The findings underscored that augmenting the number of antennas at the BS or relays significantly improves the overall performance of CNOMA schemes. Furthermore, the incorporation of a relay selection paradigm yielded additional enhancements in system performance. Importantly, the adverse effects of impairments were alleviated through the strategic application of selection criteria for antennas and/or relays.

In summary, the alignment between analytical, asymptotic, and simulated results establishes the robustness and accuracy of the analytical framework presented in this study. These insights contribute to advancing the understanding of selection strategies in CNOMA systems, with implications for optimizing performance in practical communication scenarios.

General conclusion

Non-orthogonal multiple access (NOMA), with its unique capabilities in resource allocation and spectral efficiency enhancement, is positioned to shape the trajectory of future wireless communication systems. Its adaptability in power allocation and support for diverse services make it an appealing choice for advancing communication paradigms. Anticipating the future, NOMA's impact is expected to extend beyond current capabilities, playing a crucial role in advancing connectivity, setting higher performance standards, and optimizing resource utilization. This forward-looking vision positions NOMA as a major contributor to the ongoing evolution of advanced communication standards, facilitating transformative applications in the dynamic digital era.

On the flip side, multiple input multiple output (MIMO) technology plays a pivotal role in shaping the future of mobile networks, contributing to enhanced overall performance. Its capacity to boost data rates establishes it as a fundamental technology, essential for addressing the requirements of advanced applications during the transition from the 4^{th} generation (4G) to the 5^{th} generation (5G) and beyond.

This thesis is committed to evaluating the impact of MIMO technology on NOMA systems, seeking to comprehend how the use of multiple antennas improves the overall performance of NOMA systems. To assess the realistic capabilities of NOMA, various practical impairments, including successive interference cancellation (SIC) error, channel estimation error (CEE), and feedback delay error, are systematically considered. This approach enhances our understanding of the challenges and interactions posed by these errors, facilitating the development of mitigation strategies and performance benchmarks for NOMA in practical scenarios.

In the first chapter, we have presented a thorough exploration of future generations of mobile wireless communication and the fundamentals of NOMA and MIMO paradigms. The initial segment of this chapter included a detailed literature review covering the requirements, features, and use cases of B5G and 6G. While the following section delved into the fundamental principles of NOMA in the power domain. Additionally, we explored various concepts related to multiple antennas.

In the second chapter of our thesis, we conducted an in-depth examination of practical impairments, encompassing SIC error, CEE, and feedback delay, affecting both downlink and uplink SISO-NOMA systems. The analysis in this context has centered on key metrics such as ergodic capacity (EC), outage probability (OP), and bit error rate (BER). Our comprehensive findings underscored the adverse effects of these impairments.

In chapter three, our investigation delved into the examination of the Ergodic Capacity (EC) of MIMO-NOMA utilizing the joint transmit and receive antenna selection (JTRAS) protocol for two distinct scenarios: a two-user scenario and a multi-user scenario. We thoroughly analyzed and juxtaposed the EC of the proposed MIMO-NOMA with JTRAS against MIMO-OMA under varied imperfections. The results unmistakably highlighted the superiority of the NOMA system over OMA when utilizing MIMO techniques. Moreover, both successive interference cancellation (SIC) and channel estimation error (CEE) imperfections contributed to capacity degradation. Furthermore, an increment in the number of users detrimentally affected the EC, while an increase in the number of antennas positively influenced the EC.

In the fourth chapter, we have investigated the outage probability (OP) and throughput of cooperative non-orthogonal multiple access (CNOMA) using the transmit antenna selection (TAS) protocol to enhance the performance of SISO-NOMA systems. To achieve this goal, two strategies, namely partial relay selection (PRS) and best relay selection (BRS), are employed in the presence and absence of certain imperfections. The results demonstrated that increasing the number of antennas at the base station (BS) or relays has contributed to the overall improvement of the CNOMA scheme's performance. Additionally, the integration of relay selection and antenna selection paradigms further enhanced system performance. Conversely, the impact of impairments was mitigated by incorporating selection criteria for antennas and/or relays.

This thesis conducts a thorough analysis of the results obtained from antenna selection strategies in MIMO-NOMA systems and advocates for their implementation in the unmanned aerial vehicle (UAV), high altitude platform station (HAPS), and integrated space and terrestrial network (ISTN) networks. Furthermore, it recommends further exploration into the utilization of intelligent antenna arrays, specifically reconfigurable intelligent surfaces (RIS) and large intelligent surfaces (LIS). In addition, the introduction of artificial intelligence (AI) is suggested as a novel paradigm, aiming to significantly improve the efficiency, reliability, and capability of wireless communication systems through the integration of multiple antennas and NOMA.

Appendix A

Appendix A: Proof of equation (2.10)

The achievable rates of UE_1 given as follows

$$R_1 = \log_2\left(1 + \frac{\alpha_1\gamma_0\left|\hat{h}_1^{(\tau)}\right|^2}{\alpha_2\gamma_0\left|\hat{h}_1^{(\tau)}\right|^2 + \frac{\gamma_0}{\rho^2}\left(\sigma_\kappa^2 + \sigma_{f_d\tau}^2\right) + \frac{1}{\rho^2}}\right). \tag{A.1}$$

After simplifying (A.1) we obtain

$$R_1 = \log_2\left(\frac{\beta + \gamma_0\left|\hat{h}_1^{(\tau)}\right|^2}{\beta + \alpha_2\gamma_0\left|\hat{h}_1^{(\tau)}\right|^2}\right), \tag{A.2}$$

where, $\beta = \frac{\gamma_0}{\rho^2}\left(\sigma_\kappa^2 + \sigma_{f_d\tau}^2\right) + \frac{1}{\rho^2}$
Then, by using $\log_2\left(\frac{x}{y}\right) = \log_2(x) - \log_2(y)$, Eq (A.2) became

$$R_1 = \log_2\left(\beta + \gamma_0\left|\hat{h}_1^{(\tau)}\right|^2\right) - \log_2\left(\beta + \alpha_2\gamma_0\left|\hat{h}_1^{(\tau)}\right|^2\right). \tag{A.3}$$

Let us suppose $X_1 = \gamma_0\left|\hat{h}_1^{(\tau)}\right|^2$, and $Y_1 = \alpha_2\gamma_0\left|\hat{h}_1^{(\tau)}\right|^2$ as a exponential random variables, so the ergodic capacity was defined as

$$C_{j,erg} = E\left[R_j\right] = \int_0^\infty \log_2(\beta + x)\, f_{X_j}(x)\, dx - \int_0^\infty \log_2(\beta + y)\, f_{Y_j}(y)\, dy \tag{A.4}$$

By using ([95], Eq (11)), the Eq (A.4) can be written as

$$C_{j,erg} = \underbrace{\frac{1}{\ln(2)}\int_0^\infty \frac{1 - F_{X_j}(x)}{\beta + x}dx}_{I_1} - \underbrace{\frac{1}{\ln(2)}\int_0^\infty \frac{1 - F_{Y_j}(y)}{\beta + y}dy}_{I_2} \tag{A.5}$$

To calculate the ergodic capacity of each component using the PDF of X_1 and Y_1 defined in (2.14), followed by some mathematical simplification. The CDF calculated as follow

$$F_{X_1}(x) = p_r\left(\gamma_0\left|\hat{h}_1^{(\tau)}\right|^2 < x\right) = p_r\left(\left|\hat{h}_1^{(\tau)}\right|^2 < \frac{x}{\gamma_0}\right)$$
$$= \int_0^{\frac{x}{\gamma_0}} f_{\left|\hat{h}_1^{(\tau)}\right|^2}(x)\,dx \quad = 1 - \exp\left(-\frac{x}{\gamma_0\widehat{\sigma}_1^2}\right). \tag{A.6}$$

$$F_{Y_1}(y) = p_r\left(\alpha_2\gamma_0\left|\hat{h}_1^{(\tau)}\right|^2 < y\right) = p_r\left(\left|\hat{h}_1^{(\tau)}\right|^2 < \frac{y}{\alpha_2\gamma_0}\right)$$
$$= \int_0^{\frac{y}{\alpha_2\gamma_0}} f_{\left|\hat{h}_1^{(\tau)}\right|^2}(y)\,dy \quad = 1 - \exp\left(-\frac{y}{\alpha_2\gamma_0\widehat{\sigma}_1^2}\right). \tag{A.7}$$

Applying ([93], Eq (3.352.4)), also, by substituting (A.6) in I_1 and by substituting (A.7) into I_2 we obtain

$$I_1 = \frac{1}{\ln(2)}\left(-\exp\left(\frac{\frac{\gamma_0}{\rho^2}\left(\sigma_\kappa^2 + \sigma_{f_d\tau}^2\right) + \frac{1}{\rho^2}}{\gamma_0\widehat{\sigma}_1^2}\right) Ei\left(-\frac{\frac{\gamma_0}{\rho^2}\left(\sigma_\kappa^2 + \sigma_{f_d\tau}^2\right) + \frac{1}{\rho^2}}{\gamma_0\widehat{\sigma}_1^2}\right)\right) \tag{A.8}$$

$$I_2 = \frac{1}{\ln(2)}\left(-\exp\left(\frac{\frac{\gamma_0}{\rho^2}\left(\sigma_\kappa^2 + \sigma_{f_d\tau}^2\right) + \frac{1}{\rho^2}}{\gamma_0\alpha_2\widehat{\sigma}_1^2}\right) Ei\left(-\frac{\frac{\gamma_0}{\rho^2}\left(\sigma_\kappa^2 + \sigma_{f_d\tau}^2\right) + \frac{1}{\rho^2}}{\gamma_0\alpha_2\widehat{\sigma}_1^2}\right)\right) \tag{A.9}$$

where Ei(.) denotes the exponential integral function.

Finally, after substituting (A.8) and (A.9) into (A.5) we obtain the ergodic capacity for UE_1 expressed as in (2.10).

The proof is completed.

Appendix B

Appendix B: Proof of equation (2.17)

$$
\begin{aligned}
P_{out.1} &= Pr(\gamma_1 < \gamma_{th,1}) \\
&= Pr\left(\frac{\alpha_1\gamma_0\left|\hat{h}_1^{(\tau)}\right|^2}{\alpha_2\gamma_0\left|\hat{h}_1^{(\tau)}\right|^2 + \frac{\gamma_0}{\rho^2}\left(\sigma_\kappa^2 + \sigma_{f_d\tau}^2\right) + \frac{1}{\rho^2}} < \gamma_{th,1}\right) \\
&= \Pr\left(\left|\widehat{h}_1^{(\tau)}\right|^2 < \frac{\frac{\gamma_{th,1}}{\rho^2}\left(1 + \gamma_0\left(\sigma_\kappa^2 + \sigma_{f_d\tau}^2\right)\right)}{\gamma_0\left(\alpha_1 - \alpha_2\gamma_{th.1}\right)}\right) \qquad \text{(B.1)} \\
&= \int_0^{\frac{\frac{\gamma_{th,1}}{\rho^2}\left(1+\gamma_0\left(\sigma_\kappa^2+\sigma_{f_d\tau}^2\right)\right)}{\gamma_0\left(\alpha_1-\alpha_2\gamma_{th.1}\right)}} \frac{1}{\sigma_1^2}\exp\left(-\frac{x}{\sigma_1^2}\right)dx.
\end{aligned}
$$

After evaluating the integral, we obtain the OP for UE_1 as follow

$$
P_{out.1} = 1 - \exp\left(\frac{-\left(\frac{\gamma_{th,1}}{\rho^2}\left(1 + \gamma_0\left(\sigma_{\kappa_j}^2 + \sigma_{fd_j}^2\right)\right)\right)}{\gamma_0\hat{\sigma}_1^2\left(\alpha_1 - \alpha_2\gamma_{th.1}\right)}\right). \qquad \text{(B.2)}
$$

The proof is completed.

Appendix C

Appendix C: Proof of equation (2.27)

The average bit error rate (ABER) at the UE_1 can be presented as in [163]

$$P_{UE_1} = \frac{1}{2}\left(\sum_{i=1}^{2}\left(\int_0^{\infty} Q(\Gamma_i) f_{\Gamma_i}(\Gamma_i) d_{\Gamma_i}\right)\right), \tag{C.1}$$

where $f_{\Gamma_i}(\Gamma_i)$ is the Rayleigh distributed probability density function which is given as

$$f_{\Gamma_i}(\Gamma_i) = \frac{1}{\bar{\Gamma_i}} \exp\left(\frac{-\Gamma_i}{\bar{\Gamma_i}}\right). \tag{C.2}$$

An alternative representation of the Q-function as specified by Craig's formulation as in [164].

$$Q(x) = \frac{1}{\pi}\int_0^{\frac{\pi}{2}} \exp\left(\frac{-x^2}{2sin^2(\theta)}\right). \tag{C.3}$$

Furthermore, the moment-generating function (MGF) is defined as follows

$$MGF_{\Gamma}(x) = \int_0^{\infty} \exp(x\Gamma) f_{\Gamma}(\Gamma) d_{\Gamma}. \tag{C.4}$$

Then, the ABER can be given as:

$$P_{UE_1} = \frac{1}{2}\left(\sum_{i=1}^{2}\left(\frac{1}{\pi}\int_0^{\frac{\pi}{2}} MGF_{\Gamma_i}\left(\frac{-1}{2sin^2(\theta)}\right) d\theta\right)\right). \tag{C.5}$$

with

$$MGF_{\Gamma_i}(x) = (1 - x\bar{\Gamma_i})^{-1} \tag{C.6}$$

Replacing (C.6) into (C.5), it becomes

$$P_{UE_1} = \frac{1}{2}\left(\sum_{i=1}^{2}\left(\frac{1}{\pi}\int_0^{\frac{\pi}{2}}\left(1 + \frac{\bar{\Gamma_i}}{2sin^2(\theta)}\right)^{-1}\right)\right). \tag{C.7}$$

However, according to [163], the term of (C.7) can be presented as

$$\frac{1}{\pi}\int_0^{\frac{\pi}{2}}\left(1 + \frac{\overline{\Gamma_i}}{2sin^2(\theta)}\right)^{-1} d\theta = \frac{1}{2}\left(1 - \sqrt{\frac{\overline{\Gamma_i}}{2 + \overline{\Gamma_i}}}\right). \tag{C.8}$$

Appendix D

Appendix D: Proof of equation (2.32)

The ABER at the UE_2 can be presented as

$$\begin{aligned} P_{UE_2} =& \frac{1}{2}\Big[\int_0^\infty Q(\Gamma_3) f_{\Gamma_3}(\Gamma_3) d_{\Gamma_3} + \int_0^\infty Q(\Gamma_4) f_{\Gamma_4}(\Gamma_4) d_{\Gamma_4} + \int_0^\infty Q(\Gamma_5) f_{\Gamma_5}(\Gamma_5) d_{\Gamma_5} \\ &+ \int_0^\infty Q(\Gamma_6) f_{\Gamma_6}(\Gamma_6) d_{\Gamma_6} + \int_0^\infty Q(\Gamma_7) f_{\Gamma_7}(\Gamma_7) d_{\Gamma_7} + \int_0^\infty Q(\Gamma_8) f_{\Gamma_8}(\Gamma_8) d_{\Gamma_8}\Big], \end{aligned} \tag{D.1}$$

According to (C.3) we can write (D.1) as

$$\begin{aligned} P_{UE_2} =& \frac{1}{2}\Big[\int_0^\infty \frac{1}{\pi}\int_0^{\frac{\pi}{2}} \exp\left(\frac{-\Gamma_3}{2sin^2(\theta)}\right) f_{\Gamma_3}(\Gamma_3) d_{\Gamma_3} + \int_0^\infty \frac{1}{\pi}\int_0^{\frac{\pi}{2}} \exp\left(\frac{-\Gamma_4}{2sin^2(\theta)}\right) f_{\Gamma_4}(\Gamma_4) d_{\Gamma_4} \\ &+ \int_0^\infty \frac{1}{\pi}\int_0^{\frac{\pi}{2}} \exp\left(\frac{-\Gamma_5}{2sin^2(\theta)}\right) f_{\Gamma_5}(\Gamma_5) d_{\Gamma_5} + \int_0^\infty \frac{1}{\pi}\int_0^{\frac{\pi}{2}} \exp\left(\frac{-\Gamma_6}{2sin^2(\theta)}\right) f_{\Gamma_6}(\Gamma_6) d_{\Gamma_6} \\ &+ \int_0^\infty \frac{1}{\pi}\int_0^{\frac{\pi}{2}} \exp\left(\frac{-\Gamma_7}{2sin^2(\theta)}\right) f_{\Gamma_7}(\Gamma_7) d_{\Gamma_7} + \int_0^\infty \frac{1}{\pi}\int_0^{\frac{\pi}{2}} \exp\left(\frac{-\Gamma_8}{2sin^2(\theta)}\right) f_{\Gamma_8}(\Gamma_8) d_{\Gamma_8}\Big] \end{aligned} \tag{D.2}$$

Using the MGF expression and some algebraic manipulations, we can obtain

$$\begin{aligned} P_{UE_2} =& \frac{1}{2}\Big[\frac{1}{\pi}\int_0^{\frac{\pi}{2}} \left(1 + \frac{\bar{\Gamma_3}}{2sin^2(\theta)}\right)^{-1} d\theta + \frac{1}{\pi}\int_0^{\frac{\pi}{2}} \left(1 + \frac{\bar{\Gamma_4}}{2sin^2(\theta)}\right)^{-1} d\theta \\ &+ \frac{1}{\pi}\int_0^{\frac{\pi}{2}} \left(1 + \frac{\bar{\Gamma_5}}{2sin^2(\theta)}\right)^{-1} d\theta + \frac{1}{\pi}\int_0^{\frac{\pi}{2}} \left(1 + \frac{\bar{\Gamma_6}}{2sin^2(\theta)}\right)^{-1} d\theta \\ &+ \frac{1}{\pi}\int_0^{\frac{\pi}{2}} \left(1 + \frac{\bar{\Gamma_7}}{2sin^2(\theta)}\right)^{-1} d\theta + \frac{1}{\pi}\int_0^{\frac{\pi}{2}} \left(1 + \frac{\bar{\Gamma_8}}{2sin^2(\theta)}\right)^{-1} d\theta\Big] \end{aligned} \tag{D.3}$$

Using (C.8) we can express (2.32).

Scientific Production

Authored paper

- Saber Menaa, Abdellatif Khelil, Khaled M. Rabie, Xingwang Li & Galymzhan Nauryzbayev: **"On the ergodic capacity of MIMO-NOMA systems with JTRAS protocol under imperfect SIC and CSI"**, International Journal of Electronics Taylor & Trancis (2023), DOI: 10.1080/00207217.2023.2240077.

- Saber Menaa & Abdellatif Khelil: **"Performance Analysis of Antenna-Relay Selection in CNOMA Systems under Practical Impairments"**, submitted to Journal of Telecommunications and Information Technology (JTIT 2024). Decision : Accepted.

Conference paper

- Saber Menaa & Abdellatif Khelil: **"On the Performance of SISO, SIMO and MISO-NOMA Systems under Perfect and Imperfect SIC"**, The 19th IEEE International Multi-Conference on Systems, Signals & Devices SSD'2022 – Setif –.

Bibliography

[1] J. M. Velazquez-Gutierrez and C. Vargas-Rosales, "Sequence sets in wireless communication systems: A survey," *IEEE Communications Surveys & Tutorials*, vol. 19, no. 2, pp. 1225–1248, 2016.

[2] M. A. Albreem, "5g wireless communication systems: Vision and challenges," in *2015 International Conference on Computer, Communications, and Control Technology (I4CT)*, pp. 493–497, IEEE, 2015.

[3] O. Maraqa, A. S. Rajasekaran, S. Al-Ahmadi, H. Yanikomeroglu, and S. M. Sait, "A survey of rate-optimal power domain noma with enabling technologies of future wireless networks," *IEEE Communications Surveys & Tutorials*, vol. 22, no. 4, pp. 2192–2235, 2020.

[4] M. Agiwal, A. Roy, and N. Saxena, "Next generation 5g wireless networks: A comprehensive survey," *IEEE communications surveys & tutorials*, vol. 18, no. 3, pp. 1617–1655, 2016.

[5] R. IslamSM, D. AvazovN, *et al.*, "Power domain non orthogonal multiple access (noma) in 5g systems: Potentials and challenges," *IEEE communications Surveys & Tutorials*, vol. 19, no. 2, p. 721, 2017.

[6] A. Akbar, S. Jangsher, and F. A. Bhatti, "Noma and 5g emerging technologies: A survey on issues and solution techniques," *Computer Networks*, vol. 190, p. 107950, 2021.

[7] H. Tabassum, M. S. Ali, E. Hossain, M. J. Hossain, and D. I. Kim, "Non-orthogonal multiple access (noma) in cellular uplink and downlink: Challenges and enabling techniques," *arXiv preprint arXiv:1608.05783*, 2016.

[8] A. S. Shah, A. N. Qasim, M. A. Karabulut, H. Ilhan, and M. B. Islam, "Survey and performance evaluation of multiple access schemes for next-generation wireless communication systems," *IEEE Access*, vol. 9, pp. 113428–113442, 2021.

[9] H. Tabassum, M. S. Ali, E. Hossain, M. J. Hossain, and D. I. Kim, "Uplink vs. downlink noma in cellular networks: Challenges and research directions," in *2017 IEEE 85th vehicular technology conference (VTC Spring)*, pp. 1–7, IEEE, 2017.

[10] B. Makki, K. Chitti, A. Behravan, and M.-S. Alouini, "A survey of noma: Current status and open research challenges," *IEEE Open Journal of the Communications Society*, vol. 1, pp. 179–189, 2020.

[11] A. Kassir, R. A. Dziyauddin, H. M. Kaidi, and M. A. M. Izhar, "Power domain non orthogonal multiple access: A review," in *2018 2nd International Conference on Telematics and Future Generation Networks (TAFGEN)*, pp. 66–71, IEEE, 2018.

[12] Q. Wang, R. Zhang, L.-L. Yang, and L. Hanzo, "Non-orthogonal multiple access: A unified perspective," *IEEE Wireless Communications*, vol. 25, no. 2, pp. 10–16, 2018.

[13] Y. Wu, C. Xiao, Z. Ding, X. Gao, and S. Jin, "A survey on mimo transmission with finite input signals: Technical challenges, advances, and future trends," *Proceedings of the IEEE*, vol. 106, no. 10, pp. 1779–1833, 2018.

[14] L. Juho, H. Jin-Kyu, and Z. Jianzhong, "Mimo technologies in 3gpp lte and lte-advanced," *WCN-EURASIP Journal on Wireless Communications and Networking*, vol. 2009, no. 1, p. 302092, 2009.

[15] R. S. Blum and J. H. Winters, "On optimum mimo with antenna selection," in *2002 IEEE International Conference on Communications. Conference Proceedings. ICC 2002 (Cat. No. 02CH37333)*, vol. 1, pp. 386–390, IEEE, 2002.

[16] S. Sanayei and A. Nosratinia, "Antenna selection in mimo systems," *IEEE Communications magazine*, vol. 42, no. 10, pp. 68–73, 2004.

[17] F. Khennoufa and K. Abdellatif, "Ber performance of co-operative relay noma-assisted ps protocol with imperfect sic and csi," *International Journal of Sensors Wireless Communications and Control*, vol. 13, no. 2, pp. 99–107, 2023.

[18] F. Khennoufa, A. Khelil, K. Rabie, H. Kaya, and X. Li, "An efficient hybrid energy harvesting protocol for cooperative noma systems: Error and outage performance," *Physical Communication*, vol. 58, p. 102061, 2023.

[19] S. Menaa, A. Khelil, K. M. Rabie, X. Li, and G. Nauryzbayev, "On the ergodic capacity of mimo-noma systems with jtras protocol under imperfect sic and csi," *International Journal of Electronics*, pp. 1–20, 2023.

[20] L. Pang, W. Wu, Y. Zhang, Y. Yuan, Y. Chen, A. Wang, and J. Li, "Joint power allocation and hybrid beamforming for downlink mmwave-noma systems," *IEEE Transactions on Vehicular Technology*, vol. 70, no. 10, pp. 10173–10184, 2021.

[21] M. Ad and A. Khelil, "Outage performance of underlay cr-noma-based d2d communications under imperfect csi and sic," *International Journal of Sensors, Wireless Communications and Control*, vol. 8, pp. 128942–128953, 2024.

[22] H. Marshoud, V. M. Kapinas, G. K. Karagiannidis, and S. Muhaidat, "Non-orthogonal multiple access for visible light communications," *IEEE photonics technology letters*, vol. 28, no. 1, pp. 51–54, 2015.

[23] H. Lee, S. Kim, and J.-H. Lim, "Multiuser superposition transmission (must) for lte-a systems," in *2016 IEEE International Conference on Communications (ICC)*, pp. 1–6, IEEE, 2016.

[24] P. Sharma, "Evolution of mobile wireless communication networks-1g to 5g as well as future prospective of next generation communication network," *International Journal of Computer Science and Mobile Computing*, vol. 2, no. 8, pp. 47–53, 2013.

[25] L. J. Vora, "Evolution of mobile generation technology: 1g to 5g and review of upcoming wireless technology 5g," *International journal of modern trends in engineering and research*, vol. 2, no. 10, pp. 281–290, 2015.

[26] J. Xia, "The third-generation-mobile (3g) policy and deployment in china: Current status, challenges, and prospects," *Telecommunications Policy*, vol. 35, no. 1, pp. 51–63, 2011.

[27] E. Ezhilarasan and M. Dinakaran, "A review on mobile technologies: 3g, 4g and 5g," in *2017 second international conference on recent trends and challenges in computational models (ICRTCCM)*, pp. 369–373, IEEE, 2017.

[28] M. Agiwal, H. Kwon, S. Park, and H. Jin, "A survey on 4g-5g dual connectivity: road to 5g implementation," *Ieee Access*, vol. 9, pp. 16193–16210, 2021.

[29] O. T. Eluwole, N. Udoh, M. Ojo, C. Okoro, and A. J. Akinyoade, "From 1g to 5g, what next?," *IAENG International Journal of Computer Science*, vol. 45, no. 3, 2018.

[30] M. Series, "Imt vision–framework and overall objectives of the future development of imt for 2020 and beyond," *Recommendation ITU*, vol. 2083, no. 0, 2015.

[31] G. Liu, Y. Huang, N. Li, J. Dong, J. Jin, Q. Wang, and N. Li, "Vision, requirements and network architecture of 6g mobile network beyond 2030," *China Communications*, vol. 17, no. 9, pp. 92–104, 2020.

[32] M. Series, "Minimum requirements related to technical performance for imt-2020 radio interface (s)," *Report*, vol. 2410, pp. 2410–2017, 2017.

[33] Z. Zhang, Y. Xiao, Z. Ma, M. Xiao, Z. Ding, X. Lei, G. K. Karagiannidis, and P. Fan, "6g wireless networks: Vision, requirements, architecture, and key technologies," *IEEE vehicular technology magazine*, vol. 14, no. 3, pp. 28–41, 2019.

[34] W. Jiang, B. Han, M. A. Habibi, and H. D. Schotten, "The road towards 6g: A comprehensive survey," *IEEE Open Journal of the Communications Society*, vol. 2, pp. 334–366, 2021.

[35] X. Wei, *Resource Allocation Techniques for Non-Orthogonal Multiple Access in Beyond 5G*. PhD thesis, University of York, 2022.

[36] O. O. Erunkulu, A. M. Zungeru, C. K. Lebekwe, M. Mosalaosi, and J. M. Chuma, "5g mobile communication applications: A survey and comparison of use cases," *IEEE Access*, vol. 9, pp. 97251–97295, 2021.

[37] I. A. Alimi, R. K. Patel, N. J. Muga, A. N. Pinto, A. L. Teixeira, and P. P. Monteiro, "Towards enhanced mobile broadband communications: A tutorial on enabling technologies, design considerations, and prospects of 5g and beyond fixed wireless access networks," *Applied Sciences*, vol. 11, no. 21, p. 10427, 2021.

[38] S. Krishna Sharma and X. Wang, "Towards massive machine type communications in ultra-dense cellular iot networks: Current issues and machine learning-assisted solutions," *arXiv e-prints*, pp. arXiv–1808, 2018.

[39] M. Rasti, S. K. Taskou, H. Tabassum, and E. Hossain, "Evolution toward 6g wireless networks: A resource management perspective," *arXiv preprint arXiv:2108.06527*, 2021.

[40] L. Bariah, L. Mohjazi, S. Muhaidat, P. C. Sofotasios, G. K. Kurt, H. Yanikomeroglu, and O. A. Dobre, "A prospective look: Key enabling technologies, applications and open research topics in 6g networks," *IEEE access*, vol. 8, pp. 174792–174820, 2020.

[41] Y. Niu, Y. Li, D. Jin, L. Su, and A. V. Vasilakos, "A survey of millimeter wave communications (mmwave) for 5g: opportunities and challenges," *Wireless networks*, vol. 21, pp. 2657–2676, 2015.

[42] X. Wang, L. Kong, F. Kong, F. Qiu, M. Xia, S. Arnon, and G. Chen, "Millimeter wave communication: A comprehensive survey," *IEEE Communications Surveys & Tutorials*, vol. 20, no. 3, pp. 1616–1653, 2018.

[43] G. Wang, H. Gu, X. Li, Z. Yu, O. Li, Q. Liu, K. Zeng, J. He, Y. Chen, J. Lu, *et al.*, "Terahertz sensing and communication towards future intelligence connected networks," *Communications of Huawei Research*, no. 2, pp. 54–79, 2022.

[44] M. S. Akbar, Z. Hussain, Q. Z. Sheng, and S. Mukhopadhyay, "6g survey on challenges, requirements, applications, key enabling technologies, use cases, ai integration issues and security aspects," *arXiv preprint arXiv:2206.00868*, 2022.

[45] N. Chi, Y. Zhou, Y. Wei, and F. Hu, "Visible light communication in 6g: Advances, challenges, and prospects," *IEEE Vehicular Technology Magazine*, vol. 15, no. 4, pp. 93–102, 2020.

[46] X. Zhu, C.-X. Wang, J. Huang, M. Chen, and H. Haas, "A novel 3d non-stationary channel model for 6g indoor visible light communication systems," *IEEE Transactions on Wireless Communications*, vol. 21, no. 10, pp. 8292–8307, 2022.

[47] S. Sun, T. S. Rappaport, and M. Shaft, "Hybrid beamforming for 5g millimeter-wave multi-cell networks," in *IEEE INFOCOM 2018-IEEE Conference on Computer Communications Workshops (INFOCOM WKSHPS)*, pp. 589–596, IEEE, 2018.

[48] E. J. Black, "Holographic beam forming and mimo," *Pivotal Commware*, pp. 1–8, 2017.

[49] E. Björnson, L. Sanguinetti, H. Wymeersch, J. Hoydis, and T. L. Marzetta, "Massive mimo is a reality—what is next?: Five promising research directions for antenna arrays," *Digital Signal Processing*, vol. 94, pp. 3–20, 2019.

[50] M. Di Renzo, A. Zappone, M. Debbah, M.-S. Alouini, C. Yuen, J. De Rosny, and S. Tretyakov, "Smart radio environments empowered by reconfigurable intelligent surfaces: How it works, state of research, and the road ahead," *IEEE journal on selected areas in communications*, vol. 38, no. 11, pp. 2450–2525, 2020.

[51] M. A. ElMossallamy, H. Zhang, L. Song, K. G. Seddik, Z. Han, and G. Y. Li, "Reconfigurable intelligent surfaces for wireless communications: Principles, challenges, and opportunities," *IEEE Transactions on Cognitive Communications and Networking*, vol. 6, no. 3, pp. 990–1002, 2020.

[52] M. Jian, G. C. Alexandropoulos, E. Basar, C. Huang, R. Liu, Y. Liu, and C. Yuen, "Reconfigurable intelligent surfaces for wireless communications: Overview of hardware designs, channel models, and estimation techniques," *Intelligent and Converged Networks*, vol. 3, no. 1, pp. 1–32, 2022.

[53] X. Ba, Y. Wang, H. Hai, Y. Chen, and Z. Liu, "Performance comparison of multi-connectivity with comp in 5g ultra-dense network," in *2018 IEEE 87th Vehicular Technology Conference (VTC Spring)*, pp. 1–5, IEEE, 2018.

[54] F. Irram, M. Ali, Z. Maqbool, F. Qamar, and J. J. Rodrigues, "Coordinated multi-point transmission in 5g and beyond heterogeneous networks," in *2020 IEEE 23rd International Multitopic Conference (INMIC)*, pp. 1–6, IEEE, 2020.

[55] E. Björnson and L. Sanguinetti, "Cell-free versus cellular massive mimo: What processing is needed for cell-free to win?," in *2019 IEEE 20th International Workshop on Signal Processing Advances in Wireless Communications (SPAWC)*, pp. 1–5, IEEE, 2019.

[56] Y. Liu, Z. Qin, M. Elkashlan, Z. Ding, A. Nallanathan, and L. Hanzo, "Nonorthogonal multiple access for 5g and beyond," *Proceedings of the IEEE*, vol. 105, no. 12, pp. 2347–2381, 2017.

[57] O. Kucur, G. Karabulut Kurt, M. Z. Shakir, and I. S. Ansari, "Nonorthogonal multiple access for 5g and beyond," 2018.

[58] S. R. Islam, M. Zeng, O. A. Dobre, and K.-S. Kwak, "Resource allocation for downlink noma systems: Key techniques and open issues," *IEEE Wireless Communications*, vol. 25, no. 2, pp. 40–47, 2018.

[59] M. A. Habibi, M. Nasimi, B. Han, and H. D. Schotten, "A comprehensive survey of ran architectures toward 5g mobile communication system," *Ieee Access*, vol. 7, pp. 70371–70421, 2019.

[60] A. Laghrissi and T. Taleb, "A survey on the placement of virtual resources and virtual network functions," *IEEE Communications Surveys & Tutorials*, vol. 21, no. 2, pp. 1409–1434, 2018.

[61] S. E. Elayoubi, S. B. Jemaa, Z. Altman, and A. Galindo-Serrano, "5g ran slicing for verticals: Enablers and challenges," *IEEE Communications Magazine*, vol. 57, no. 1, pp. 28–34, 2019.

[62] M. A. Habibi, B. Han, and H. D. Schotten, "Network slicing in 5g mobile communication architecture, profit modeling, and challenges," *arXiv preprint arXiv:1707.00852*, 2017.

[63] A. Patil and H. Sawant, "Technical specification group services and system aspects ip multimedia subsystem (ims)," *Int. J. Electron. Commun. Comput. Eng.*, vol. 3, no. 2, pp. 234–238, 2012.

[64] A. Napolitano, A. Giorgetti, K. Kondepu, L. Valcarenghi, and P. Castoldi, "Network slicing: an overview," in *2018 IEEE 4th International Forum on Research and Technology for Society and Industry (RTSI)*, pp. 1–4, IEEE, 2018.

[65] I. Afolabi, T. Taleb, K. Samdanis, A. Ksentini, and H. Flinck, "Network slicing and softwarization: A survey on principles, enabling technologies, and solutions," *IEEE Communications Surveys & Tutorials*, vol. 20, no. 3, pp. 2429–2453, 2018.

[66] K. B. Letaief, W. Chen, Y. Shi, J. Zhang, and Y.-J. A. Zhang, "The roadmap to 6g: Ai empowered wireless networks," *IEEE communications magazine*, vol. 57, no. 8, pp. 84–90, 2019.

[67] J. Liu, Y. Shi, Z. M. Fadlullah, and N. Kato, "Space-air-ground integrated network: A survey," *IEEE Communications Surveys & Tutorials*, vol. 20, no. 4, pp. 2714–2741, 2018.

[68] A. Mohammed, A. Mehmood, F.-N. Pavlidou, and M. Mohorcic, "The role of high-altitude platforms (haps) in the global wireless connectivity," *Proceedings of the IEEE*, vol. 99, no. 11, pp. 1939–1953, 2011.

[69] A. Fotouhi, H. Qiang, M. Ding, M. Hassan, L. G. Giordano, A. Garcia-Rodriguez, and J. Yuan, "Survey on uav cellular communications: Practical aspects, standardization advancements, regulation, and security challenges," *IEEE Communications surveys & tutorials*, vol. 21, no. 4, pp. 3417–3442, 2019.

[70] L. Dai, B. Wang, Z. Ding, Z. Wang, S. Chen, and L. Hanzo, "A survey of non-orthogonal multiple access for 5g," *IEEE communications surveys & tutorials*, vol. 20, no. 3, pp. 2294–2323, 2018.

[71] M. Aldababsa, M. Toka, S. Gökçeli, G. K. Kurt, and O. Kucur, "A tutorial on nonorthogonal multiple access for 5g and beyond," *Wireless communications and mobile computing*, vol. 2018, 2018.

[72] I. Budhiraja, N. Kumar, S. Tyagi, S. Tanwar, Z. Han, M. J. Piran, and D. Y. Suh, "A systematic review on noma variants for 5g and beyond," *IEEE Access*, vol. 9, pp. 85573–85644, 2021.

[73] D. Tse and P. Viswanath, *Fundamentals of wireless communication*. Cambridge university press, 2005.

[74] Z. Ding, F. Adachi, and H. V. Poor, "The application of mimo to non-orthogonal multiple access," *IEEE Transactions on Wireless Communications*, vol. 15, no. 1, pp. 537–552, 2015.

[75] A. Yılmaz and O. Kucur, "Unified analysis of transmit, receive and hybrid diversity techniques over generalized-k channels," *Wireless Communications and Mobile Computing*, vol. 16, no. 13, pp. 1798–1808, 2016.

[76] M. Aldababsa and O. Kucur, "Performance of cooperative multiple-input multiple-output noma in nakagami-m fading channels with channel estimation errors," *IET Communications*, vol. 14, no. 2, pp. 274–281, 2020.

[77] M. K. Simon and M.-S. Alouini, "Digital communications over fading channels (mk simon and ms alouini; 2005)[book review]," *IEEE Transactions on Information Theory*, vol. 54, no. 7, pp. 3369–3370, 2008.

[78] L. Dai, B. Wang, Y. Yuan, S. Han, I. Chih-Lin, and Z. Wang, "Non-orthogonal multiple access for 5g: solutions, challenges, opportunities, and future research trends," *IEEE Communications Magazine*, vol. 53, no. 9, pp. 74–81, 2015.

[79] Y. Saito, A. Benjebbour, Y. Kishiyama, and T. Nakamura, "System-level performance of downlink non-orthogonal multiple access (noma) under various environments," in *2015 IEEE 81st vehicular technology conference (VTC Spring)*, pp. 1–5, IEEE, 2015.

[80] K. Lu, Z. Wu, and X. Shao, "A survey of non-orthogonal multiple access for 5g," in *2017 IEEE 86th vehicular technology conference (VTC-Fall)*, pp. 1–5, IEEE, 2017.

[81] Y. Liu, G. Pan, H. Zhang, and M. Song, "On the capacity comparison between mimo-noma and mimo-oma," *IEEE Access*, vol. 4, pp. 2123–2129, 2016.

[82] M. Zeng, A. Yadav, O. A. Dobre, G. I. Tsiropoulos, and H. V. Poor, "On the sum rate of mimo-noma and mimo-oma systems," *IEEE Wireless communications letters*, vol. 6, no. 4, pp. 534–537, 2017.

[83] Z. Ding, Z. Yang, P. Fan, and H. V. Poor, "On the performance of non-orthogonal multiple access in 5g systems with randomly deployed users," *IEEE signal processing letters*, vol. 21, no. 12, pp. 1501–1505, 2014.

[84] Z. Yang, Z. Ding, P. Fan, and G. K. Karagiannidis, "On the performance of non-orthogonal multiple access systems with partial channel information," *IEEE Transactions on Communications*, vol. 64, no. 2, pp. 654–667, 2015.

[85] F. Kara and H. Kaya, "Ber performances of downlink and uplink noma in the presence of sic errors over fading channels," *IET Communications*, vol. 12, no. 15, pp. 1834–1844, 2018.

[86] M. Jain, S. Soni, N. Sharma, and D. Rawal, "Performance analysis at far and near user in noma based system in presence of sic error," *AEU-International Journal of Electronics and Communications*, vol. 114, p. 152993, 2020.

[87] T. Assaf, A. Al-Dweik, M. El Moursi, and H. Zeineldin, "Exact ber performance analysis for downlink noma systems over nakagami-m fading channels," *IEEE Access*, vol. 7, pp. 134539–134555, 2019.

[88] M. Zeng, W. Hao, O. A. Dobre, and Z. Ding, "Cooperative noma: State of the art, key techniques, and open challenges," *IEEE Network*, vol. 34, no. 5, pp. 205–211, 2020.

[89] F. Khennoufa, K. Abdellatif, and F. Kara, "Bit error rate and outage probability analysis for multi-hop decode-and-forward relay-aided noma with imperfect sic and imperfect csi," *AEU-International Journal of Electronics and Communications*, vol. 147, p. 154124, 2022.

[90] S. Menaa and A. Khelil, "On the performance of siso, simo and miso-noma systems under perfect and imperfect sic," in *2022 19th International Multi-Conference on Systems, Signals & Devices (SSD)*, pp. 458–463, IEEE, 2022.

[91] M. Aldababsa and O. Kucur, "Outage and ergodic sum-rate performance of cooperative mimo-noma with imperfect csi and sic," *International Journal of Communication Systems*, vol. 33, no. 11, p. e4405, 2020.

[92] M. Toka and O. Kucur, "Performance analyses of tas/alamouti-mrc noma system with channel estimation error, feedback delay, and imperfect sic," *Transactions on Emerging Telecommunications Technologies*, vol. 32, no. 12, p. e4359, 2021.

[93] I. S. Gradshteyn and I. M. Ryzhik, *Table of integrals, series, and products*. Academic press, 2014.

[94] S. M. Ross, "A first course in probability," 2014.

[95] X. Xie, J. Liu, J. Huang, and S. Zhao, "Ergodic capacity and outage performance analysis of uplink full-duplex cooperative noma system," *IEEE Access*, vol. 8, pp. 164786–164794, 2020.

[96] M. Vaezi, R. Schober, Z. Ding, and H. V. Poor, "Non-orthogonal multiple access: Common myths and critical questions," *IEEE Wireless Communications*, vol. 26, no. 5, pp. 174–180, 2019.

[97] M. Vaezi, Z. Ding, and H. V. Poor, *Multiple access techniques for 5G wireless networks and beyond*, vol. 159. Springer, 2019.

[98] S. R. Islam, N. Avazov, O. A. Dobre, and K.-S. Kwak, "Power-domain non-orthogonal multiple access (noma) in 5g systems: Potentials and challenges," *IEEE Communications Surveys & Tutorials*, vol. 19, no. 2, pp. 721–742, 2016.

[99] Z. Ding, X. Lei, G. K. Karagiannidis, R. Schober, J. Yuan, and V. K. Bhargava, "A survey on non-orthogonal multiple access for 5g networks: Research challenges and future trends," *IEEE Journal on Selected Areas in Communications*, vol. 35, no. 10, pp. 2181–2195, 2017.

[100] K. M. Rabie, B. Adebisi, E. H. Yousif, H. Gacanin, and A. M. Tonello, "A comparison between orthogonal and non-orthogonal multiple access in cooperative relaying power line communication systems," *IEEE access*, vol. 5, pp. 10118–10129, 2017.

[101] J. A. Oviedo and H. R. Sadjadpour, "A fair power allocation approach to noma in multiuser siso systems," *IEEE Transactions on Vehicular Technology*, vol. 66, no. 9, pp. 7974–7985, 2017.

[102] D.-T. Do and C.-B. Le, "Ergodic capacity computation in cognitive radio aided non-orthogonal multiple access systems," *Bulletin of Electrical Engineering and Informatics*, vol. 11, no. 1, pp. 270–277, 2022.

[103] X. Li, X. Gao, Y. Liu, G. Huang, M. Zeng, and D. Qiao, "Overlay cognitive radio-assisted noma intelligent transportation systems with imperfect sic and cees," *Chin. J. Electron.*, 2022.

[104] A. Rauniyar, P. Engelstad, and O. N. sterb, "Ergodic sum capacity analysis of noma-swipt enabled iot relay systems," *Internet Technology Letters*, vol. 4, no. 2, p. e218, 2021.

[105] H. V. Toan, T. M. Hoang, T. T. Duy, and L. T. Dung, "Outage probability and ergodic capacity of a two-user noma relaying system with an energy harvesting full-duplex relay and its interference at the near user," *Sensors*, vol. 20, no. 22, p. 6472, 2020.

[106] D.-T. Do, T.-L. Nguyen, K. M. Rabie, X. Li, and B. M. Lee, "Throughput analysis of multipair two-way replaying networks with noma and imperfect csi," *IEEE Access*, vol. 8, pp. 128942–128953, 2020.

[107] J. Zhang, L. Dai, R. Jiao, X. Li, and Y. Liu, "Performance analysis of relay assisted cooperative non-orthogonal multiple access systems," *submitted to IEEE Wireless Commun. Lett*, 2017.

[108] J.-B. Kim and I.-H. Lee, "Capacity analysis of cooperative relaying systems using non-orthogonal multiple access," *IEEE Communications Letters*, vol. 19, no. 11, pp. 1949–1952, 2015.

[109] K. Rabie, A. U. Makarfi, R. Kharel, O. Badarneh, B. Adebisi, X. Li, Z. Ding, *et al.*, "On the performance of non-orthogonal multiple access over composite fading channels," *arXiv preprint arXiv:2004.07860*, 2020.

[110] S. Beddiaf, A. Khelil, F. Khennoufa, F. Kara, H. Kaya, X. Li, K. Rabie, and H. Yanikomeroglu, "A unified performance analysis of cooperative noma with practical constraints: hardware impairment, imperfect sic and csi," *IEEE Access*, vol. 10, pp. 132931–132948, 2022.

[111] Y. Liu, G. Pan, H. Zhang, and M. Song, "On the capacity comparison between mimo-noma and mimo-oma," *IEEE Access*, vol. 4, pp. 2123–2129, 2016.

[112] M. Zeng, A. Yadav, O. A. Dobre, G. I. Tsiropoulos, and H. V. Poor, "Capacity comparison between mimo-noma and mimo-oma with multiple users in a cluster," *IEEE Journal on Selected Areas in Communications*, vol. 35, no. 10, pp. 2413–2424, 2017.

[113] Q. Sun, S. Han, I. Chin-Lin, and Z. Pan, "On the ergodic capacity of mimo noma systems," *IEEE Wireless Communications Letters*, vol. 4, no. 4, pp. 405–408, 2015.

[114] Q. Sun, S. Han, Z. Pan, *et al.*, "On the ergodic capacity and energy efficiency for fading mimo noma systems," *Journal of Signal Processing Systems*, vol. 83, no. 2, pp. 165–175, 2016.

[115] T. M. Hoang, B. C. Nguyen, X. N. Tran, *et al.*, "Outage probability and ergodic capacity of user clustering and beamforming mimo-noma relay system with imperfect csi over nakagami-m fading channels," *IEEE Systems Journal*, vol. 15, no. 2, pp. 2398–2409, 2020.

[116] M. Aldababsa and O. Kucur, "Outage and ergodic sum-rate performance of cooperative mimo-noma with imperfect csi and sic," *International Journal of Communication Systems*, vol. 33, no. 11, p. e4405, 2020.

[117] H. Lei, J. Zhang, K.-H. Park, P. Xu, I. S. Ansari, G. Pan, B. Alomair, and M.-S. Alouini, "On secure noma systems with transmit antenna selection schemes," *IEEE Access*, vol. 5, pp. 17450–17464, 2017.

[118] S. Mondal, S. Dhar Roy, and S. Kundu, "Outage analysis for noma-based energy harvesting relay network with imperfect csi and transmit antenna selection," *IET Communications*, vol. 14, no. 14, pp. 2240–2249, 2020.

[119] D.-T. Do, T.-L. Nguyen, and B. M. Lee, "Transmit antenna selection schemes for noma with randomly moving interferers in interference-limited environment," *Electronics*, vol. 9, no. 1, p. 36, 2019.

[120] D.-T. Do, C.-B. Le, and B. M. Lee, "Robust transmit antenna design for performance improvement of cell-edge users: Approach of noma and outage/ergodic capacity analysis," *Sensors*, vol. 19, no. 22, p. 4907, 2019.

[121] B. Demirkol and O. Kucur, "Outage performance of antenna selection schemes in noma networks using amplify-and-forward energy harvesting relay," in *2020 28th Signal Processing and Communications Applications Conference (SIU)*, pp. 1–4, IEEE, 2020.

[122] M. Aldababsa and E. Basar, "Joint transmit-and-receive antenna selection system for mimo-noma with energy harvesting," *IEEE Systems Journal*, 2021.

[123] M. Aldababsa, E. Güven, M. A. Durmaz, C. Göztepe, G. K. Kurt, and O. Kucur, "Unified performance analysis of antenna selection schemes for cooperative mimo-noma with practical impairments," *IEEE Transactions on Wireless Communications*, vol. 21, no. 6, pp. 4364–4378, 2021.

[124] M. Aldababsa, C. Göztepe, G. K. Kurt, and O. Kucur, "Bit error rate for noma network," *IEEE Communications Letters*, vol. 24, no. 6, pp. 1188–1191, 2020.

[125] M. Aldababsa and O. Kucur, "Ber performance of noma network with majority based jtras scheme in practical impairments," *AEU-International Journal of Electronics and Communications*, vol. 129, p. 153523, 2021.

[126] R. C. Kizilirmak and H. K. Bizaki, "Non-orthogonal multiple access (noma) for 5g networks," *Towards 5G Wireless Networks-A Physical Layer Perspective*, vol. 83, pp. 83–98, 2016.

[127] H. Tullberg, P. Popovski, Z. Li, M. A. Uusitalo, A. Hoglund, O. Bulakci, M. Fallgren, and J. F. Monserrat, "The metis 5g system concept: Meeting the 5g requirements," *IEEE Communications magazine*, vol. 54, no. 12, pp. 132–139, 2016.

[128] W. Shin, M. Vaezi, B. Lee, D. J. Love, J. Lee, and H. V. Poor, "Non-orthogonal multiple access in multi-cell networks: Theory, performance, and practical challenges," *IEEE Communications Magazine*, vol. 55, no. 10, pp. 176–183, 2017.

[129] B. Selim, S. Muhaidat, P. C. Sofotasios, A. Al-Dweik, B. S. Sharif, and T. Stouraitis, "Radio-frequency front-end impairments: Performance degradation in nonorthogonal multiple access communication systems," *IEEE Vehicular Technology Magazine*, vol. 14, no. 1, pp. 89–97, 2019.

[130] Z. Yang, Z. Ding, P. Fan, and N. Al-Dhahir, "A general power allocation scheme to guarantee quality of service in downlink and uplink noma systems," *IEEE transactions on wireless communications*, vol. 15, no. 11, pp. 7244–7257, 2016.

[131] Y. Saito, A. Benjebbour, Y. Kishiyama, and T. Nakamura, "System-level performance evaluation of downlink non-orthogonal multiple access (noma)," in *2013 IEEE 24th annual international symposium on personal, indoor, and mobile radio communications (PIMRC)*, pp. 611–615, IEEE, 2013.

[132] H. Liu, Z. Ding, K. J. Kim, K. S. Kwak, and H. V. Poor, "Decode-and-forward relaying for cooperative noma systems with direct links," *IEEE Transactions on Wireless Communications*, vol. 17, no. 12, pp. 8077–8093, 2018.

[133] D.-T. Do, M. Vaezi, and T.-L. Nguyen, "Wireless powered cooperative relaying using noma with imperfect csi," in *2018 IEEE Globecom Workshops (GC Wkshps)*, pp. 1–6, IEEE, 2018.

[134] J.-B. Kim and I.-H. Lee, "Non-orthogonal multiple access in coordinated direct and relay transmission," *IEEE Communications Letters*, vol. 19, no. 11, pp. 2037–2040, 2015.

[135] G. Li, D. Mishra, and H. Jiang, "Cooperative noma with incremental relaying: Performance analysis and optimization," *IEEE Transactions on Vehicular Technology*, vol. 67, no. 11, pp. 11291–11295, 2018.

[136] A. Tregancini, E. E. B. Olivo, D. P. M. Osorio, C. H. De Lima, and H. Alves, "Performance analysis of full-duplex relay-aided noma systems using partial relay selection," *IEEE Transactions on Vehicular Technology*, vol. 69, no. 1, pp. 622–635, 2019.

[137] L. Zhang, J. Liu, M. Xiao, G. Wu, Y.-C. Liang, and S. Li, "Performance analysis and optimization in downlink noma systems with cooperative full-duplex relaying," *IEEE Journal on Selected Areas in Communications*, vol. 35, no. 10, pp. 2398–2412, 2017.

[138] S. M. Ibraheem, W. Bedawy, W. Saad, and M. Shokair, "Outage performance of noma-based df relay sharing networks over nakagami-m fading channels," in *2018 13th International Conference on Computer Engineering and Systems (ICCES)*, pp. 512–517, IEEE, 2018.

[139] X. Liang, Y. Wu, D. W. K. Ng, Y. Zuo, S. Jin, and H. Zhu, "Outage performance for cooperative noma transmission with an af relay," *IEEE Communications Letters*, vol. 21, no. 11, pp. 2428–2431, 2017.

[140] A. A. Hamza, I. Dayoub, I. Alouani, and A. Amrouche, "On the error rate performance of full-duplex cooperative noma in wireless networks," *IEEE Transactions on Communications*, vol. 70, no. 3, pp. 1742–1758, 2021.

[141] X. Yue, Y. Liu, S. Kang, A. Nallanathan, and Z. Ding, "Exploiting full/half-duplex user relaying in noma systems," *IEEE Transactions on Communications*, vol. 66, no. 2, pp. 560–575, 2017.

[142] N. Guo, J. Ge, Q. Bu, and C. Zhang, "Multi-user cooperative non-orthogonal multiple access scheme with hybrid full/half-duplex user-assisted relaying," *IEEE Access*, vol. 7, pp. 39207–39226, 2019.

[143] V. Aswathi and A. Babu, "Full/half duplex cooperative noma under imperfect successive interference cancellation and channel state estimation errors," *IEEE Access*, vol. 7, pp. 179961–179984, 2019.

[144] Z. Ding, H. Dai, and H. V. Poor, "Relay selection for cooperative noma," *IEEE Wireless Communications Letters*, vol. 5, no. 4, pp. 416–419, 2016.

[145] Y. Li, Y. Li, X. Chu, Y. Ye, and H. Zhang, "Performance analysis of relay selection in cooperative noma networks," *IEEE Communications Letters*, vol. 23, no. 4, pp. 760–763, 2019.

[146] Z. Yang, Z. Ding, Y. Wu, and P. Fan, "Novel relay selection strategies for cooperative noma," *IEEE Transactions on Vehicular Technology*, vol. 66, no. 11, pp. 10114–10123, 2017.

[147] S. Lee, D. B. Da Costa, Q.-T. Vien, T. Q. Duong, and R. T. de Sousa Jr, "Non-orthogonal multiple access schemes with partial relay selection," *IET Communications*, vol. 11, no. 6, pp. 846–854, 2017.

[148] P. Xu, Z. Yang, Z. Ding, and Z. Zhang, "Optimal relay selection schemes for cooperative noma," *IEEE Transactions on Vehicular Technology*, vol. 67, no. 8, pp. 7851–7855, 2018.

[149] J. Ju, W. Duan, Q. Sun, S. Gao, and G. Zhang, "Performance analysis for cooperative noma with opportunistic relay selection," *IEEE Access*, vol. 7, pp. 131488–131500, 2019.

[150] T.-T. Thi Nguyen, D.-T. Do, Y.-C. Chen, C. So-In, and M. A. Rahman, "New look on relay selection strategies for full-duplex multiple-relay noma over nakagami-m fading channels," *Wireless Networks*, vol. 27, no. 6, pp. 3827–3843, 2021.

[151] H. Lei, Z. Yang, K.-H. Park, I. S. Ansari, Y. Guo, G. Pan, and M.-S. Alouini, "Secrecy outage analysis for cooperative noma systems with relay selection schemes," *IEEE Transactions on Communications*, vol. 67, no. 9, pp. 6282–6298, 2019.

[152] I. Umakoglu, M. Namdar, A. Basgumus, F. Kara, H. Kaya, and H. Yanikomeroglu, "Ber performance comparison of af and df assisted relay selection schemes in cooperative noma systems," in *2021 IEEE International Black Sea Conference on Communications and Networking (BlackSeaCom)*, pp. 1–6, IEEE, 2021.

[153] K. Sultan, "Best relay selection schemes for noma based cognitive relay networks in underlay spectrum sharing," *IEEE Access*, vol. 8, pp. 190160–190172, 2020.

[154] S. Asaad, A. M. Rabiei, and R. R. Müller, "Massive mimo with antenna selection: Fundamental limits and applications," *IEEE Transactions on Wireless Communications*, vol. 17, no. 12, pp. 8502–8516, 2018.

[155] A. P. Shrestha, T. Han, Z. Bai, J. M. Kim, and K. S. Kwak, "Performance of transmit antenna selection in non-orthogonal multiple access for 5g systems," in *2016 Eighth International Conference on Ubiquitous and Future Networks (ICUFN)*, pp. 1031–1034, IEEE, 2016.

[156] A. Dua, K. Medepalli, and A. J. Paulraj, "Receive antenna selection in mimo systems using convex optimization," *IEEE Transactions on Wireless Communications*, vol. 5, no. 9, pp. 2353–2357, 2006.

[157] T.-N. Tran and M. Voznak, "On secure system performance over siso, miso and mimo-noma wireless networks equipped a multiple antenna based on tas protocol," *EURASIP Journal on Wireless Communications and Networking*, vol. 2020, no. 1, pp. 1–22, 2020.

[158] M. Mohammadi, Z. Mobini, H. A. Suraweera, and Z. Ding, "Antenna selection in full-duplex cooperative noma systems," in *2018 IEEE International Conference on Communications (ICC)*, pp. 1–6, IEEE, 2018.

[159] M. Aldababsa, E. Güven, M. A. Durmaz, C. Göztepe, G. K. Kurt, and O. Kucur, "Unified performance analysis of antenna selection schemes for cooperative mimo-noma with practical impairments," *IEEE Transactions on Wireless Communications*, vol. 21, no. 6, pp. 4364–4378, 2021.

[160] Y. Yu, H. Chen, Y. Li, Z. Ding, L. Song, and B. Vucetic, "Antenna selection for mimo nonorthogonal multiple access systems," *IEEE Transactions on vehicular technology*, vol. 67, no. 4, pp. 3158–3171, 2017.

[161] Y. Yu, H. Chen, Y. Li, Z. Ding, and L. Zhuo, "Antenna selection in mimo cognitive radio-inspired noma systems," *IEEE Communications Letters*, vol. 21, no. 12, pp. 2658–2661, 2017.

[162] S. Beddiaf, A. Khelil, F. Khennoufa, F. Kara, K. Rabie, X. Li, H. Kaya, A. Emir, and H. Yanikomeroglu, "Impact of hardware impairment on the uplink simo cooperative noma with selection relay under imperfect csi," *IEEE Access*, 2023.

[163] M. K. Simon and M.-S. Alouini, *Digital communication over fading channels*. New York: Wiley, 2001.

[164] J. W. Craig, "A new, simple and exact result for calculating the probability of error for two-dimensional signal constellations," in *MILCOM 91-Conference record*, pp. 571–575, IEEE, 1991.